MICROCOPY RESOLUTION TEST CHART
NATIONAL BUREAU OF STANDARDS-1963-A

DAVID W. TAYLOR NAVAL SHIP RESEARCH AND DEVELOPMENT CENTER

Bethesda, Maryland 20084

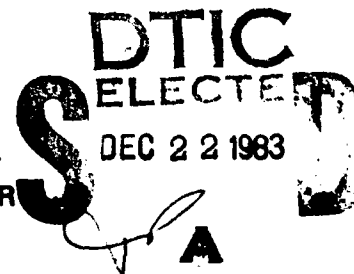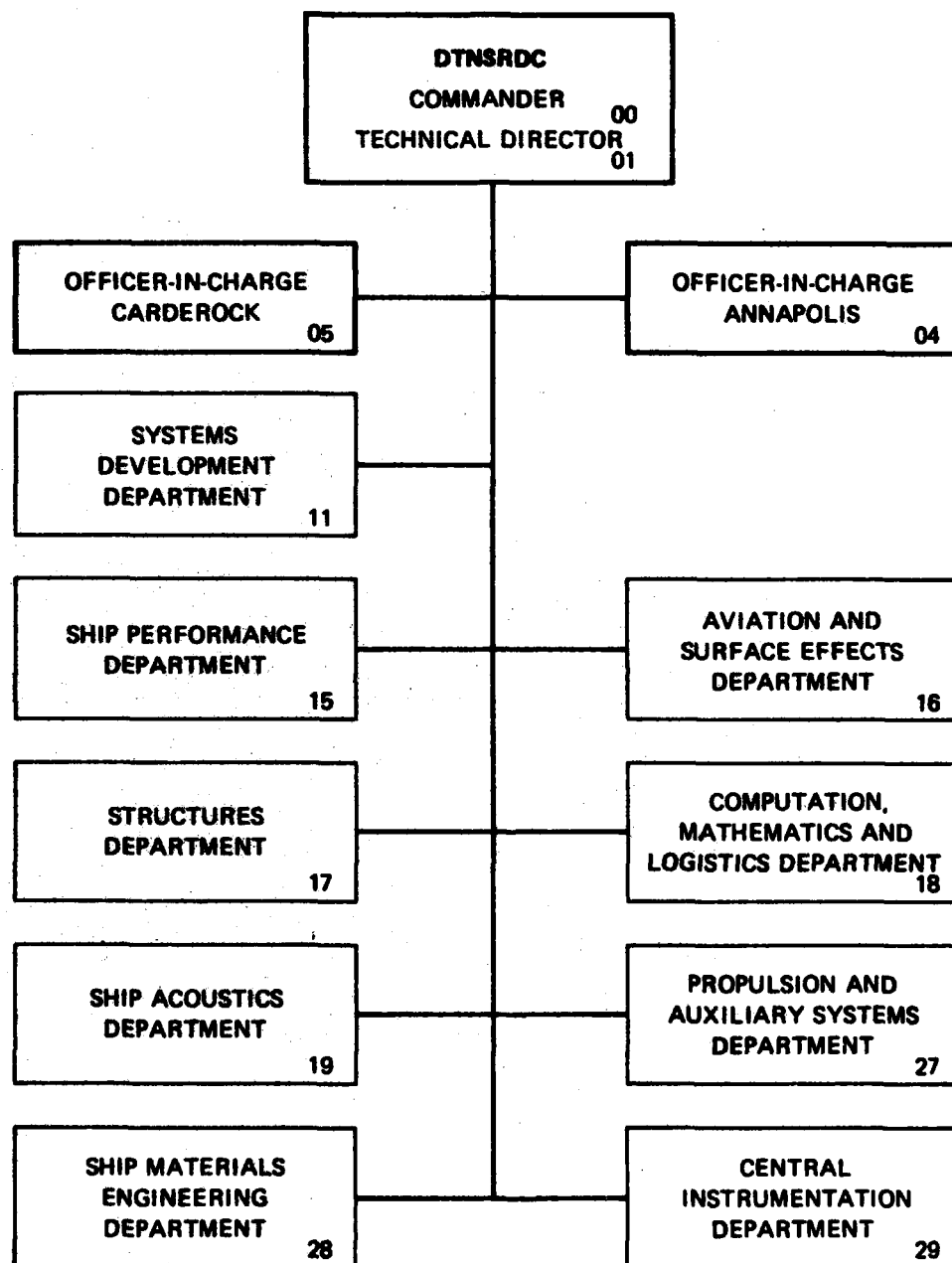## A CALCULATION OF THE PARABOLIZED NAVIER-STOKES EQUATIONS FOR TURBULENT AXISYMMETRIC FLOWS USING STREAMLINE COORDINATES AND THE k–ε TURBULENCE MODEL

by

Timothy F. Hogan

APPROVED FOR PUBLIC RELEASE: DISTRIBUTION UNLIMITED

DTIC
ELECTE
DEC 2 2 1983
S
A

SHIP PERFORMANCE DEPARTMENT
RESEARCH AND DEVELOPMENT REPORT

November 1983   DTNSRDC-83/070

MAJOR DTNSRDC ORGANIZATIONAL COMPONENTS

```
                        ┌──────────────────────────┐
                        │        DTNSRDC           │
                        │       COMMANDER       00 │
                        │   TECHNICAL DIRECTOR     │
                        │                       01 │
                        └──────────────────────────┘
                                    │
   ┌──────────────────────────┐     │     ┌──────────────────────────┐
   │   OFFICER-IN-CHARGE       │─────┼─────│   OFFICER-IN-CHARGE       │
   │   CARDEROCK           05  │     │     │   ANNAPOLIS           04  │
   └──────────────────────────┘     │     └──────────────────────────┘
                                     │
   ┌──────────────────────────┐     │
   │   SYSTEMS                 │─────┤
   │   DEVELOPMENT             │     │
   │   DEPARTMENT          11  │     │
   └──────────────────────────┘     │
                                     │
   ┌──────────────────────────┐     │     ┌──────────────────────────┐
   │   SHIP PERFORMANCE        │─────┼─────│   AVIATION AND            │
   │   DEPARTMENT          15  │     │     │   SURFACE EFFECTS         │
   └──────────────────────────┘     │     │   DEPARTMENT          16  │
                                     │     └──────────────────────────┘
   ┌──────────────────────────┐     │     ┌──────────────────────────┐
   │   STRUCTURES              │─────┼─────│   COMPUTATION,            │
   │   DEPARTMENT          17  │     │     │   MATHEMATICS AND         │
   └──────────────────────────┘     │     │   LOGISTICS DEPARTMENT 18 │
                                     │     └──────────────────────────┘
   ┌──────────────────────────┐     │     ┌──────────────────────────┐
   │   SHIP ACOUSTICS          │─────┼─────│   PROPULSION AND          │
   │   DEPARTMENT          19  │     │     │   AUXILIARY SYSTEMS       │
   └──────────────────────────┘     │     │   DEPARTMENT          27  │
                                     │     └──────────────────────────┘
   ┌──────────────────────────┐     │     ┌──────────────────────────┐
   │   SHIP MATERIALS          │─────┴─────│   CENTRAL                 │
   │   ENGINEERING             │           │   INSTRUMENTATION         │
   │   DEPARTMENT          28  │           │   DEPARTMENT          29  │
   └──────────────────────────┘           └──────────────────────────┘
```

SECURITY CLASSIFICATION OF THIS PAGE *(When Data Entered)*

REPORT DOCUMENTATION PAGE		READ INSTRUCTIONS BEFORE COMPLETING FORM
1. REPORT NUMBER DTNSRDC-83/070	2. GOVT ACCESSION NO.	3. RECIPIENT'S CATALOG NUMBER
4. TITLE *(and Subtitle)* A CALCULATION OF THE PARABOLIZED NAVIER-STOKES EQUATIONS FOR TURBULENT AXISYMMETRIC FLOWS USING STREAMLINE COORDINATES AND THE k-ε TURBULENCE MODEL		5. TYPE OF REPORT & PERIOD COVERED Formal
		6. PERFORMING ORG. REPORT NUMBER
7. AUTHOR(s) Timothy F. Hogan		8. CONTRACT OR GRANT NUMBER(s)
9. PERFORMING ORGANIZATION NAME AND ADDRESS David W. Taylor Naval Ship Research and Development Center Bethesda, Maryland 20084		10. PROGRAM ELEMENT, PROJECT, TASK AREA & WORK UNIT NUMBERS Program Element 61153N Task Area SR0230101 Work Unit 1542-101
11. CONTROLLING OFFICE NAME AND ADDRESS Naval Sea Systems Command (Code 05R24) Washington, D.C. 20362		12. REPORT DATE November 1983
		13. NUMBER OF PAGES 129
14. MONITORING AGENCY NAME & ADDRESS*(if different from Controlling Office)*		15. SECURITY CLASS. *(of this report)* UNCLASSIFIED
		15a. DECLASSIFICATION/DOWNGRADING SCHEDULE

16. DISTRIBUTION STATEMENT *(of this Report)*

APPROVED FOR PUBLIC RELEASE: DISTRIBUTION UNLIMITED

17. DISTRIBUTION STATEMENT *(of the abstract entered in Block 20, if different from Report)*

18. SUPPLEMENTARY NOTES

19. KEY WORDS *(Continue on reverse side if necessary and identify by block number)*

Axisymmetric Bodies	Thick Stern Boundary Layer
k-ε Turbulence Model	Turbulent Boundary Layers and Wakes
Parabolized Navier-Stokes	
Streamline	

20. ABSTRACT *(Continue on reverse side if necessary and identify by block number)*

     A numerical method for calculating turbulent axisymmetric flows at the stern and in the wake of bodies of revolution is presented. A partially parabolic marching technique in a streamline coordinate system is used together with the k-ε turbulence model. In the viscous sublayer region, the velocity is calculated using a mixing length argument instead of the wall function method.

(Continued on reverse side)

DD $_{1\ JAN\ 73}^{FORM}$ 1473   EDITION OF 1 NOV 65 IS OBSOLETE
S/N 0102-LF-014-6601

SECURITY CLASSIFICATION OF THIS PAGE *(When Data Entered)*

(Block 20 continued)

The numerical procedure starts at a station on the body where the boundary layer is thin and is pursued several body lengths downstream into the wake. The numerical solution is obtained by marching downstream and iteratively solving for each flow variable. The axial and normal corrections to the pressure are calculated by solving a kinematic compatibility equation for the position of the streamlines. The boundary conditions for the pressure are set by calculating the potential flow about an equivalent displacement body. The numerical marching scheme is repeated, restarting at the initial station, until convergence is achieved. Comparisons are made between the numerical results and the experimental data for four different bodies.

TABLE OF CONTENTS

LIST OF FIGURES

NOTATION

$A_{j-1/2}$	Coefficient of a tridiagonal system of equations
$B_{j-1/2}$	Coefficient of a tridiagonal system of equations
$C_{j-1/2}$	Coefficient of a tridiagonal system of equations
C_p	Numerical constant in the k-ϵ model = 0.09
c_p	Coefficient of pressure = $\dfrac{p - p_o}{1/2 \rho U_o^2}$
C_1	Numerical constant in the k-ϵ model = 1.44
C_2	Numerical constant in the k-ϵ model = 1.90
C_3	Numerical constant in the k-ϵ model = 4.44
$D_{J-1/2}$	Coefficient of a tridiagonal system of equations
$f(r_o, \delta)$	Factor used to reduce the turbulent outer mixing length viscosity
h_i	Scale factors of the natural coordinate system
K	The total number of streamline points
k	Turbulent kinetic energy
L	Length of the body
ℓ	Mixing length
n	Distance measured normal to the mean streamlines
P	Production of turbulent kinetic energy
P_E	Production of turbulent kinetic energy dissipation
p	Mean pressure
p'	Correction to the pressure to satisfy the streamline kinematic relation
p^*	Total corrected pressure = $p + p^*$

P_o	Upstream pressure
R	Radius of curvature of a streamline
Re	Reynolds number of the flow = $\rho U_o L/\nu$
r	Radial position of a streamline
r_{max}	Maximum radius of the body
r_o	Radial position of the surface of the body
s	Distance measured along a streamline
U	Total mean velocity
U'	Correction to the mean velocity
U^*	Total mean corrected velocity = $U + U'$
U_e	Potential flow velocity on the displacement body
U_o	Upstream velocity
u'	Turbulent velocity in the s-direction
u_j	Mean velocity in the x_j-direction
u_r	Mean radial velocity
u_x	Mean axial velocity
u^*	Friction velocity = τ_w/ρ
v'	Turbulent velocity in the n-direction
w'	Turbulent velocity in the θ-direction
x	Coordinate measured along the axis of the body
x_b	Beginning x-station of the partially parabolic k-ϵ integrations
x_e	Final x-station of the numerical integration

x_i	i^{th} x-station of the numerical integration
x_j	j^{th} cartesian coordinate
$y+$	Normal law of the wall distance
$y+^*$	Critical law of the wall distance for the k-ε model
α	Angle of streamline with the x-axis
α'	Correction to α to satisfy the streamline kinematic relation
α^*	Total corrected angle $= \alpha + \alpha'$
γ	Intermittency factor
ΔA_j	Control area for U, k, and ε equations
$\Delta A_j'$	Control area for the α equations
δ	Boundary layer thickness = position where the velocity is 99.5% of the potential flow velocity
δ^*	Displacement body
ε	Turbulent kinetic energy dissipation
η	Distance measured in the θ-direction
θ	Azimuthal angle
κ	von Karman constant = 0.40
ν	Molecular viscosity
ν_e	Total effective viscosity $= \nu + \nu_T$
ν_i	Inner viscosity used in the Huang/Wang boundary layer program
ν_o	Outer viscosity used in the Huang/Wang boundary layer program
ν_T	Turbulent eddy viscosity

$\upsilon_{T_{m\ell}}$ Turbulent eddy viscosity in the viscous sublayer

ξ_i Curvilinear coordinate of the natural coordinate system

ρ Constant fluid density

σ_k Turbulent Prandtl number used in the k equation $= 1.0$

σ_ε Turbulent Prandtl number used in the ε equation $= 1.30$

τ_w Wall shear stress

ψ Stream function

ψ_j j^{th} streamline grid number

ψ_T Outer streamline grid number

ABSTRACT

A numerical method for calculating tur-
bulent axisymmetric flows at the stern and
in the wake of bodies of revolution is
presented. A partially parabolic marching
technique in a streamline coordinate system
is used together with the k-ε turbulence model.
In the viscous sublayer region, the velocity
is calculated using a mixing length argument
instead of the wall function method. The
numerical procedure starts at a station on the
body where the boundary layer is thin and is
pursued several body lengths downstream into the
wake. The numerical solution is obtained by
marching downstream and iteratively solving for
each flow variable. The axial and normal cor-
rections to the pressure are calculated by solving
a kinematic compatibility equation for the position
of the streamlines. The boundary conditions for
the pressure are set by calculating the potential
flow about an equivalent displacement body. The
numerical marching scheme is repeated, restarting
at the initial station, until convergence is
achieved. Comparisons are made between the numer-
ical results and the experimental data for four
different bodies.

1. INTRODUCTION

The present study presents a numerical scheme for calculating steady, axisym-
metric, turbulent, incompressible flow about bodies of revolution. To fully describe
the steady flow past a body requires a solution of the elliptic Navier-Stokes
equations. Since this is a difficult task for complicated turbulent motion, the
turbulence must be modeled. As a minimum criterion, the turbulence model must

describe turbulent motion effects on the time averaged or mean flow. The present numerical scheme uses the turbulent kinetic energy and turbulent kinetic energy dissipation (k-ϵ) model together with the mean axisymmetric Navier-Stokes equations.

Even with a turbulent model, sophisticated and time consuming numerical methods are needed to solve the resulting elliptical Navier-Stokes equations. However, under certain conditions (partially parabolic flow conditions) certain diffusive terms are small. Neglecting these terms, and using a known pressure field, the mean steady equations become parabolic. Simpler marching techniques can then be employed which require less computer time to calculate the solution.

PARTIALLY PARABOLIC FLOW METHOD

General Discussion

The partially parabolic flow conditions are:

1. There is a predominant direction of flow;

2. The diffusion of momentum, k and ϵ along this direction can be neglected; and

3. Pressure is the main carrier of downstream effects to the upstream flow.

A simple example below illustrates the key points of the partially parabolic flow assumptions. For two-dimensional, steady, incompressible, laminar flow, the equations for the velocity components u and v and the normalized pressure p are

$$\frac{\partial u}{\partial x} + \frac{\partial v}{\partial y} = 0 \tag{1.1}$$

$$L(u) = -\frac{\partial p}{\partial x} + \nu \left(\frac{\partial^2 u}{\partial x^2} + \frac{\partial^2 u}{\partial y^2} \right) \tag{1.2}$$

$$L(v) = -\frac{\partial p}{\partial y} + \nu \left(\frac{\partial^2 v}{\partial x^2} + \frac{\partial^2 v}{\partial y^2} \right) \tag{1.3}$$

2

where the first order operation L is the advection operator. Assuming that the partially parabolic flow conditions are valid and that the predominant direction of the flow is along the x-axis, then the momentum Equations (1.2) and (1.3) can be approximated by

$$L(u) \approx -\frac{\partial p}{\partial x} + \nu \frac{\partial^2 u}{\partial y^2} \qquad (1.4)$$

$$L(v) \approx -\frac{\partial p}{\partial y} + \nu \frac{\partial^2 v}{\partial y^2} \qquad (1.5)$$

The system of equations, given by (1.4) and (1.5), is parabolic if the pressure field is known. The downstream flow field can then be calculated from the u and v boundary conditions. However, pressure is also unknown; an equation for p can be obtained by eliminating the diffusive terms in Equations (1.4) and (1.5), and using the continuity Equation (1.1). The result is

$$\frac{\partial^2 p}{\partial x^2} + \frac{\partial^2 p}{\partial y^2} = -\left[\frac{\partial L(u)}{\partial x} + \frac{\partial L(v)}{\partial y}\right] \qquad (1.6)$$

which is a Poisson equation. To obtain the solution for the pressure, boundary conditions must be given on the entire outer boundary of the flow domain, and the solution depends on upstream and downstream flow fields. It is directly through the pressure solution that downstream effects are communicated to the upstream.

The partially parabolic flow assumptions have been applied to internal and external flows. Briley (1974),[1*] Patankar et al. (1974),[2] and Roberts and Forester (1979)[3] have applied the assumptions successfully to solve for high Reynolds number flows in ducts and pipes. For external flows, the assumptions have been used to solve for two-dimensional flows by Markatos and Wills (1980),[4] for axisymmetric flow

---

*A complete listing of references is given on page 111.

3

problems by Muraoka (1980),[5] and for three-dimensional flow past surface ships by Abdelmeguid et al. (1978)[6] and Muraoka (1978).[7] For external flows, the agreement with experimental data is not as satisfactory as it is for internal flows. The principle disagreement between calculated and experimental results for external flows occurs in the stern/wake region of the flow. In this region the flow is often near separation, and in regions where the flow separates, the partially parabolic flow equations cannot adequately describe the motion.

Discrepancies between experiments and numerical results, however, may also be attributable to other sources. Among these are the choice of the predominant direction, the manner in which the pressure is calculated, and the approximations used in the turbulence model.

Predominate Direction of Flow

To apply the partially parabolic flow assumptions, a direction must be specified along which the diffusion is small compared with the other terms in the equations. Among the possibilities for this direction are the axis of the body (Abdelmeguid et al. 1978[6] and Muraoka 1978,[7] 1980[5]), the direction parallel to the surface of the body (Pratap and Spalding 1975[8]), the external potential flow direction (Briley, 1974[1]), and the mean flow direction (Markatos and Wills, 1980[4]). With each choice of the predominant direction, parabolic equations are obtained for momentum, k and ε, but each choice results in a different approximation to the turbulent diffusive mechanism.

The choice of the axis of the body may not be appropriate for bodies with a steep turn at the stern. In such a case, in the stern region, the direction of the flow is sizably different from the direction of the axis, and there would be a non-negligible contribution of diffusion in the axis direction. The selection of the direction parallel to the surface of the body, suitable for the flow near the body, becomes a poorer approximation to the flow direction as the distance away from the body increases. An additional difficulty with this choice is that, at the tail of the body, the flow is oriented at a nonzero angle, while in the wake the flow is along the axis of the body. This can lead to a singularity of the coordinate system. The choice of the external potential flow direction for external partially parabolic schemes is proper for the external regions of the flow but can be a poor approximation to the flow direction near the body.

4

In the present study, the predominant flow direction is the mean flow direction. The major advantage of this choice over the others for use in a partially parabolic method is that the direction of the mean flow coincides with the same direction that the diffusion is neglected in. As long as the Reynolds number remains large and the flow does not separate, the diffusion along the mean flow direction is small. Additional advantages of this selection are: there is no singularity at the tail of the coordinate system, and the surface of the body lies along a coordinate line. The disadvantage of this choice is that additional equations are needed to specify the positions of the streamlines.

Pressure Field

The analysis leading to Equation (1.6) shows that the pressure satisfies an elliptic differential equation. Instead of solving an equation of the form (1.6), the partially parabolic scheme employs the continuity equation to solve for the pressure field. Returning to the example of two-dimensional, incompressible, steady, laminar flow, let u^* and v^* represent the solution to Equations (1.4) and (1.5) for a given pressure field p^*. In general, u^* and v^* will not satisfy the continuity Equation (1.1), and therefore, u^*, v^*, and p^* must be corrected so that the continuity equation is satisfied. If the corrections to the velocity and pressure are denoted by primes, then the corrected u, v, and p fields are given by:

$$
\begin{aligned}
u &= u^* + u' \\
v &= v^* + v' \\
p &= p^* + p'
\end{aligned}
\tag{1.7}
$$

where u' and v' must be related by the equation

$$
\frac{\partial u'}{\partial x} + \frac{\partial v'}{\partial y} = -\left(\frac{\partial u^*}{\partial x} + \frac{\partial v^*}{\partial y}\right)
\tag{1.8}
$$

Using Equations (1.4) and (1.5), u' and v' can be expressed in terms of the derivatives of p':

5

$$u' = f\left(\frac{\partial p'}{\partial x}\right)$$

(1.9)

$$v' = g\left(\frac{\partial p'}{\partial y}\right)$$

and inserting (1.9) into (1.8) leads to

$$\frac{\partial f}{\partial\left[\frac{\partial p'}{\partial x}\right]}\frac{\partial^2 p'}{\partial x^2} + \frac{-\partial g}{\partial\left[\frac{\partial p'}{\partial y}\right]}\frac{\partial^2 p'}{\partial y^2} = -\left(\frac{\partial u^*}{\partial x} + \frac{\partial v^*}{\partial y}\right)$$

(1.10)

The functions f and g in Equation (1.9) must be determined numerically. The solution to Equation (1.10) together with the forms of f and g determine the corrected flow field.

Many partially parabolic schemes have solved the pressure correction equation by assuming that p' is independent of the predominant direction of the flow. For external flows, the derivatives of the pressure with respect to the predominant direction is set equal to the value of the derivative in this direction at the edge of the boundary layer (Patankar and Spalding, 1975).[9] In this way, a fast convergent scheme can be obtained. However, treating of the x and y derivatives of the pressure as independent of one another restricts the downstream influence of the pressure. This can also lead to poor results in the thick boundary layer region of the flow where the longitudinal and normal pressure variations can be large. In the present numerical scheme, the derivatives of the pressure are not assumed to be independent. This slows down the convergence, but it leads to a more accurate calculation of the flow field. The full details of the present numerical scheme are presented in the Numerical Procedure Section.

6

For external flow problems, the pressure must be specified on an outer boundary away from the body. Far away from the surface of the body, the pressure is equal to the free-stream pressure. This boundary condition has been used by Markatos and Wills (1980)[4] for two-dimensional flows. The difficulty with using this boundary condition is that special care must be taken to avoid pressure oscillations that can develop in the outer regions of the flow.

As an alternative to using this boundary condition, the potential flow solution can be used to set the pressure on a surface away from the body. Outside the boundary layer region, viscous effects are negligible and the flow equations are given by the inviscid equations. For three-dimensional flows Abdelmeguid et al. (1978)[6] and Muraoka (1978)[7] have applied the potential flow solution past a surface ship to set the outer boundary condition for pressure. In this paper, the method of using the potential flow to set the boundary condition is extended by using the potential flow past a displacement body (Lighthill, 1958).[10] The displacement body concept is that the actual body is thickened so that outside the viscous flow region, the streamline positions calculated from the potential flow about the displacement body match the streamline positions calculated from the viscous flow about the actual body. Therefore, the iteratively calculated displacement body positions and the potential flow about this displacement body are important calculations in the numerical procedure.

TURBULENCE MODEL

The turbulence model used in this study is the k-ε model (Launder and Spalding, 1974).[11] This turbulence model is a two-equation model, characterized by partial differential equations for k and for ε. The interaction of the turbulence with the mean flow is specified through an eddy viscosity which is a function of k and ε.

The k-ε model has gained acceptance over mixing length models and the k-ε model lacks much of the arbitrariness of mixing length arguments. However, there is a drawback to the use of the k-ε equations, that is: the k-ε model is not valid in the viscous region of the turbulent flow. There have been two approaches to circumvent this difficulty: (1) modify the k-ε equations near the body so that

7

they are valid throughout the entire flow region (low Reynolds number model method, Jones and Launder, 1971,[12] 1973[13]); and (2) instead of solving in the viscous sublayer region, specify how the velocity varies in this region (wall function method; Launder and Spalding 1974[11]). The first method is numerically time consuming and the second method does not calculate the flow in a region where the velocity has its greatest variation.

As an alternative to these two methods, the present study specifies the eddy viscosity near to the body by a mixing length model and then calculates the velocity in this region. In this manner the problem of time consuming calculations is avoided while the velocity is calculated in the viscous sublayer region.

Another difficulty with solving the k-ε model has been found by Hanjalic and Launder (1980[14]). With partially parabolic schemes, the k-ε equations have been solved by neglecting both the diffusion of k and ε in the predominant direction and the generation of k and ε due to mean shear in the predominant direction. Hanjalic and Launder (1980[14]) retained the generation terms and found considerable improvement in the consistency of the numerical results with the experimental data. These mean shear generation terms will be retained in the k-ε equations used in the present method.

SUMMARY

In summary, the present numerical scheme contains the following features not included in most partially parabolic schemes using the k-ε turbulence model.

1. A streamline coordinate system is used so that the diffusive terms in the flow equations are neglected in the actual mean flow direction;

2. The longitudinal and normal variation of the pressure field are not treated as independent quantities;

3. The displacement body concept is used to calculate the external boundary condition for the pressure;

4. A mixing length argument is employed to specify the eddy viscosity in the viscous sublayer region; and

5. The generation terms of k and ε due to longitudinal mean shear are retained in the k-ε equations.

8

The Equation Section discusses: the geometry of the streamline coordinate system, the theoretical framework of the k-ε turbulence model, and the time averaged equations. Also, the final coordinate system is established together with the equations and their boundary conditions. In the Numerical Procedure Section, the details of the numerical scheme are given. Finally, in the Numerical Results Section, results for four bodies of revolution are presented together with their comparisons with experimental data.

2. EQUATIONS

NATURAL COORDINATE SYSTEM

The flow equations are expressed in the natural coordinate system so that the second partially parabolic flow condition (see the Partially Parabolic Flow Method Section) can be applied in the streamline direction. A natural coordinate system is one in which one coordinate lies along the streamline and the other two are normal to the streamline (Liepmann and Roshko, 1957).[15] Assuming axisymmetric flow, one of the normal directions is in the azimuthal direction.

Differential distances in the streamline direction, the normal direction, and the azimuthal direction are denoted as (ds, dn, dz). If the curvilinear coordinates for this coordinate system are denoted by (ξ_1, ξ_2, θ) and the corresponding scale factors by (h_1, h_2, r), then the differential distances are given by

$$
\left.
\begin{aligned}
\partial s &= h_1 \, d \, \xi_1 \\
\partial n &= h_2 \, d \, \xi_2 \\
\partial z &= r \, d \, \theta
\end{aligned}
\right\}
\qquad (2.1)
$$

where θ is the azimuthal angle and r is the radial position. The derivatives of any quantity are given by

$$
\left.
\begin{aligned}
\frac{\partial}{\partial s} &= \frac{1}{h_1} \frac{\partial}{\partial \xi_1} \\
\frac{\partial}{\partial n} &= \frac{1}{h_2} \frac{\partial}{\partial \xi_2} \\
\frac{\partial}{\partial z} &= \frac{1}{r} \frac{\partial}{\partial \theta} \equiv 0
\end{aligned}
\right\}
\qquad (2.2)
$$

9

In the relation (2.2), the derivative with respect to θ is set equal to zero because there is no variation of the flow in the azimuthal direction for axisymmetric flow.

In the natural coordinate system the distance along the axis of symmetry, x, the radial position, r, and the scale factors, h_1 and h_2, must be determined in terms of ξ_1 and ξ_2. As shown in Figure 1 and using Equation (2.1), the derivatives of x and r in the streamline direction are

$$\frac{\partial x}{\partial \xi_1} = h_1 \cos \alpha \qquad (2.3a)$$

$$\frac{\partial r}{\partial \xi_1} = h_1 \sin \alpha \qquad (2.3b)$$

where α is the angle between the streamline and the x-axis direction. Similarly, using Figure 1 and Equation (2.1) the derivatives of x and r in the n direction are given by

$$\frac{\partial x}{\partial \xi_2} = - h_2 \sin \alpha \qquad (2.3c)$$

$$\frac{\partial r}{\partial \xi_2} = h_2 \cos \alpha \qquad (2.3d)$$

An equation for the scale factors can be obtained by first differentiating Equation (2.3a) with respect to ξ_2 and then differentiating Equation (2.3c) with respect to ξ_1. Performing these operations, the resulting left-hand sides are the same and therefore the right-hand sides are equal. The result is:

10

$$\frac{\partial h_1}{\partial \xi_2} \cos \alpha - h_1 \sin \alpha \frac{\partial \alpha}{\partial \xi_2} = - \frac{\partial h_2}{\partial \xi_1} \sin \alpha - h_2 \sin \alpha \frac{\partial \alpha}{\partial \xi_1} \qquad (2.4a)$$

A second equation for the scale factors can be obtained by applying the same differentiations to Equations (2.3b) and (2.3d), respectively, and the resulting equation is

$$\frac{\partial h_1}{\partial \xi_2} \sin \alpha + h_1 \cos \alpha \frac{\partial \alpha}{\partial \xi_2} = - \frac{\partial h_2}{\partial \xi_1} \cos \alpha - h_2 \sin \alpha \frac{\partial \alpha}{\partial \xi_1} \qquad (2.4b)$$

A simpler equation can be obtained for the scale factors by multiplying Equation (2.4a) by - sin α and multiplying Equation (2.4b) by cos α and adding the two resulting equations, which yields:

$$h_1 \frac{\partial \alpha}{\partial \xi_2} = \frac{\partial h_2}{\partial \xi_1} \qquad (2.5a)$$

Similarly, multiplying Equation (2.4a) by cos α and multiplying Equation (2.4b) by sin α and adding the two resulting equations gives the result

$$\frac{\partial h_1}{\partial \xi_2} = - h_2 \frac{\partial \alpha}{\partial \xi_1} \qquad (2.5b)$$

Equation (2.5b) can be put into a more familiar form by dividing Equation (2.5b) through by $h_1 h_2$. Using Equation (2.2) the result is

$$\frac{1}{h_1} \frac{\partial h_1}{\partial n} = - \frac{\partial \alpha}{\partial s} \equiv \frac{1}{R} \qquad (2.6)$$

where R is the radius of curvature of the streamlines. Equations (2.3) and (2.5) determine the positions and the scale factors in the natural coordinate system.

REYNOLDS EQUATIONS IN THE NATURAL COORDINATE SYSTEM AND TURBULENT EDDY VISCOSITY

The time averaged, steady, axisymmetric, incompressible continuity and momentum equations will now be given in the natural coordinate system for the mean flow fields. In this coordinate system, the variable s denotes the distance measured along the time-averaged streamline and n denotes the variable measured normal to this streamline direction. Using the results of the Natural Coordinate System Section the continuity and momentum equations are expressed as

$$\frac{1}{h_2 r} \; \frac{\partial}{\partial s} \; (r U h_2) = 0 \tag{2.7}$$

$$
\begin{aligned}
U \frac{\partial U}{\partial s} = & -\frac{1}{\rho} \frac{\partial p}{\partial s} - \frac{1}{r} \frac{\partial}{\partial n} (r \; \overline{u'v'}) - \frac{1}{r} \frac{\partial}{\partial s} (r \overline{u'^2}) \\[1mm]
& + (\overline{u'^2} - \overline{v'^2}) \frac{1}{r} \frac{\partial r}{\partial s} + \frac{1}{U} \frac{\partial U}{\partial s} + \frac{\overline{w'^2}}{r} \frac{\partial r}{\partial s} \\[1mm]
& + 2 \; \overline{u'v'} \; \frac{\partial \alpha}{\partial s} + 2 \; \nu \frac{\partial^2 U}{\partial s^2} + \nu \frac{\partial}{\partial n} \left(\frac{\partial U}{\partial n} + U \frac{\partial \alpha}{\partial s} \right) \\[1mm]
& + \nu \, \frac{\partial U}{\partial s} \left(\frac{1}{h_2} \frac{\partial h_2}{\partial n} + \frac{\partial r}{\partial s} \right) \\[1mm]
& - \nu \left(\frac{\partial U}{\partial n} + U \frac{\partial \alpha}{\partial s} \right) \left[2 \frac{\partial \alpha}{\partial s} - \frac{1}{r} \frac{\partial r}{\partial n} \right] \\[1mm]
& - 2\nu \frac{U}{h_2^2} \left(\frac{\partial h_2}{\partial n} \right)^2 - 2\nu \frac{U}{r^2} \left(\frac{\partial r}{\partial s} \right)^2
\end{aligned}
\tag{2.8}
$$

$$U^2 \frac{\partial \alpha}{\partial s} = -\frac{1}{\rho} \frac{\partial p}{\partial n} - \frac{1}{r} \frac{\partial}{\partial n} (\overline{rv'^2}) - \frac{1}{r} \frac{\partial}{\partial s} (\overline{ru'v'})$$

$$- \frac{\partial \alpha}{\partial s} \overline{(u'^2 - v'^2)} + \overline{w'^2} \frac{\partial r}{\partial n} + 2 \overline{u'v'} \left(\frac{1}{r} \frac{\partial r}{\partial s} + \frac{1}{U} \frac{\partial U}{\partial s} \right)$$

$$+ \nu \frac{\partial^2 U}{\partial s \partial n} - \nu \frac{\partial}{\partial s} \left(\frac{U}{h_1} \frac{\partial h_1}{\partial s} \right) + 2 \nu \frac{\partial}{\partial n} \left(\frac{U}{h_2} \frac{\partial h_2}{\partial s} \right)$$

$$+ \left(\frac{2\nu}{h_2} \frac{\partial h_2}{\partial s} + \frac{\nu}{r} \frac{\partial r}{\partial s} \right) \left[\frac{\partial U}{\partial n} + U \frac{\partial \alpha}{\partial s} \right] - \frac{2\nu}{h_1} \frac{\partial h_1}{\partial s} \frac{\partial U}{\partial s}$$

$$- \nu \frac{U}{r^2} \frac{\partial r}{\partial s} \frac{\partial r}{\partial n} + \frac{2\nu}{h_1 h_2} U \frac{\partial h_1}{\partial n} \frac{\partial h_2}{\partial s} + \frac{2\nu}{h_1 r} U \frac{\partial r}{\partial n} \frac{\partial h_2}{\partial s} \qquad (2.9)$$

In the above equations, U is the total time averaged velocity and its direction coincides with the direction of the mean streamlines. The variable α is the angle between the mean streamline and the direction of the x-axis, p is the mean pressure, ρ is the constant density of the fluid, ν is the molecular viscosity, and r is the radial position from the x-axis. The velocities u', v', and w' are the turbulent velocities measured in the s-direction, in the n-direction, and in the θ-direction, respectively. A bar above the product of two turbulent velocities indicates that the time average of the product is taken. These time averaged product terms are the Reynolds stress terms, which are the stress on the mean flow due to the turbulent motion. The continuity Equation (2.7) states that the mass contained between two streamlines, which is $r\, U\, h_2\, \Delta \xi_2 = r\, U\, \Delta n$, is conserved. Equation (2.8) states that the advection of U in the streamline direction is given by the sum of the pressure gradient, the turbulent Reynolds stresses, and the molecular viscous forces in the streamline direction. Equation (2.9) gives the balance of the centrifugal force with the normal pressure gradient and the normal turbulent and molecular viscous forces.

To solve Equations (2.8) and (2.9), additional equations are needed to describe the Reynolds stress terms. These terms are related to the mean shear through an eddy viscosity ν_T. In cartesian coordinates, the Reynolds stresses, $-\overline{u_i' u_j'}$, are assumed to be given by

$$-\overline{u_i' u_j'} + \frac{2}{3} \delta_{ij} k = \nu_T \left(\frac{\partial u_i}{\partial x_j} + \frac{\partial u_j}{\partial x_i} \right) \tag{2.10}$$

where the subscript on the variables indicates the direction of the flow: (1) is along the x-axis, (2) is along the y-axis, and (3) is along the z-axis. Transformed to the (s,n) coordinate system the Reynolds stresses in Equation (2.10) are given by

$$-\overline{u'v'} = \nu_T \frac{\partial U}{\partial n} + U \frac{\partial \alpha}{\alpha s}$$

$$2/3 k - \overline{u'^2} = 2\nu_T \frac{\partial U}{\partial s}$$

$$2/3 k - \overline{v'^2} = \frac{-2\nu_T}{r} \frac{\partial}{\partial s} (r, U) \tag{2.11}$$

$$2/3 k - \overline{w'^2} = 2\nu_T \frac{U}{r} \frac{\partial r}{\partial s}$$

$$-\overline{u'w'} = -\overline{v'w'} = 0$$

The last two terms are zero in Equation (2.11) since they are related to the variation of the mean flow in the θ-direction.

Combining Equations (2.8) and (2.9) with Equation (2.11), the momentum equations are written

$$U \frac{\partial U}{\partial s} = -\frac{1}{\rho} \frac{\partial p}{\partial s} + \frac{1}{r} \frac{\partial}{\partial n} \left[\nu_e r \frac{\partial U}{\partial n} \right] + \frac{1}{r} \frac{\partial}{\partial n} \left[\nu_e U \frac{\partial \alpha}{\partial s} \right]$$

$$+ \frac{1}{r} \frac{\partial}{\partial s} \left[2\nu_e r \frac{\partial U}{\partial s} \right] - \left(\frac{1}{r} \frac{\partial r}{\partial s} + \frac{1}{U} \frac{\partial U}{\partial s} \right) \left[2\nu_e \frac{\partial U}{\partial s} - \frac{2\nu_e}{r} \frac{\partial [r, U]}{\partial s} \right]$$

$$- 2\nu_e U \left[\frac{1}{r} \frac{\partial r}{\partial s} \right]^2 - 2\nu_e \frac{\partial \alpha}{\partial s} \left[\frac{\partial U}{\partial n} + U \frac{\partial \alpha}{\partial s} \right] \qquad (2.12)$$

$$U^2 \frac{\partial \alpha}{\partial s} = -\frac{1}{\rho} \frac{\partial p}{\partial n} + \frac{1}{r} \frac{\partial}{\partial n} \left[2\nu_e \frac{\partial}{\partial s} (rU) \right]$$

$$- \frac{1}{r} \frac{\partial}{\partial s} \left[r \nu_e \frac{\partial U}{\partial n} + Ur \nu_e \frac{\partial \alpha}{\partial s} \right] - 2\nu_e \frac{U}{r^2} \frac{\partial r}{\partial n} \frac{\partial r}{\partial s}$$

$$+ 2\nu_e \frac{\partial \alpha}{\partial s} \left[\frac{\partial U}{\partial s} + \frac{1}{r} \frac{\partial}{\partial s} (rU) \right]$$

$$- 2\nu_e \left[\frac{\partial U}{\partial n} + U \frac{\partial \alpha}{\partial s} \right] \left(\frac{1}{r} \frac{\partial r}{\partial s} + \frac{1}{U} \frac{\partial U}{\partial s} \right) \qquad (2.13)$$

The variable ν_e is the total effective viscosity, given by the sum of the molecular viscosity and the turbulent viscosity:

$$\nu_e = \nu + \nu_T \qquad (2.14)$$

Once ν_T is specified, a complete system of equations is obtained for the variables x, r, h_1, h_2, U, α, and p. The turbulent viscosity will be given by the k-ε turbulent model.

15

THE k-ε TURBULENT MODEL

The k-ε turbulent model assumes that the interaction of the turbulence on the mean flow can be described by an eddy viscosity that is a function of the turbulent kinetic energy k and the rate of turbulent kinetic energy dissipation ε. In cartesian coordinates, k and ε are defined as

$$k = \frac{\overline{u_1'^2} + \overline{u_2'^2} + \overline{u_3'^2}}{2} \tag{2.15}$$

and

$$\varepsilon = 2\nu \overline{\left[\frac{\partial u_i'}{\partial x_j} + \frac{\partial u_j'}{\partial x_i} \right] \left(\frac{\partial u_i'}{\partial x_j} + \frac{\partial u_j'}{\partial x_i} \right)} \tag{2.16}$$

where the summation over the indices i and j from 1 to 3 is implied in Equation (2.16). Since ν_T is a function of k and ε, it can be shown by dimensional analysis that it is a function of the single variable k^2/ε. It is assumed further that the function is linear and ν_T is given by

$$\nu_T = \frac{C_p k^2}{\varepsilon} \tag{2.17}$$

Equations must be supplied to describe the behavior of k and ε. The k equation is derived by considering the exact turbulent kinetic energy budget which is given by Tennekes and Lumley (1972)[16] in cartesian coordinates as

$$u_j \frac{\partial}{\partial x_j} k = - \frac{\partial}{\partial x_j} \left[\frac{1}{\rho} \overline{u_j' p'} + 1/2 \overline{u_i' u_i' u_j'} - \nu \overline{u_i' \left(\frac{\partial u_i'}{\partial x_j} + \frac{\partial u_j'}{\partial x_i} \right)} \right]$$

$$- \overline{u_i' u_j'} \left[\frac{\partial u_i}{\partial x_j} + \frac{\partial u_j}{\partial x_i} \right] - \varepsilon \tag{2.18}$$

16

where summation is implied over the indices. The left-hand side of (2.18) is the advection of k by the mean flow. The first three terms on the right-hand side are transport terms: the transport of k by the turbulent pressure gradient, by the turbulent velocity fluctuations, and by the turbulent deformation field. The fourth term on the right-hand side is the production of k and the fifth term is the rate of dissipation of k. The transport terms are parameterized by assuming that the three bracket terms in Equation (2.18) are proportional to the gradient of k:

$$- \left[\frac{1}{\rho} \overline{u_j' p'} + 1/2 \overline{u_i' u_i' u_j'} - \nu \overline{u_i' \left(\frac{\partial u_i'}{\partial x_j} + \frac{\partial u_j'}{\partial x_i} \right)} \right] = \frac{\nu_T}{\sigma_k} \frac{\partial k}{\partial x_j} \qquad (2.19)$$

where σ_k is a constant. The Reynolds stress terms $\overline{-u_i' u_j'}$ in Equation (2.18) are given by Equation (2.10). Combining these relations, the k equation is given by

$$u_j \frac{\partial k}{\partial x_j} = \frac{\partial}{\partial x_j} \left[\frac{\nu_T}{\sigma_k} \frac{\partial k}{\partial x_j} \right] + \nu_T \left[\frac{\partial u_i}{\partial x_j} + \frac{\partial u_j}{\partial x_i} \right] \frac{\partial u_i}{\partial x_j} - \varepsilon \qquad (2.20)$$

The ε equation is derived by forcing it to take the same form as the k equation (see Launder and Spalding, 1974)[11]. It is given by

$$u_j \frac{\partial \varepsilon}{\partial x_j} = \frac{\partial}{\partial x_j} \left[\frac{\nu_T}{\sigma_\varepsilon} \frac{\partial \varepsilon}{\partial x_j} \right] + C_1 \nu_T \frac{\varepsilon}{k} \left[\frac{\partial u_i}{\partial x_j} + \frac{\partial u_j}{\partial x_i} \right] \frac{\partial u_i}{\partial x_j} - C_2 \varepsilon^2/k \qquad (2.21)$$

where C_1, C_2, and σ_ε are additional constants that must be specified. The constants C_μ, C_1, C_2, σ_k, and σ_ε used to give the best results for boundary layer and wake flows are given by Hanjalic and Launder (1980)[14]:

$$\left. \begin{aligned} C_\mu &= 0.09 \\ C_1 &= 1.44 \\ C_2 &= 1.90 \\ \sigma_k &= 1.0 \\ \sigma_\varepsilon &= 1.30 \end{aligned} \right\} \qquad (2.22)$$

17

In the (s,n) coordinate system, the k and ε equations are expressed as

$$U \frac{\partial k}{\partial s} = \frac{1}{h_2 r} \frac{\partial}{\partial s} \left[\frac{\nu_T h_2 r}{\sigma_k} \frac{\partial k}{\partial s} \right] + \frac{1}{h_1 r} \frac{\partial}{\partial n} \left[\frac{\nu_T}{\sigma_k} h_1 r \frac{\partial k}{\partial n} \right] + P - \varepsilon \quad (2.23)$$

and

$$U \frac{\partial \varepsilon}{\kappa s} = \frac{1}{h_2 r} \frac{\partial}{\partial s} \left[\frac{\nu_T h_2 r}{\sigma_\varepsilon} \frac{\partial \varepsilon}{\partial s} \right] + \frac{1}{hr} \frac{\partial}{\partial n} \left[\frac{\nu_T}{\sigma_e} h_1 r \frac{\partial \varepsilon}{\partial n} \right]$$

$$+ C_1 \frac{\varepsilon}{k} P - C_2 \frac{\varepsilon^2}{k} \quad (2.24)$$

where the production P of turbulent kinetic energy is given by

$$P = \nu_T \left[\frac{\partial U}{\partial n} + U \frac{\partial \alpha}{\partial s} \right]^2 + 2 \nu_T \left[\frac{\partial U}{\partial s} \right]^2$$

$$+ 2 \frac{\nu_T}{r^2} \left[\frac{\partial}{\partial s} (rU) \right]^2 + 2 \nu_T \left[\frac{U}{r} \frac{\partial r}{\partial s} \right]^2 \quad (2.25)$$

In the viscous sublayer region, Equations (2.23) and (2.24) do not adequately describe the variations of k and ε. One approach to remedy this problem is to add additional terms to Equations (2.23) and (2.24) to describe the behavior of k and ε near the body (Jones and Launder, 1972[12], 1973[13]). This approach has not been used often since the extra terms greatly increase the computational time needed to calculate the flow field. Another approach has been used to solve the flow equations starting at a point above the viscous sublayer region, using the law of the wall to obtain the lower boundary conditions for U, k, and ε (Launder and Spalding, 1974).[11] The distance above the wall is characterized by

18

$$y_+ = \frac{(y-y_o)\, u_*}{\nu} \tag{2.26a}$$

and

$$u_* = \sqrt{\tau_w/\rho} \tag{2.26b}$$

where y is a point above the body, y_o is the coordinate of the surface, and τ_w is the shear stress at y_o. At a sufficiently large value of y_+, given by y_+^*, it is assumed that the production of turbulent kinetic energy P is equal to the rate of dissipation of turbulent kinetic energy ε. With $P = \varepsilon$, the velocity field U, the turbulent kinetic energy k, and the rate of dissipation ε are given at $y_+ = y_+^*$ as

$$U = u_* \left[\frac{1}{\kappa} \ell n y_+^* + 5.24 \right] \tag{2.28a}$$

$$k = u_*^2 / \sqrt{C_\mu} \tag{2.28b}$$

$$\varepsilon = \frac{u_*^3}{\kappa(y-y_o)} \tag{2.28c}$$

where κ is the von Karman constant (κ=0.40). The procedure is to determine κ at y_+^* by solving Equation (2.23) in the region between $y_+ = 0$ and $y_+ = y_+^*$, assuming that the diffusion of k is zero. The value of ε in Equation (2.23) is set equal to the average energy dissipation rate in the region $y_+ = 0$ to $y_+ = y_+^*$ by integrating Equation (2.28c). Once k is known at y_+^*, u_*, U, and ε can be determined at y_+^* from Equations (2.28a, b, c). These values of U, k, and ε serve as the lower boundary conditions for the flow equations.

An alternate procedure to the two methods discussed above is to specify the viscosity in the region between $y_+ = 0$ to $y_+ = y_+^*$ by a mixing length, eddy viscosity. This is the approach used in the present study. A mixing length, eddy

19

viscosity, denoted by $\nu_{T_{m\ell}}$ (whose form will be given later), is assumed in the region between the wall and y_+^*. Using this eddy viscosity, τ_w can be calculated. The value of k at y_+^* is determined using Equation (2.28b), while ε at y_+^* is given by Equation (2.17) as

$$\varepsilon = \frac{C_\mu k^2}{\nu_{T_{m\ell}}} \quad \text{at } y_+ = y_+^* \qquad (2.29)$$

With these boundary conditions, the k and ε equations are solved in the region $y_+ > y_+^*$. Using Equation (2.29) as the value of ε at y_+^* ensures that the eddy viscosity calculated from the mixing length argument matches the eddy viscosity calculated from the k-ε equations. This procedure provides a continuous variation of the eddy viscosity.

THE PARTIALLY PARABOLIC ASSUMPTIONS AND THE HANJALIC AND LAUNDER CORRECTION TO THE k-ε MODEL

The partially parabolic flow assumptions given in the Partially Parabolic Flow Method Section will be applied to the momentum Equations (2.12) and (2.13), and the k-ε Equations (2.23) and (2.24). The predominant direction in which the diffusion terms are neglected is taken to be along the mean streamline direction. Neglecting all s derivative terms in the diffusion terms of Equations (2.12) and (2.13), the momentum equations are approximated by

$$U \frac{\partial U}{\partial s} = -\frac{1}{\rho} \frac{\partial p}{\partial s} + \frac{1}{r} \frac{\partial}{\partial n} \left[\nu_e \, r \, \frac{\partial U}{\partial n} \right] \qquad (2.30)$$

and

$$U^2 \frac{\partial \alpha}{\partial s} = -\frac{1}{\rho} \frac{\partial p}{\partial n} \qquad (2.31)$$

Patel et al. (1973)[17] have shown that the terms neglected in Equations (2.30) and (2.31) are small for axisymmetric flows. Using integral methods, Dyne (1978)[18] has solved Equations (2.30) and (2.31) and has obtained good agreement with experimental data.

Equation (2.30) states that the momentum calculated along the streamline direction is increased by the pressure force and removed by the normal Reynolds stresses. Equation (2.31) states that the centrifugal force is exactly balanced by the normal variations of the pressure.

The partially parabolic flow assumptions are also applied to the k and ε equations. Neglecting the turbulent diffusive terms in Equations (2.23) and (2.24) in the s-direction, the k and ε equations are approximated by

$$U \frac{\partial k}{\partial s} = \frac{1}{h_1 r} \frac{\partial}{\partial n} \left[\frac{\nu_T}{\sigma_k} h_1 r \frac{\partial k}{\partial n} \right] + P - \varepsilon \qquad (2.32)$$

$$U \frac{\partial \varepsilon}{\partial s} = \frac{1}{h_1 r} \frac{\partial}{\partial n} \left[\frac{\nu_T}{\sigma_\varepsilon} h_1 r \frac{\partial \varepsilon}{\partial n} \right] + C_1 \frac{\varepsilon}{k} P - C_2 \frac{\varepsilon^2}{k} \qquad (2.33)$$

Using the partially parabolic flow assumptions Abdelmeguid et al. (1978)[6] and Muraoka (1978)[7] have neglected all production terms containing derivatives in the predominant direction. In the (s,n) coordinate system, with this approximation

$$P = \nu_T \left[\frac{\partial U}{\partial n} \right]^2 \qquad (2.34)$$

Hanjalic and Launder (1980)[14], however, have recommended the retention of the $(\partial U/\partial s)$ terms to emphasize the role of irrotational deformations in promoting energy transfer. Keeping the $\partial U/\partial s$ terms in P and using Relations (2.11), P is approximated by

$$P = \nu_T \left[\frac{\partial U}{\partial n} \right]^2 - (\overline{u'^2} - \overline{v'^2}) \frac{\partial U}{\partial s} \qquad (2.35)$$

21

The difference in the Reynolds stresses appearing in Equation (2.35) is expressed in terms of the turbulent kinetic energy by (see Hanjalic and Launder, 1980)[14]:

$$(\overline{u'^2} - \overline{v'^2}) = \frac{1}{3} k \tag{2.36}$$

Equations (2.35) and (2.36) are used for the production term in Equation (2.32). For the ε Equation (2.33), Hanjalic and Launder (1980)[14] recommend the form for the production of ε, P_ε, as

$$P_\varepsilon = C_1 \frac{\varepsilon}{k} \nu_T \left(\frac{\partial U}{\partial n}\right)^2 - C_3 (\overline{u'^2} - \overline{v'^2}) \frac{\partial U}{\partial s} \tag{2.37}$$

where

$$C_3 = 4.44 \tag{2.38}$$

Combining Equations (2.32), (2.33), (2.35), (2.36), and (2.37), the final k and ε equations become

$$U \frac{\partial k}{\partial s} = \frac{1}{h_2 r} \frac{\partial}{\partial n} \left(\frac{\nu_T}{\sigma_k} h_1 r \frac{\partial k}{\partial n}\right) + \nu_T \left(\frac{\partial U}{\partial n}\right)^2 - \frac{1}{3} k \frac{\partial U}{\partial s} - \varepsilon \tag{2.39}$$

and

$$U \frac{\partial \varepsilon}{\partial s} = \frac{1}{h_1 r} \frac{\partial}{\partial n} \left(\frac{\nu_T}{\sigma_\varepsilon} h_1 r \frac{\partial \varepsilon}{\partial n}\right) + C_1 \frac{\varepsilon}{k} \nu_T \left(\frac{\partial U}{\partial n}\right)^2 - C_3 \varepsilon \frac{\partial U}{\partial s} - C_2 \frac{\varepsilon^2}{k} \tag{2.40}$$

with the constants given in Equations (2.22) and (2.38).

THE (x,ψ) COORDINATE SYSTEM

The 10 unknown flow variables are x, r, h_1, h_2, U, α, p, k, ε, and ν_T or $\nu_{T_{m\ell}}$ in the viscous sublayer region. The equations describing their behavior are (2.3c), (2.3d), (2.5a), (2.5b), (2.7), (2.30), (2.31), (2.39), (2.40), and (2.17). To integrate these equations, the curvilinear coordinates ξ_1 and ξ_2 must be specified. The coordinate ξ_1 should be chosen so that it is the arc-length of some known streamline. The choice for ξ_2 can be obtained from the continuity Equation (2.7). This equation implies that rUh_2 is a function of only ξ_2, which is written

$$rUh_2 = \frac{\partial \psi}{\partial \xi_2} \tag{2.41}$$

The function ψ is the streamfunction and ξ_2 should be set equal to ψ (Patankar and Spalding, 1967).[19] Setting $\xi_2 = \psi$ and solving Equation (2.41) for h_2 gives the relation

$$h_2 = \frac{1}{rU} \tag{2.42}$$

For numerical calculations, it is advantageous to make one final coordinate transformation of the equations in order to replace ξ_1 by the x-axis. The transformation of the equations to the (x,ψ) coordinate system can be obtained by considering the variation of a function f whose variables are x and ψ. The differential of f is given by

$$df = \left(\frac{\partial f}{\partial x}\right) dx + \left(\frac{\partial f}{\partial \psi}\right) d\psi \tag{2.43}$$

Using Equations (2.2), (2.3), (2.42), and (2.43) the derivatives of f with respect to s and n are given by:

$$\frac{\partial f}{\partial s} = \cos \alpha \left(\frac{\partial f}{\partial x}\right) \tag{2.44}$$

and

$$\frac{\partial f}{\partial n} = U\left(\frac{\partial f}{\partial \psi}\right) - \sin\,\alpha\,\left(\frac{\partial f}{\partial x}\right) \qquad (2.45)$$

the Equations (for the radial position) (2.3b) and (2.3d), using Equations (2.44) and (2.45), become

$$\frac{\partial r}{\partial x} = \tan\,\alpha \qquad (2.46a)$$

and

$$\frac{\partial r}{\partial \psi} = \frac{1}{rU\,\cos\,\alpha} \qquad (2.46b)$$

Since ψ is a coordinate, the conservation of mass is automatically satisfied. In place of a conservation of mass equation, a kinematic relation can be obtained for the (x,ψ) coordinate system by differentiating Equation (2.46a) by ψ and differentiating Equation (2.46b) by x and subtracting the two resulting equations. The result is

$$\frac{\partial}{\partial x}\left(\frac{1}{rU\,\cos\,\alpha}\right) = \frac{\partial}{\partial \psi}\,(\tan\,\alpha) \qquad (2.46c)$$

which expresses that the radial position of the streamline calculated in the x-direction from Equation (2.46a) matches the radial position of the streamline calculated in the normal direction from Equation (2.46b). The equations for U, α, k, and ε are obtained as above by applying Equations (2.44) and (2.45) to Equations (2.30), (2.31), (2.39), and (2.40). These are given by

24

$$U \cos \alpha \, \frac{\partial U}{\partial x} = - \cos \alpha \, \frac{\partial}{\partial x} \left[\frac{p}{\rho} \right] + \frac{\sin \alpha}{r} \, \frac{\partial}{\partial x} \left[r \, \nu_e \, \sin \alpha \, \frac{\partial U}{\partial x} \right]$$

$$- \frac{\sin \alpha}{r} \, \frac{\partial}{\partial x} \left[r^2 \, \nu_e \, U \, \frac{\partial U}{\partial \psi} \right] - U \, \frac{\partial}{\partial \psi} \left[r \, \nu_e \, \sin \alpha \, \frac{\partial U}{\partial x} \right]$$

$$+ U \, \frac{\partial}{\partial \psi} \left[r^2 \, \nu_e \, U \, \frac{\partial U}{\partial \psi} \right] \tag{2.46d}$$

$$U^2 \cos \alpha \, \frac{\partial \alpha}{\partial x} = \sin \alpha \, \frac{\partial}{\partial x} \left[\frac{p}{\rho} \right] - r \, U \, \frac{\partial}{\partial \psi} \left[\frac{p}{\rho} \right] \equiv - \frac{\partial p}{\partial n} \tag{2.46e}$$

$$U \cos \alpha \, \frac{\partial k}{\partial x} = \frac{\sin \alpha}{r} \, \frac{\partial}{\partial x} \left[\frac{r \nu_e}{\sigma_k} \sin \alpha \, \frac{\partial k}{\partial x} \right] - \frac{\sin \alpha}{r} \, \frac{\partial}{\partial x} \left[\frac{r^2 \nu_e}{\sigma_k} U \, \frac{\partial k}{\partial \psi} \right]$$

$$- U \, \frac{\partial}{\partial \psi} \left[\frac{r \nu_e}{\sigma_k} \sin \alpha \, \frac{\partial k}{\partial x} \right] + U \, \frac{\partial}{\partial \psi} \left[\frac{r^2 \nu_e}{\sigma_k} U \, \frac{\partial k}{\partial \psi} \right]$$

$$+ \nu_T \left[r \, U \, \frac{\partial U}{\partial \psi} - \sin \alpha \, \frac{\partial U}{\partial x} \right]^2 - 1/3 \, k \cos \alpha \, \frac{\partial U}{\partial x} - \epsilon \tag{2.46f}$$

25

$$U \cos \alpha \frac{\partial \varepsilon}{\partial x} = \frac{\sin \alpha}{r} \frac{\partial}{\partial x} \left[\frac{r \nu_e}{\sigma_\varepsilon} \sin \alpha \frac{\partial \varepsilon}{\partial x} \right] - \frac{\sin \alpha}{r} \frac{\partial}{\partial x} \left[\frac{r^2 \nu_e}{\sigma_\varepsilon} U \frac{\partial \varepsilon}{\partial \psi} \right]$$

$$- U \frac{\partial}{\partial \psi} \left[\frac{r \nu_e}{\sigma_\varepsilon} \sin \alpha \frac{\partial \varepsilon}{\partial x} \right] + U \frac{\partial}{\partial \psi} \left[\frac{r^2 \nu_e}{\sigma_\varepsilon} U \frac{\partial \varepsilon}{\partial \psi} \right]$$

$$+ C_1 \frac{\varepsilon}{k} \nu_T \left[r U \frac{\partial U}{\partial \psi} - \sin \alpha \frac{\partial U}{\partial x} \right]^2$$

$$- 1/3 \, C_3 \, \varepsilon \cos \alpha \frac{\partial U}{\partial x} - C_2 \frac{\varepsilon^2}{k} \tag{2.46g}$$

In Equations (2.46f) and (2.46g) the variations of h_1 in the n-direction have been neglected since they are given by $(\partial \alpha / \partial s)$ in Equation (2.7), and this term is taken to be small compared to the normal variations of k and ε. Outside the viscous sub-layer $(y_+ > y_+^*)$ ν_T is given by

$$\nu_T = \gamma \, C_\mu \frac{k^2}{\varepsilon} \tag{2.46h}$$

where γ is an intermittency factor used to reduce the turbulent eddy viscosity outside the boundary layer region. The factor is given by

$$\gamma = \begin{cases} 1 & \text{for } \frac{r-r_o}{\delta} < 0.1 \\ \dfrac{1}{1 + 5.5 \left(\dfrac{r-r_o}{\delta} \right)^6} & \text{for } \frac{r-r_o}{\delta} \geq 0.1 \end{cases} \tag{2.46i}$$

where r_o is the radial position of the body $(r_o = 0$ in the wake) and δ is the boundary layer thickness. In the viscous sublayer region $(y_+ \leq y_+^*)$ the mixing length eddy viscosity is the one used by Wang and Huang (1979)[20] in the viscous sublayer region as follows:

26

$$\nu_{T_{m\ell}} = \ell^2 \left(\frac{r}{r_o}\right) \left[rU \frac{\partial U}{\partial \psi} - \sin \alpha \frac{\partial U}{\partial x}\right] \qquad (2.46\text{j})$$

where

$$\ell = \kappa r_o \ln \left(\frac{r}{r_o}\right) \left\{1 - \exp \left[-r_o \ln \left(\frac{u_* r}{26 \, \nu r_o}\right)\right]\right\} \qquad (2.46\text{k})$$

Once the boundary conditions are specified, the system of equations listed under Equation (2.46) are solved for r, u, α, p, k, ε, and ν_T.

THE BOUNDARY CONDITIONS

The solution to the equations listed under (2.46) is calculated in a domain in (x, ψ) space. This domain begins at x_b, which is an x-station on the body where the boundary layer is thin, and ends at an x-station in the wake, x_e, such that $x_e/L = 4.0$, where L is the length of the body. At x_b all flow variables must be given so that the boundary conditions at $x = x_b$ are

$$\left.\begin{aligned}
r &= r_b \\
U &= U_b \\
\alpha &= \alpha_b \\
p &= p_b \\
k &= k_b \\
\varepsilon &= \varepsilon_b \\
\nu_T &= \nu_{T_b}
\end{aligned}\right\} \text{ at } x = x_b \qquad (2.47\text{a})$$

27

At x_e the pressure is the only variable that is specified so that

$$p = p_e \text{ at } x = x_e \qquad (2.47b)$$

The lower ψ boundary is the streamline that lies along the body's surface and along $r = 0$ in the wake. This streamline is set as $\psi = 0$. The boundary conditions on the body ($\psi=0$) are

$$\left.\begin{array}{l} r = r_o \\[4pt] U = 0 \\[4pt] \alpha = \alpha_o \\[10pt] \dfrac{\partial p}{\partial n} \equiv \left[r\, U\, \dfrac{\partial p}{\partial \psi} - \sin \alpha\, \dfrac{\partial p}{\partial x} \right] = 0 \end{array}\right\} \begin{array}{l} \psi = 0 \text{ and} \\[4pt] x/L \leq 1.0 \end{array} \qquad (2.47c)$$

where r_o is the radial position of the body's surface and α_o is the angle of the surface with respect to the x-axis. The pressure boundary condition in Equation (2.47c) is obtained by setting $U = 0$ in Equation (2.46e). The boundary conditions for k and ϵ are not given at $\psi = 0$. These boundary conditions are given outside the viscous sublayer region by Equations (2.27) and (2.29) on a streamline such that $y_+ = y_+^*$. Between $\psi = 0$ and $y_+ = y_+^*$ the eddy viscosity is given by (2.46j). In the wake the boundary conditions on $\psi = 0$ are

$$\left.\begin{array}{l} r = 0 \\[6pt] \dfrac{\partial U}{\partial \psi} = 0 \\[6pt] \alpha = 0 \\[6pt] \dfrac{\partial p}{\partial \psi} = 0 \\[6pt] \dfrac{\partial k}{\partial \psi} = 0 \\[6pt] \dfrac{\partial \epsilon}{\partial \psi} = 0 \end{array}\right\} \begin{array}{l} \psi = 0 \text{ and} \\[4pt] x/L > 1 \end{array} \qquad (2.47d)$$

which express the axisymmetric symmetry of the flow. For the outer boundary conditions, a streamline is selected such that it lies entirely outside the turbulent

28

boundary layer and turbulent wake region of the flow. This streamline is denoted by ψ_T and the boundary conditions on this term are

$$\left.\begin{array}{l} U = U_o\sqrt{1 - \left(\dfrac{p_T - p_o}{\rho U_o^2/2}\right)} \\[2em] p = p_T \\[1em] k = \varepsilon = 0 \end{array}\right\} \psi = \psi_T \qquad (2.47e)$$

where U_o is the far upstream constant velocity and p_o is the far upstream constant pressure.

The boundary conditions at $x = x_b$ will be given from the numerical solution of the thin boundary layer equation obtained from the Wang/Huang (1979)[20] boundary layer program. The pressure boundary conditions at x_b, x_e, and ψ_T will be specified by a potential flow calculation (Hess and Smith, 1966)[21] about the equivalent displacement body. The boundary conditions specified by Equation (2.47) are exactly those needed for partially parabolic flows, namely pressure given over the entire flow domain and U, k, and ε given on the beginning station and on the outer and bottom boundaries.

3. NUMERICAL PROCEDURE

THE (x, ψ) GRID

Initially, the solution to the boundary layer equations for the axisymmetric body is obtained from the Wang/Huang (1979)[20] boundary layer program. This program uses constant pressure profiles, given from a displacement body potential flow calculation, and a mixing length eddy viscosity. This viscosity is given by

$$\nu_T = \begin{cases} \nu_{T_i} = \nu_{T_{m\ell}}, & \text{for } \nu_{T_i} \le \nu_{T_o} \\[1.5em] \nu_{T_o} = f(r_o, \delta)\, 0.0168\, U_e\, \delta^*, & \text{for } \nu_{T_i} \ge \nu_{T_o} \end{cases} \qquad (3.1)$$

29

where ν_{T_i} is the inner viscosity and ν_{T_o} is the outer viscosity. The inner viscosity is given by Equation (2.46j). In the outer viscosity formula, U_e is the potential flow velocity on the displacement body, δ^* is the calculated displacement body thickness, δ is the boundary layer thickness, and $f(r_o, \delta)$ is a multiplicative factor used by the program to reduce the outer viscosity in the thick boundary layer region, given by

$$f(r_o, \delta) = \begin{cases} 1 & \text{for } \delta < 0.2r_o \\[3mm] \dfrac{(r_o + \delta)^2 - r_o^2}{3.33\,\delta^2} & \text{for } \delta \geq 0.2r_o \end{cases} \qquad (3.2)$$

The flow field obtained from the Wang/Huang (1979)[20] program is examined and a x-station, x_b, is selected where the boundary layer is thin ($f(r_o, \delta) = 1$). The velocity profiles obtained from the calculation serve as the boundary conditions in Equation (2.47a). The dissipation at x_b is obtained by assuming $P = \varepsilon$ and k is obtained by assuming ν_T is given by Equation (3.1) at x_b and solving for k from Equation (2.46h).

The output at x_b is given at J-1 radial stations. The corresponding streamlines for this flow data are calculated by integrating the definition of ψ in (x,r) coordinates:

$$\left. \begin{aligned} \frac{\partial \psi}{\partial r} &= rU \cos \alpha \\[4mm] \frac{\partial \psi}{\partial x} &= -rU \sin \alpha \end{aligned} \right\} \qquad (3.3)$$

setting the streamline on the surface of the body as $\psi = 0$. These streamlines are denoted as $(\psi_1, \psi_2, \ldots, \psi_J)$, where $\psi_1 = 0$. In addition to the output at x_b, the velocity field at $x/L = 1.0$ is examined. Using Equation (3.3), the corresponding streamlines are calculated at $x/L = 1.0$. An outer streamline number, ψ_T, is obtained by multiplying 1.5 times the maximum of the streamline numbers obtained

at x_b and $x/L = 1.0$. The flow calculated on $\psi = \psi_T$, therefore, should be entirely above the turbulent region. The data at x_b is extended from ψ_j to ψ_T by adding 6 more streamline numbers, assuming that r, U, α, and p are given by the displacement body, potential flow solution. The streamlines (ψ_1, ψ_2, ..., ψ_K), where K corresponds to the outer streamline number, serve as the ψ grid stations. It is emphasized that these are streamline numbers and the positions of these numbers must be calculated from Equation (2.46a) or (2.46b).

The x-stations are selected beginning at x_b and ending at x_e, such that there are many x-stations in the stern and near-wake region. In this way, a full resolution of the thick boundary layer and wake region is obtained.

Most of the variables are not evaluated at the grid points, but they were placed at staggered positions to give a better representation for the numerical calculations. If a typical grid point is denoted as (x^i, ψ_j), then the flow variables are given as $r_j^{i+1/2}$, $U_{j+1/2}^{i+1/2}$, α_j^i, $p_{j+1/2}^{i+1/2}$, $k_{j+1/2}^{i+1/2}$, $\varepsilon_{j+1/2}^{i+1/2}$, and $\nu_{Tj+1/2}^{i+1/2}$. The i+1/2 superscript indicates that the variable is evaluated at $(x^i + x^{i+1/2})/2$ and the j+1/2 subscript indicates that the position is at $(\psi_j + \psi_{j+1})/2$. In addition, all the variables are given on $\psi_1 = 0$ and ψ_K. As an example, the U field at $(x^i + x^{i+1})/2$ is given by $(U_1^{i+1/2}, U_{3/2}^{i+1/2}, U_{5/2}^{i+1/2}, \ldots, U_{K-1/2}^{i+1/2}, U_K^{i+1/2}$. The grid geometry is illustrated in Figure 2.

THE FINITE VOLUME NUMERICAL TECHNIQUE

The solution to the equations under (2.46) is obtained by marching the equations downstream in x. Given the flow conditions at $x_1 = x_b$; r, U, k, ε, and ν_T are solved for at $x_{5/2}$ and for α is solved for at x_2. With these solutions, r, U, k, ε, and ν_T are obtained at $x_{7/2}$ and α at x_3 and so on to the final station, x_e. The solution method for the downstream values of U, α, k, and ε is the finite volume numerical technique (Patankar and Spalding, 1979).[9] The values of U at $x^{i+1/2}$ are calculated dividing the flow domain from $x^{i-1/2}$ to $x^{i+1/2}$ into K-1 areas, ΔA_j, and integrating Equation (2.46d) in each ΔA_j. The control areas ΔA_j are defined as (see Figure 2)

$$\Delta A_j = \begin{cases} x^{i-1/2} \leq x \leq x^{i+1/2} \\ \\ \psi_j \leq \psi \leq \psi_{j+1} \end{cases} \tag{3.4}$$

31

The details of the integration procedure are given in Appendix A. The result, at each x-station, $x^{i+1/2}$, is a tridiagonal system of equations for $U_{j+1/2}^{i+1/2}$ (see Equation (A.6)) which is solved by the double sweep method presented in Appendix B. The solutions for k and ε are arrived at by the same method except that the lower control areas begin at the first streamline where $y_+ > y_+^*$. For smaller values of y_+, $\nu_T = \nu_{T_{m\ell}}$ given by Equation (2.46j). The value of u_* is calculated from the definition of τ_w, as follows:

$$u_*^2 \equiv \frac{\tau_w}{\rho} = \left[\nu_T \left(rU \frac{\partial U}{\partial n} - \sin \alpha \; \frac{\partial U}{\partial x} \right) \right]_{\psi = 0} \tag{3.5}$$

To solve for the downstream values of α at x^i, the flow domain from x^{i-1} to x^i is divided into K areas $\Delta A_j^{'i}$ (see Figure 2);

$$\Delta A_1^{'i} = \begin{cases} x^{i-1} \leq x \leq x^i \\[2mm] 0 \leq \psi \leq (\psi_1 + \psi_2)/2 \end{cases}$$

$$\Delta A_j^{'i} = \begin{cases} x^{i-1} \leq x \leq x^i \\[2mm] \dfrac{\psi_{j-1} + \psi_j}{2} \leq \dfrac{\psi_j + \psi_{j+1}}{2} \end{cases} \qquad \text{for } j = 2, \; \dots \; K-1 \tag{3.6}$$

$$\Delta A_K^{'i} = \begin{cases} x^{i-1} \leq x \leq x^i \\[2mm] \dfrac{(\psi_{K-1} + \psi_K)}{2} \leq \psi \leq \psi_K \end{cases}$$

and Equation (2.46e) is integrated in each $\Delta A_j^{'i}$. The downstream values of r are obtained by integrating Equation (2.46b) along $x = x^{i+1/2}$. The details of the k, ε, α, and r equation integrations are also given in Appendix A.

32

PRESSURE FIELD CALCULATIONS

The downstream solutions $U_{j+1/2}^{i+1/2}$ and $\alpha_j^{\,i}$ depend on the pressure field. Initially, the pressure profiles are given from the Wang/Huang (1979)[20] boundary layer program. However, the downstream values of U and α do not satisfy the kinematic streamline relation in Equation (2.46c). Therefore, corrections are added to the U, α, and p values in such a manner that Equation (2.46c) is satisfied. These corrections are added to the downstream values of U and α and the upstream values of p as follows:

$$\left.
\begin{aligned}
U_{j+1/2}^{*\,i+1/2} &= U_{j+1/2}^{i+1/2} + U_{j+1/2}^{'\,i+1/2} \\[2ex]
\alpha_j^{*\,i} &= \alpha_j^{\,i} + \alpha_j^{'\,i} \\[2ex]
P_{j+1/2}^{*\,i-1/2} &= P_{j+1/2}^{i-1/2} + P_{j+1/2}^{'\,i-1/2}
\end{aligned}
\right\} \tag{3.7}$$

where the primed fields are the corrections and the starred fields are the new corrected values.

It is the upstream values of pressure that are corrected which is consistent with the partially parabolic flow assumption that p communicates downstream information to the upstream. Using the finite volume numerical technique to solve Equation (2.46c), with the control areas given by Equation (3.4) and with the corrected starred fields of Equation (3.7), the integration of Equation (2.46) in the ΔA_j becomes

$$\left.
\begin{aligned}
(x^{i+1/2} &- x^{i-1/2}) \; (\tan [\alpha_j^{*\,i}] - \tan [\alpha_{j-1}^{*\,i}]) \\[2ex]
&= (\psi_j - \psi_{j-1})/ \; [(r_j^{i+1/2} + r_{j-1}^{i+1/2})/2] \; U_{j-1/2}^{*\,i+1/2} \; \cos \, [(\alpha_j^{*\,i} + \alpha_{j-1}^{*\,i})/2] \\[2ex]
&\quad - (\psi_j - \psi_{j-1})/ \; [r_j^{i-1/2} + r_{j-1}^{i-1/2})/2] \; U_{j-1/2}^{i-1/2} \; \cos \, [(\alpha_j^{i-1} + \alpha_{j-1}^{i-1})/2]
\end{aligned}
\right\} \tag{3.8}$$

The starred variables in Equation (3.8) are expanded in terms of Equation (3.7) and to first-order quantities in Equation (3.8) are given by:

$$\tan\,[\alpha_j^{*\,i}] = \tan\,[\alpha_j\,i] + \alpha_j'^{\,i}/\cos^2[\alpha_j\,i]$$

$$\cos\,[(\alpha_j^{*\,i}+\alpha_{j-1}^{*\,i})/2] = \cos\,[(\alpha_j\,^i+\alpha_{j-1}\,^i)/2] \qquad (3.9)$$

$$[i/U_{j-1/2}^{*\,i+1/2}] = [i/U_{j-1/2}^{\,i+1/2}] - [U_{j-1/2}'^{\,i+1/2}/(U_{j-1/2}^{\,i+1/2})^2]$$

Finally, $U_{j-1/2}'^{\,i+1/2}$ and $\alpha_j'^{\,i}$ are related to $p_{j-1/2}'^{\,i-1/2}$ and $p_{j-1/2}'^{\,i-1/2}$ by expanding the solution equations for $U_{j-1/2}^{\,i+1/2}$ (A.6) and for $\alpha_j\,^i$ (A.10) in power serves for $U_{j-1/2}'^{\,i+1/2}$, $\alpha_j'^{\,i}$, and $p_{j-1/2}'^{\,i-1/2}$:

$$U_{j-1/2}'^{\,i+1/2} = -F_{j-1/2}^U\,p_{j-1/2}'^{\,i-1/2}/(A_{j-1/2}^U+B_{j-1/2}^U+C_{j-1/2}^U)$$

$$\qquad (3.10)$$

$$\alpha_j'^{\,i} = B_j^\alpha\,p_{j+1/2}'^{\,i-1/2} + C_j^\alpha\,p_{j-1/2}'^{\,i-1/2}$$

Inserting Equations (3.9) and (3.10) into (3.8), a tridiagonal system of equations are obtained for the correction to the pressure field at $x^{i-1/2}$:

$$A_{j-1/2}^P\,p_{j-3/2}'^{\,i-1/2} + B_{j-1/2}^P\,p_{j-1/2}'^{\,i-1/2} + C_{j-1/2}^P\,p_{j+1/2}'^{\,i-1/2} = D_{j-1/2}^P \qquad (3.11)$$

The boundary conditions for Equation (3.11) are that

$$p'k = 0$$

$$\left.\frac{\partial p}{\partial n}\right|_{\psi=0} \equiv \left[rU\,\frac{\partial p'}{\partial \psi} - \sin\,\alpha\,\frac{\partial p'}{\partial x}\right]_{\psi=0} = 0$$

$$\qquad (3.12)$$

Solving Equation (3.11) for p' and using Equation (3.10), the corrected values for U, α, and p are obtained.

NUMERICAL MARCHING PROCEDURE

The equations under (2.46) are solved by marching downstream in x. Given the upstream conditions at x^{i-1} and $x^{i-1/2}$, the downstream flow is calculated at x^i and $x^{i+1/2}$. Once these flow conditions are obtained the flow is calculated at x^{i+1} and $x^{i+3/2}$, and so on until $x^{i+1/2} = x_e$. The numerical marching procedure is outlined below:

1. Given the upstream values of the flow at x^{i-1} and $x^{i-1/2}$, $U^{i+1/2}$ is obtained by solving Equation (A.6) and α^i is obtained by solving Equation (A.10).

2. The upstream values of p, $p^{i-1/2}$, are corrected by solving Equation (3.11). Using the new pressure field, the corrected downstream values of U and α are calculated from Equation (3.10).

3. The downstream values of r, $r^{i+1/2}$, are calculated from Equation (A.11).

4. The value of u_* is obtained from Equation (3.5), $\nu_{T_{m\ell}}$ is calculated using Equation (2.46j), k and ε are obtained by solving Equation (A.16) with the boundary condition Equations (2.27) and (2.29), and ν_T is given by Equation (2.46h).

5. Steps 1 through 4 are repeated until the flow fields converge.

6. Steps 1 through 5 are repeated at the next downstream stations, x^{i+1} and $x^{i+3/2}$, until the final x-station is reached.

7. Beginning at x_b, steps 1 through 6 are repeated until all variables converge.

8. A new displacement body is calculated and steps 1 through 7 are repeated until final convergence of the flow field.

The maximum number of iterations at a station (Step 5) is set as 5. The new displacement body (Step 8) is calculated by matching the mass flow of the turbulent flow from r_o to r_K (the radial position of ψ_K) to the mass flow calculated from the pressure field's potential flow from δ^* to r_K as follows:

35

$$\int_{r_o}^{r_K} + \delta^* \rho \, U_o \sqrt{1-c_p} \; r \cos \alpha \; dr = \int_{r_o}^{r_K} \rho U r \cos \alpha \; dr \tag{3.13}$$

where

$$c_p = 2 \, \frac{(p-p_o)}{\rho U_o^2} \tag{3.14}$$

With a new displacement body, new boundary conditions for p are established by recalculating the potential flow about the displacement body. The new pressure field is given as:

$$p_{j+1/2}^{i+1/2} = \bar{p}_{j+1/2}^{i+1/2} + (p_k^{i+1/2} - \bar{p}_k^{i+1/2}) \tag{3.15}$$

where $\bar{p}$ is the pressure field from the previous iteration (old displacement body).

In correcting the upstream pressure field (Step 2) an under-relaxation factor has been used to quicken the convergence. If $p_{j+1/2}^{i-1/2}$ is the uncorrected pressure field and $\bar{p}_{j+1/2}^{i-1/2}$ is the corrected pressure field obtained by solving Equation (3.11), then the new pressure field $p_{j+1/2}^{i-1/2}$ is given by

$$\bar{p}_{j+1/2}^{i-1/2} = \frac{(p_{j+1/2}^{i-1/2} + \bar{p}_{j+1/2}^{i-1/2})}{2} \tag{3.16}$$

With Equation (3.16), it requires about 20 total sweeps to obtain a solution that converges to 1% accuracy.

NUMERICAL DIFFICULTIES

Calculations were performed on a Burroughs B7000:168. The number of iterations needed to achieve a convergent solution depended on the complexity of the body geometry. For Afterbody 5 (see the Numerical Results Section), with 37 x-stations

and 34 streamline numbers, 23 iterations were required with 13 minutes of processor time. For Model A, however, only 9 iterations were needed with 6 minutes of processor time, using the same number of x and ψ stations. The region of the flow field where the slowest convergence occurred was the region near the body where the angle of the surface with respect to ψ is at its maximum. In this region, the flow rapidly diverges away from the body. As will be seen in the Numerical Results Section, the flow about Afterbody 5 is near separation while the flow about Model A is not. The maximum angle the program could handle was 40° in the stern region. Above this value, small regions of reverse flow were seen to develop, as indicated by the values of the streamline angle α turning negative. After this occurred, no convergent solution was obtained. If separation occurs, it is no longer advantageous to integrate along the streamlines since in the separated region the values of the streamlines become negative (assuming that the body lies along the $\psi=0$ streamline). In this case, downstream values of the flow are needed to obtain an accurate numerical solution, and the streamwise turbulent diffusion cannot be neglected in comparison with the normal turbulent diffusion terms.

4. NUMERICAL RESULTS

Using the numerical procedure developed in Section 3, calculations were performed for four bodies for which experimental data were available. These are designated as Afterbody 1 (Huang et al., 1979),[22] Afterbody 5 (Huang et al., 1980),[23] Model A, and Model B (Lyon, 1932[24] and 1934[25]). Table 1 lists the following geometric and flow parameters for each body: the length of the body L, the maximum radius of the body r_{max}, the upstream flow velocity U_o, and the upstream Reynolds number Re. The aft body geometries, together with four streamline positions, the displacement body, δ^* and the boundary layer thickness, δ, are presented in Figures 3 through 6. In these figures, the streamline numbers are normalized with respect to LU_o^2 and they correspond to (outer) streamline grid numbers 10, 22, 30, and 34. The aft body geometries for Afterbody 1 (Figure 3) and Afterbody 5 (Figure 4) are characterized by parallel middle bodies with inflected sterns. The aft body geometries for Model A (Figure 5) and Model B (Figure 6) have constantly decreasing radii, with the curvature of the surface remaining convex.

TABLE 1 - FLOW AND BODY GEOMETRY PARAMETERS

	L (m)	r_{max} (m)	U_∞ (m/s)	R_e
Afterbody 1	3.066	0.1398	30.48	6.60×10^6
Afterbody 5	2.910	0.1397	45.72	9.30×10^6
Model A	1.778	0.1778	17.88	2.09×10^6
Model B	1.778	0.1778	17.88	2.05×10^6

The numerical results display a thickening of the turbulent region in the stern/wake regions of the flows. The displacement bodies diverge significantly from the physical bodies near the stern and continue into the wake with slowly decreasing radii. In Figures 3 and 4, the computed displacement body and boundary layer thickness are compared to the values of δ^* and δ obtained from the data of Huang et al., (1979),[22] (1980)[23]. For both bodies, the computed δ^* and δ lie slightly below the experimental results in the stern/wake region, but overall the agreement with the experiments is good.

Figures 7 through 28 present a detailed comparison of the computed flow field to experimental results. In all of these figures y_+^* was set equal to 50. The distributions of the frictional velocity u_* and the wall-pressure coefficient c_p are shown in Figures 7 through 10 for the four bodies. The computed pressure distribution for Afterbody 1 (Figure 7) has a large trough at the inflected stern. At this region of the body, the surface and the streamlines near the surface have a marked change in curvature. As the streamlines change curvature from convex to concave, the pressure gradient changes from adverse to favorable. Following the concave part of the stern, the streamline curvature becomes convex again, with a corresponding rise in the pressure on the wall. The computed wall shear stress, given by ρu_*^2, drops rapidly in the adverse pressure gradient region of the flow. Accompanying the sharp drop in the wall pressure, the wall shear stress rises steeply. With the final change of curvature of the streamlines at the tail, u_* drops dramatically to zero. The computed pressure distribution agrees well with the

38

experimental data, having a maximum percentage difference of 1% of the total head $\rho U_o^2/2$. However, the computed u_* distribution reaches a smaller value than the experimental data, being 25% under the experimental result at $x/L = 0.97$. (For the pressure field, the percent difference between the computed pressure field, p_{comp}, and the experimental pressure field, p_{exp}, will be given by $100 \times |p_{exp} - p_{comp}|/\rho U_o^2$. For the velocity field the percentage difference between the computed velocity, U_{comp}, and the experimental velocity, U_{ext}, will be given by $100 \times |U_{exp} - U_{comp}|/U_o$. For all other variables, the percentage difference will be the local difference between the computed (ϕ_{comp}) and the experimental (ϕ_{exp}) given by $100 \times |\phi_{exp} - \phi_{comp}|/|\phi_{exp}|$.)

The computed u_* and c_p distributions for Afterbody 5 (Figure 8) display the same type of behavior as exhibited for Afterbody 1. For Afterbody 5, the agreement with the experimental data is good for both the wall frictional velocity and the wall pressure coefficient. As is evident by the steep drop in u_* in the adverse pressure gradient region of the flow, the flow about this body is very near to separation at $x/L = 0.93$.

The computed u_* and wall c_p for flow past Model A are given in Figure 9. As opposed to Afterbodies 1 and 5, the stern of Model A is not inflected. Therefore, over the aft region of the body, the pressure gradient remains adverse up to the tail of the body and u_* steadily decreases to zero. The computed wall-pressure distribution lies slightly above the experimental results, with a maximum difference between the computed and experimental pressure distributions of less than 3% at $x/L = 0.95$.

The shape of Model B is characterized by a sharply sloping stern region. The values of the surface angles near 90° at the stern caused some numerical difficulty for the computer code. To obtain the computed flow field, only a few x-stations were placed near the tail of the body. Despite the limited number of points, good agreement of the computed wall pressure with the experimental data is obtained, with a maximum difference of less than 4% occurring at $x/L = 0.95$ (Figure 10). The sharp decrease in u_* indicates that the flow is nearing separation as the body sharply turns downward at the tail.

39

Figures 11 through 16 present detailed comparisons of the computed velocity fields to the experimental results for the four bodies. In Figure 11, the computed velocity profiles show remarkable agreement with the experimental data for Afterbody 1 up to the tail of the body. The computed velocities near the tail and in the wake are also in good agreement with the experimental results (Figure 12). The largest discrepancy occurs immediately behind the body (x/L=1.0076), where the computed axial velocity is 8% less than the experimental value at r = 0. The cause of this large difference is not known. Farther into the wake, the agreement with the experiment is very good, as is evident by the profiles at x/L = 1.1820.

Computed and experimental velocity profiles for Afterbody 5 are presented in Figures 13 and 14. Since no measurements were made past the body, comparisons cannot be made for the wake velocity profiles. For x-stations on the body, the overall agreement with the experimental data is good. At x/L = 0.8727 (Figure 13), the computed radial velocity is 5% under the experimental results, and the computed axial velocity is 3% under the experimental data. Near the tail, at x/L = 0.9512 and x/L = 0.9874, (Figure 14), the computed axial velocities are slightly greater than the experimental profiles (2%).

Figures 15 and 16 present the total velocity profile results at several x-stations for the flows past Models A and B. The consistency of the computed velocity fields with the experimental velocities is very good with a maximum difference of less than 2%.

Extensive measurements of the pressure field were made for the flows past Afterbody 1 (Huang et al., 1979)[22] and Afterbody 5 (Huang et al., 1980).[23] Comparisons of the computed to the experimental pressure fields for the two bodies are given in Figures 17 through 20. The computed pressure profiles and the experimental pressure fields for Afterbody 1 (Figures 17 and 18) are within 1.5%; for Afterbody 5 (Figures 19 and 20) the results differ by 2%. At all the x-stations plotted, the computed pressure profiles agree very well with the experimental results above the boundary-layer region. This indicates that the displacement body concept has correctly determined the influence of the turbulent flow on the external inviscid flow.

40

The results of the turbulent kinetic energy calculations for Afterbody 1 and Afterbody 5, together with experimental results, are given at several x-stations in Figures 21 through 24. For x-stations on the bodies, the agreement of the computed k with the experimental data is good. These results are encouraging and indicate the use of the inner mixing length with the $k-\varepsilon$ model gives a good approximation to the turbulent field. In the wake, the value of k on the centerline is its average from $r = 0$ to $r = 0.2\delta$. The agreement in the wake for Afterbody 1 (Figure 22) is poor, with the computed k field 25% under the experimental value at $x/L = 1.1820$. Because of this large difference, further testing of the boundary conditions of the $k-\varepsilon$ equations is needed in the wake.

The normal Reynolds stress profiles, $-\overline{u'v'}$, are presented at several x-stations for Afterbody 1 and Afterbody 5 in Figures 25 through 28. The agreement of the computed results to the experimental data is fair in the thinner boundary layer regions and becomes poorer in the thick boundary layer/wake region of the flow. For x-stations lying on the body, the computed normal Reynolds stresses are smaller than the experimental profiles, while in the wake the computed values are greater than the experimental values.

Figures 29 through 36 present a comparison of the partially parabolic, $k-\varepsilon$ calculations to the Wang/Huang[20] mixing length, boundary layer calculations for the four bodies. Experimental data are also plotted in the figures. For Afterbody 1 (Figure 29), the u_* and c_p distributions are in general agreement up to $x/L = 0.95$. The Wang/Huang[20] calculations do not predict as steep a drop in u_* at the concave part of the body as do the $k-\varepsilon$ calculations. In addition, there is no trough at the stern in the Wang/Huang[20] pressure distribution. The velocity profiles computed for Afterbody 1 (Figure 30) from the two programs are consistent with the partially parabolic calculation agreeing slightly better with the experimental profiles at $x/L = 0.9460$. For Afterbody 5, the partially parabolic, $k-\varepsilon$ calculations correctly predict the steep drop in u_* and the pressure trough near the stern (Figure 31). The velocity profile comparisons for Afterbody 5 (Figure 32) demonstrate again the agreement of the two computer codes (within 2%), with the Wang/Huang[20] axial velocity profile agreeing slightly better with the experimental results at $x/L = 0.9874$.

The calculations for u_* and c_p for Model A (Figure 33) demonstrate that the calculations agree up to the tail of the body. At the tail, the partially parabolic u_* distribution drops rapidly to zero as opposed to the Wang/Huang[20] boundary layer code which shows a slight upturn. Both pressure distributions turn downward at the tail, with the partially parabolic pressure distribution reaching a slightly higher maximum. The computed velocity profiles for Model A (Figure 34) are again consistent. The comparisons of u_*, c_p, and velocity for Model B (Figures 35 and 36) show the same behavior as demonstrated for Model A.

In Figures 3 through 36, y_+^* was set equal to 50. To test the influence of y_+^* on the computed flow field, calculations were performed for Afterbody 5 with y_+^* equal to 100, 300, and 500. The results of these calculations are given in Figures 37 through 48. The $y_+^* = 100$ computation (Figures 37 through 40) shows little change compared to the $y_+^* = 50$ calculation. Near the stern, there is a slight increase in u_* (Figure 37). The velocity profiles (Figure 38) and the pressure profiles (Figure 39) have not moved noticeably, except for the decrease in pressure at $x/L = 0.9874$. However, the turbulent kinetic energy profiles (Figure 40) have marked dips near the body at x-stations near the stern.

The u_* distribution, calculated for $y_+^* = 300$, has further increased near the stern (Figure 41). In addition, the pressure at the wall near the stern has increased. The velocity profiles (Figure 42) have slightly decreased from the previous case of $y_+^* = 100$. This decrease in velocity is due to the increase of pressure near the stern, as evident in Figure 43. The turbulent kinetic energy at the stern (Figure 44) begins to show erratic behavior as the matching point of the k-ϵ equations and the mixing length is extended farther above the body.

As y_+^* is further increased to 500, the computed u_* distribution lies above the experimental results (Figure 45). Both the velocity profiles (Figure 46) and the pressure profiles (Figure 47) show marked movement away from the experimental values near the stern. The erratic behavior k experienced for the case of $y_+^* = 300$ is even more pronounced for $y_+^* = 500$ (Figure 48). Since the object of the study was not to determine what the optimal value of y_+^* is, no definitive statement can be made concerning the best value of y_+^* to use. However, because of the oscillatory behavior of the turbulent fields as y_+^* is increased, it is felt that the lower values of y_+^* are preferable over the higher values of y_+^*.

42

Finally, calculations were performed for flow past Afterbody 5 at Reynolds numbers of 1×10^8 and 1×10^9. At these two high Reynolds numbers, the value of y_+^* required to obtain a convergent solution had to be increased above 50. For $Re = 1 \times 10^8$ the lowest value of y_+^* for which a solution could be obtained was 100, and for $Re = 1 \times 10^9$, the minimum y_+^* was 625. The calculations for these two Reynolds numbers were performed with the same number of x-grid stations as the case of $Re = 9.3 \times 10^6$, and the number of ψ-stations were increased to 40. Comparisons of the u_* and c_p distributions, calculated from the partially parabolic, k-ϵ program, to the distributions calculated from the Wang/Huang[20] boundary layer program are given in Figure 49 for $Re = 1 \times 10^8$. Near the stern, the k-ϵ calculations predict a 36% smaller value of u_* than the mixing length theory (Figure 49). The two pressure distributions agree well up to the concave region of the body, where the partially parabolic pressure distribution has a trough. The velocity profile comparisons (Figure 50) for $Re = 1 \times 10^8$ agree within 3%. The corresponding comparisons for the case of $Re = 1 \times 10^9$ are given in Figures 51 and 52. The partially parabolic, k-ϵ code again predicts a smaller u_* and a pressure trough near the stern (Figure 51). The velocity fields are again in agreement (Figure 52), with the mixing-length profile being 5% smaller near the stern (Figure 52). The values of y_+^* used for the higher Reynolds numbers represent the minimum values attainable for this particular code. The proper value of y_+^* as a function of Reynolds number still remains to be found. The partially parabolic, k-ϵ distributions at the higher Reynolds numbers (Figures 49 and 51) contain some roughness. At these higher Reynolds numbers, more x- and ψ-stations are needed to smooth these plots. However, the number of grid points were matched to the Wang/Huang[20] boundary layer program to give a true comparison of the two computer codes.

5. CONCLUDING REMARKS

Overall, the agreement between the measured and calculated results is encouraging. For most of the flow field, the velocity, pressure, and k profiles are correctly predicted. The pressure and surface-shear-stress distributions also agree well with the experimental data. The major drawback to the present scheme is that the total number of iterations needed for the flow calculations to converge is very large when a large angle at the stern is present.
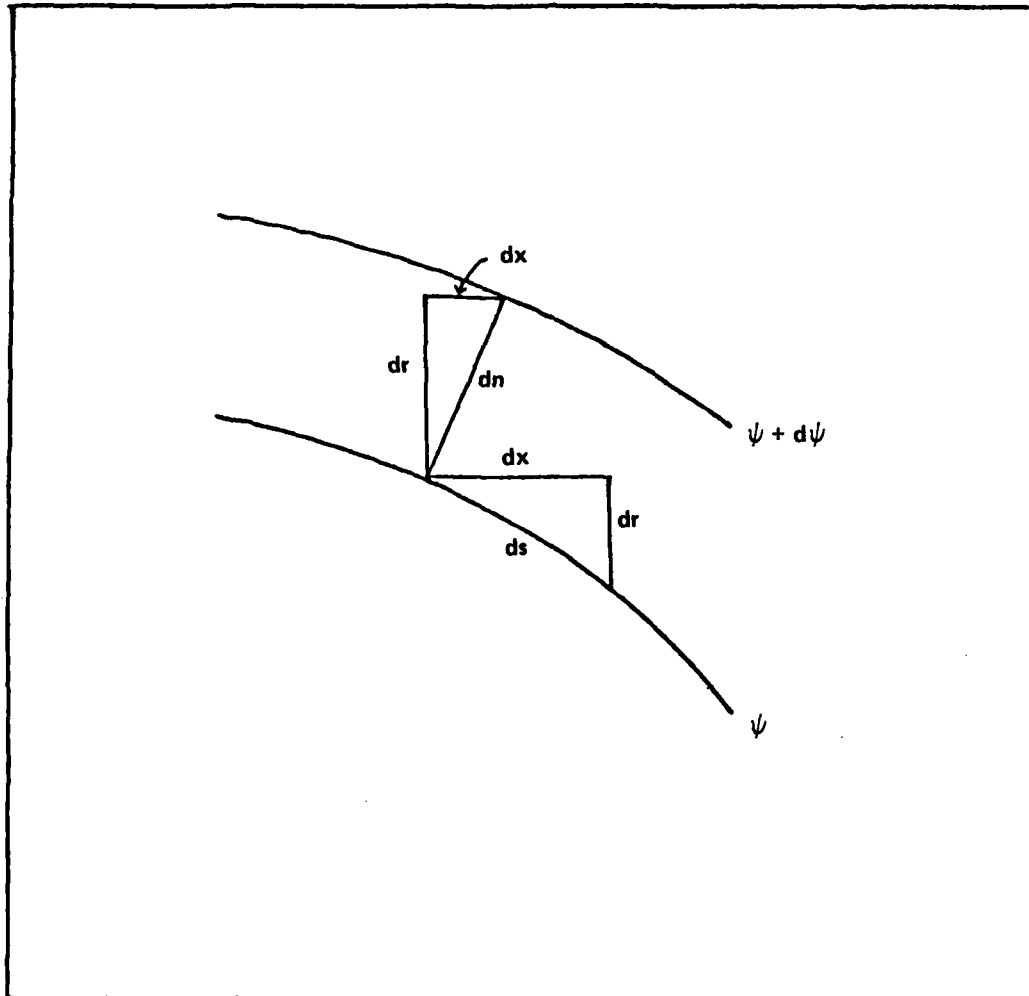
Figure 1 - The Geometry of the Natural Coordinate System

44
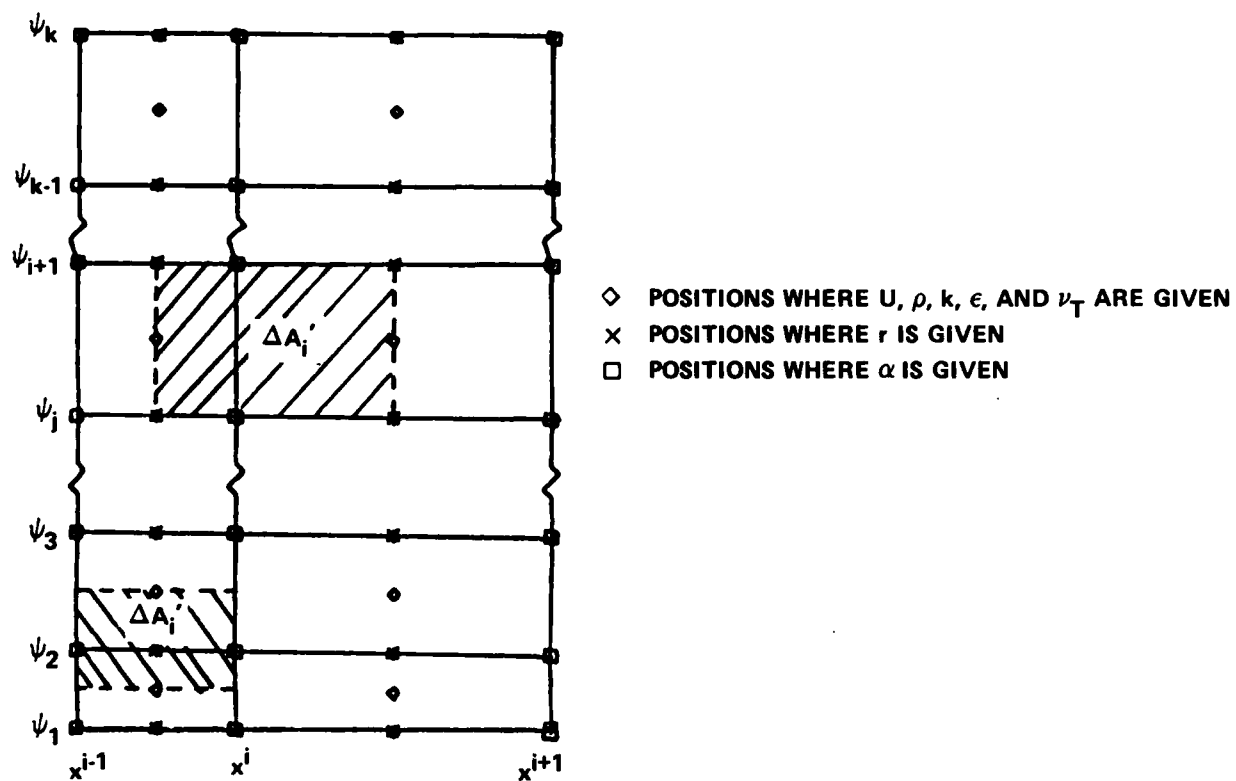
Figure 2 - The (x, ψ) Staggered Grid Geometry
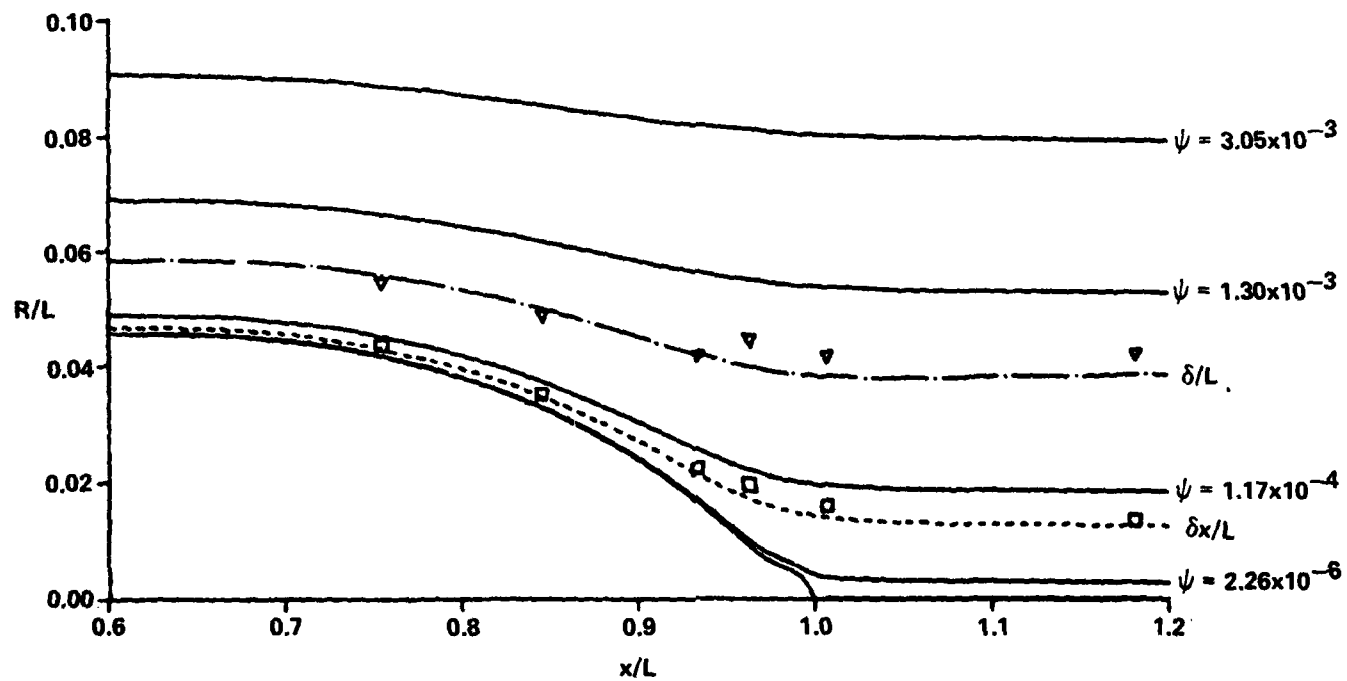
Figure 3 - The Aft Body Geometry, Four Streamline Positions, the Displacement Body δ^*, and the Boundary Layer Thickness δ for Afterbody 1

Figure 4 — The Aft Body Geometry, Four Streamline Positions, the Displacement Body
Position δ*, and the Boundary Layer Thickness for Afterbody 5
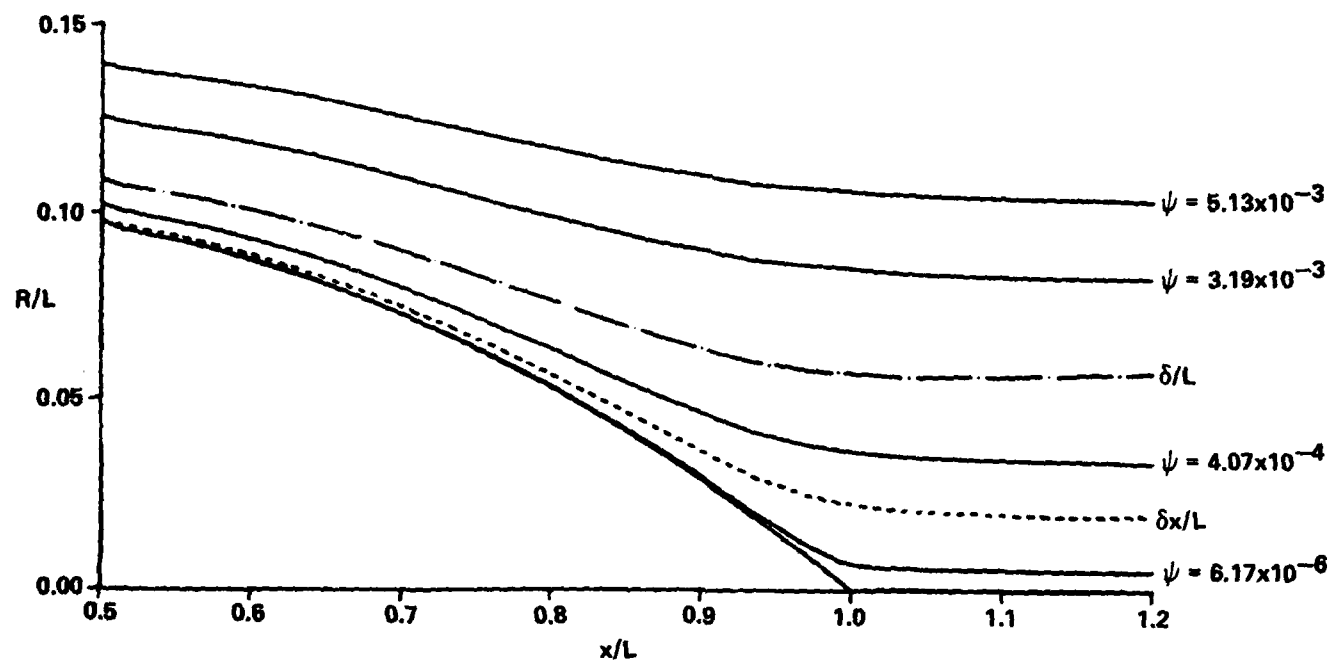
Figure 5 – The Aft Body Geometry, Four Streamline Positions, the Position of the Displacement Body $\delta*$, and the Boundary Layer Thickness δ for Model A

48
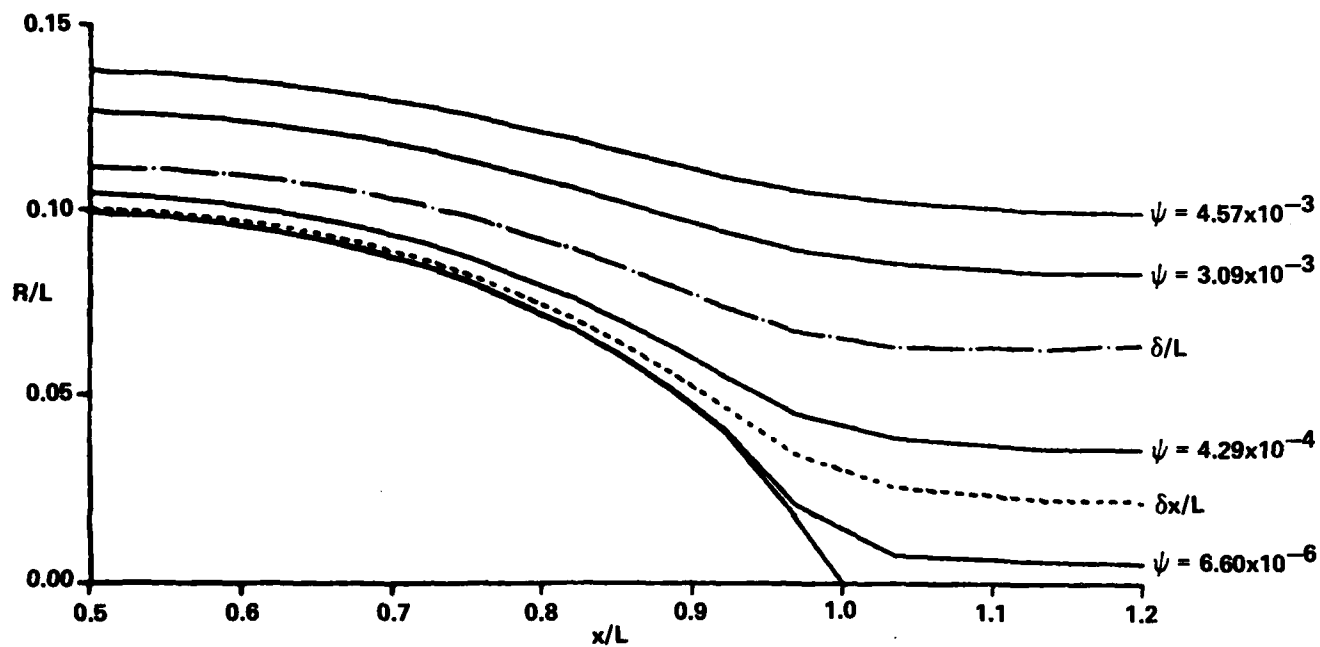
Figure 6 – The Aft Body Geometry, Four Streamline Positions, the Position of the Displacement Body δ^*, and the Boundary Layer Thickness δ for Model B

49
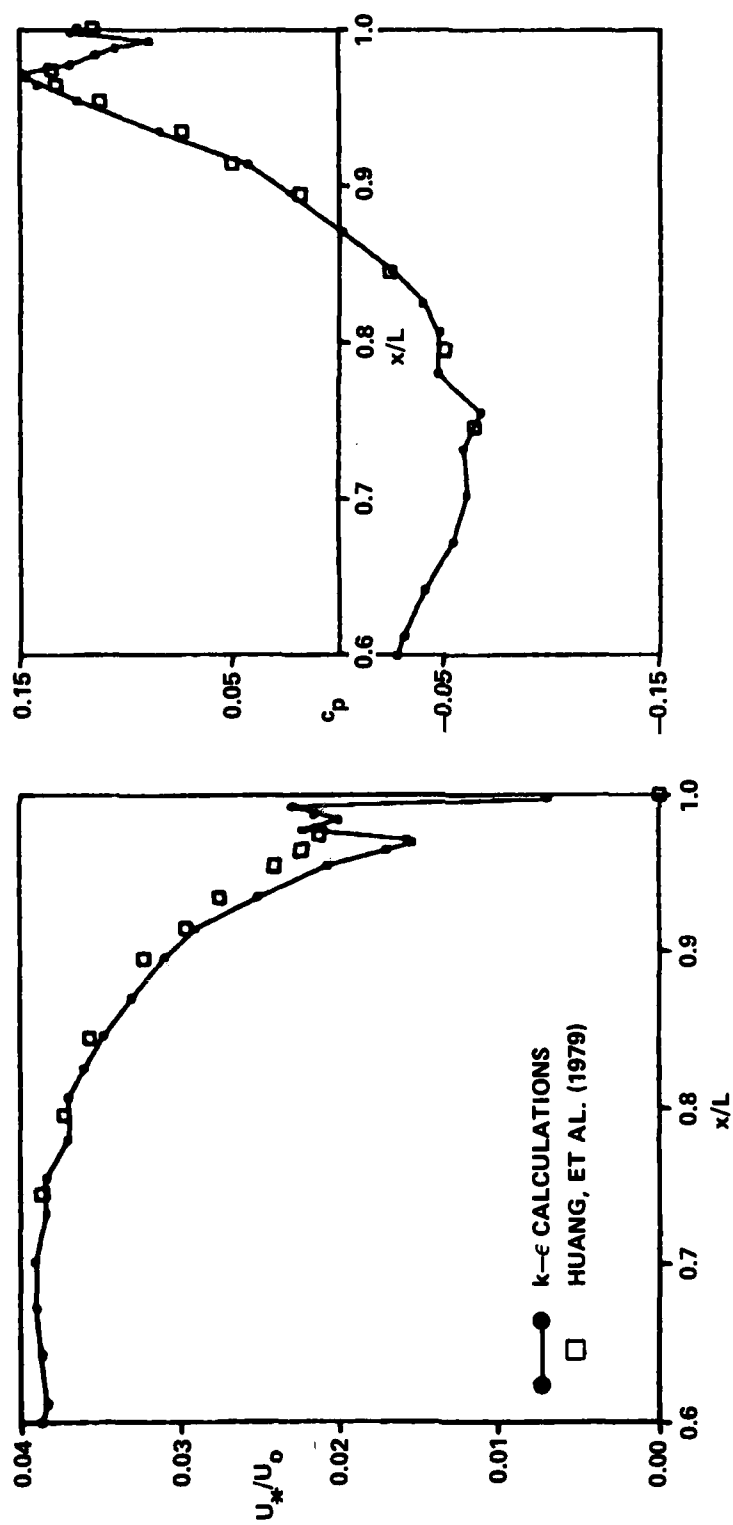
Figure 7 - The Plots of the Normalized Frictional Velocity u* and the Pressure Distribution on the Body, $c_p = (p - p_o)/1/2\rho U_o^2$, versus x/L for Afterbody 1
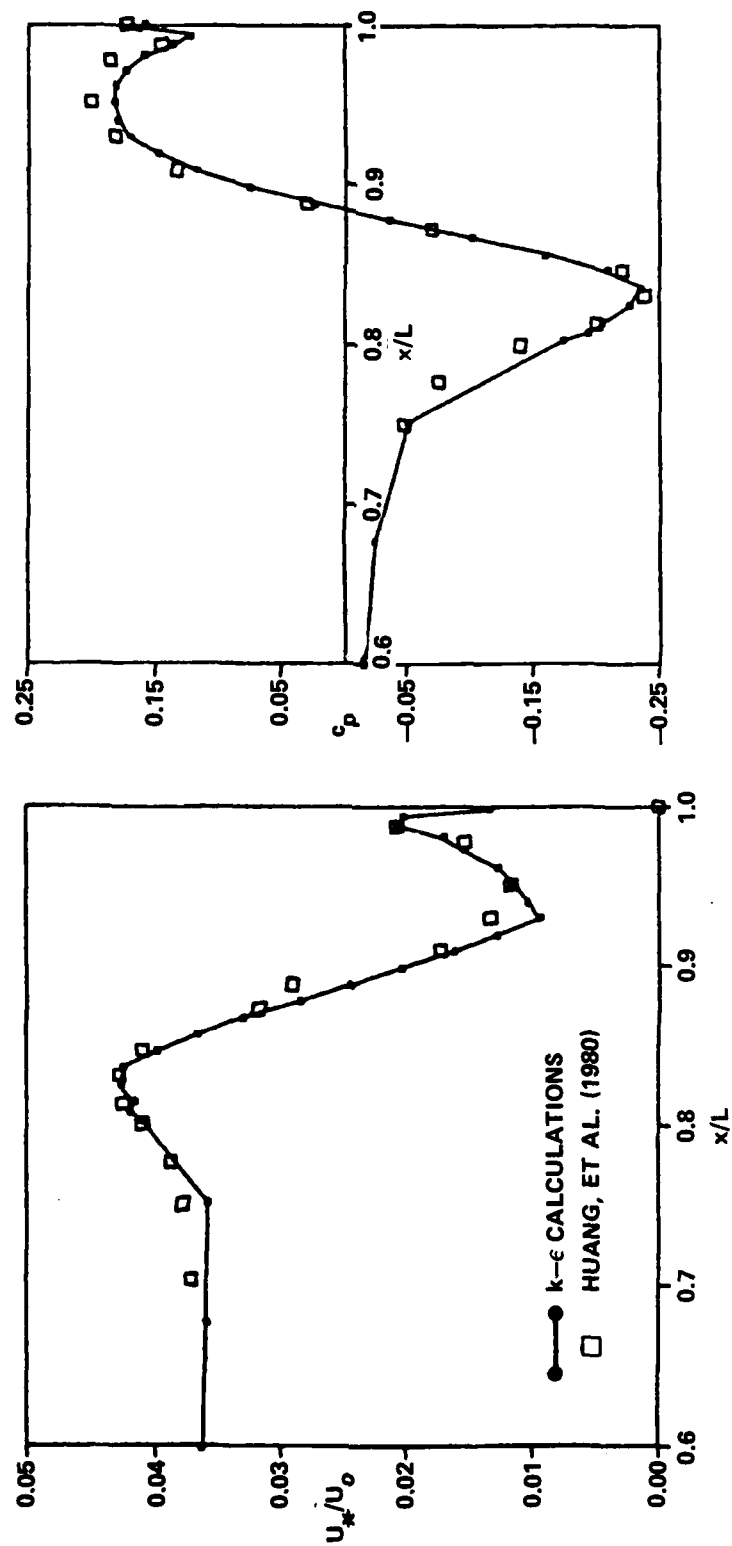
Figure 8 – The Plots for the Normalized Frictional Velocity u* and the Pressure Distribution on the Body, c_p, versus x/L for Afterbody 5
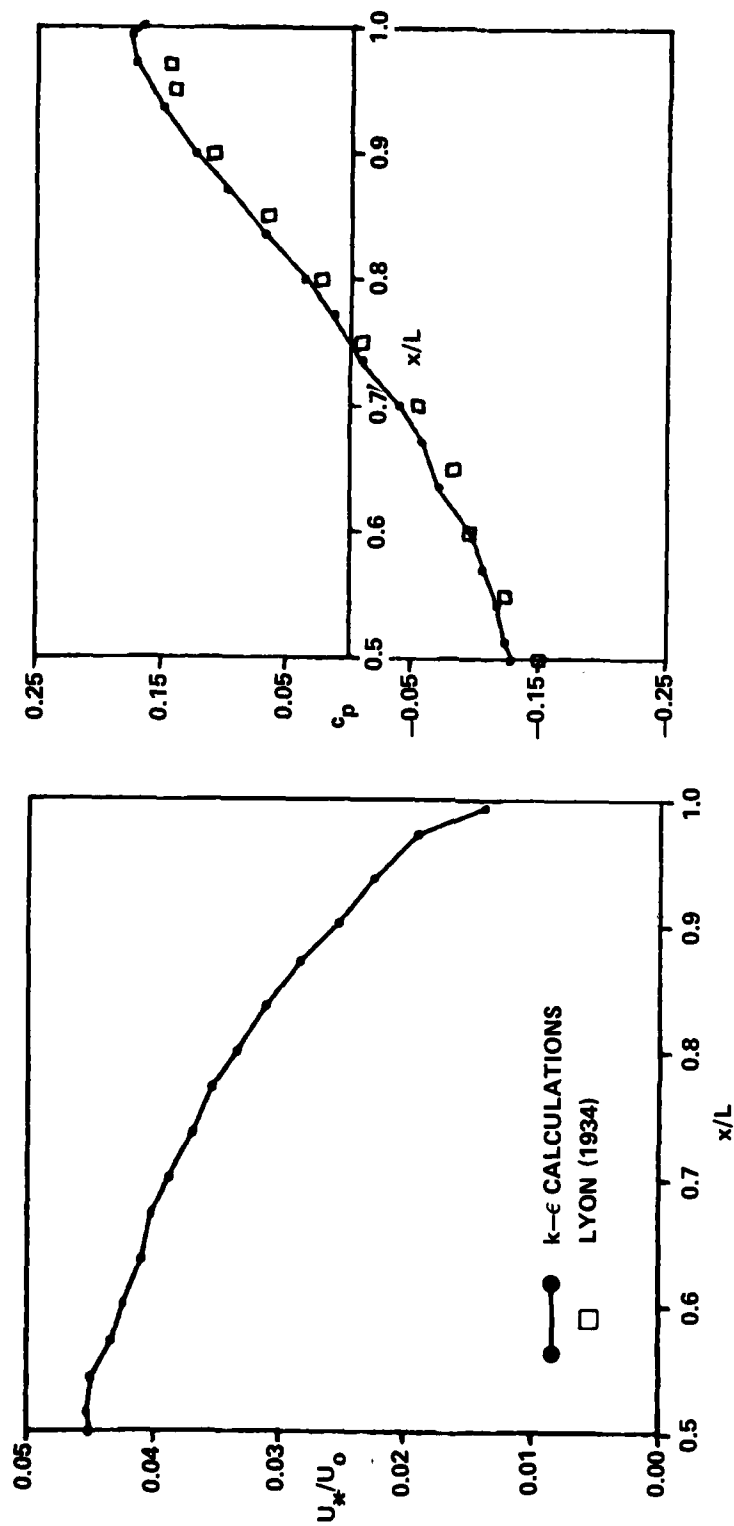
Figure 9 – The Plots of the Normalized Frictional Velocity u* and the Pressure Distribution on the Body Given by $(p_w - p_o)/1/2\rho U_o^2$, Where p_w is the Pressure at the Wall, versus x/L for Model A
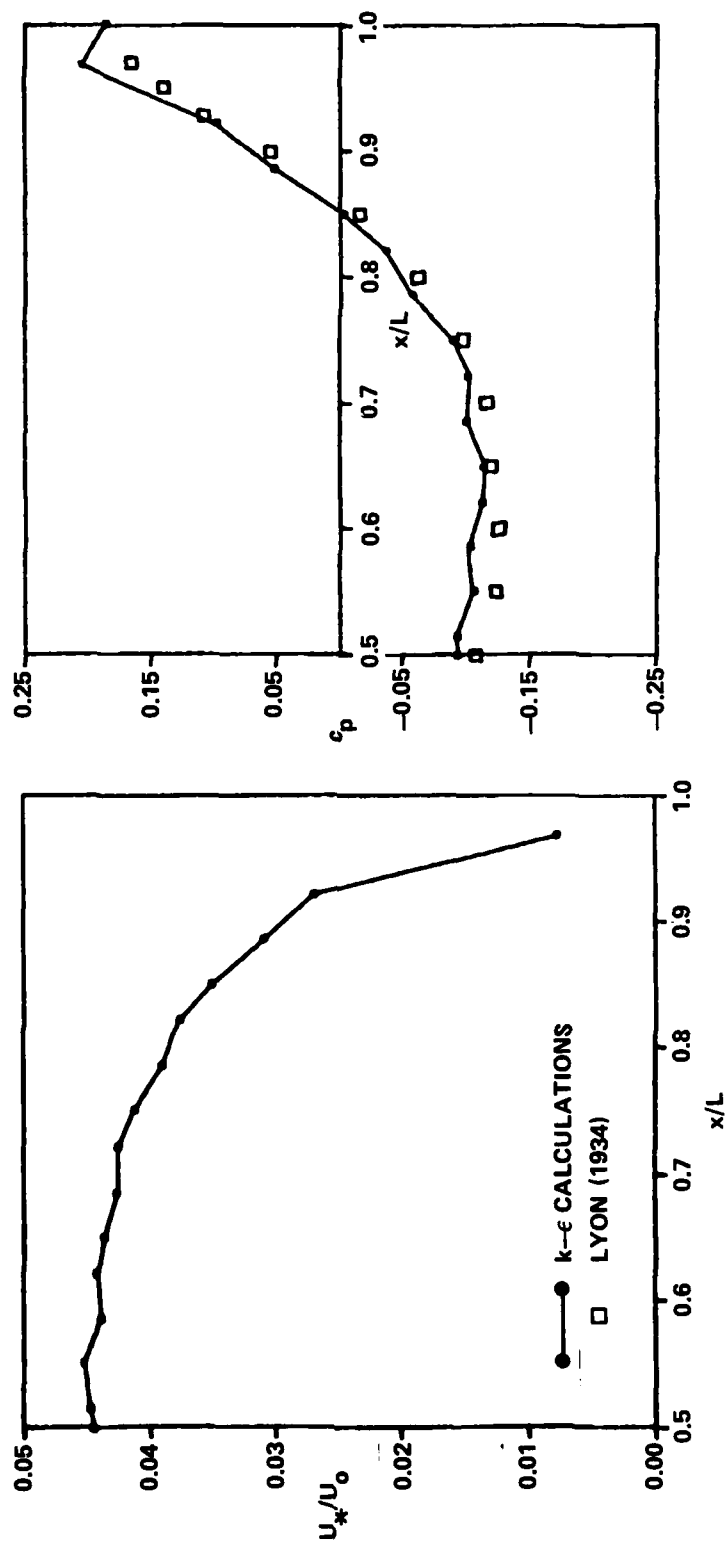
Figure 10 - The Plots of the Normalized Frictional Velocity u* and the Pressure
Distribution on the Body Given by $(p_w - p_o) 1/2 \rho U_o^2$, Where p_w is the
Pressure at the Wall, versus x/L for Model B

53
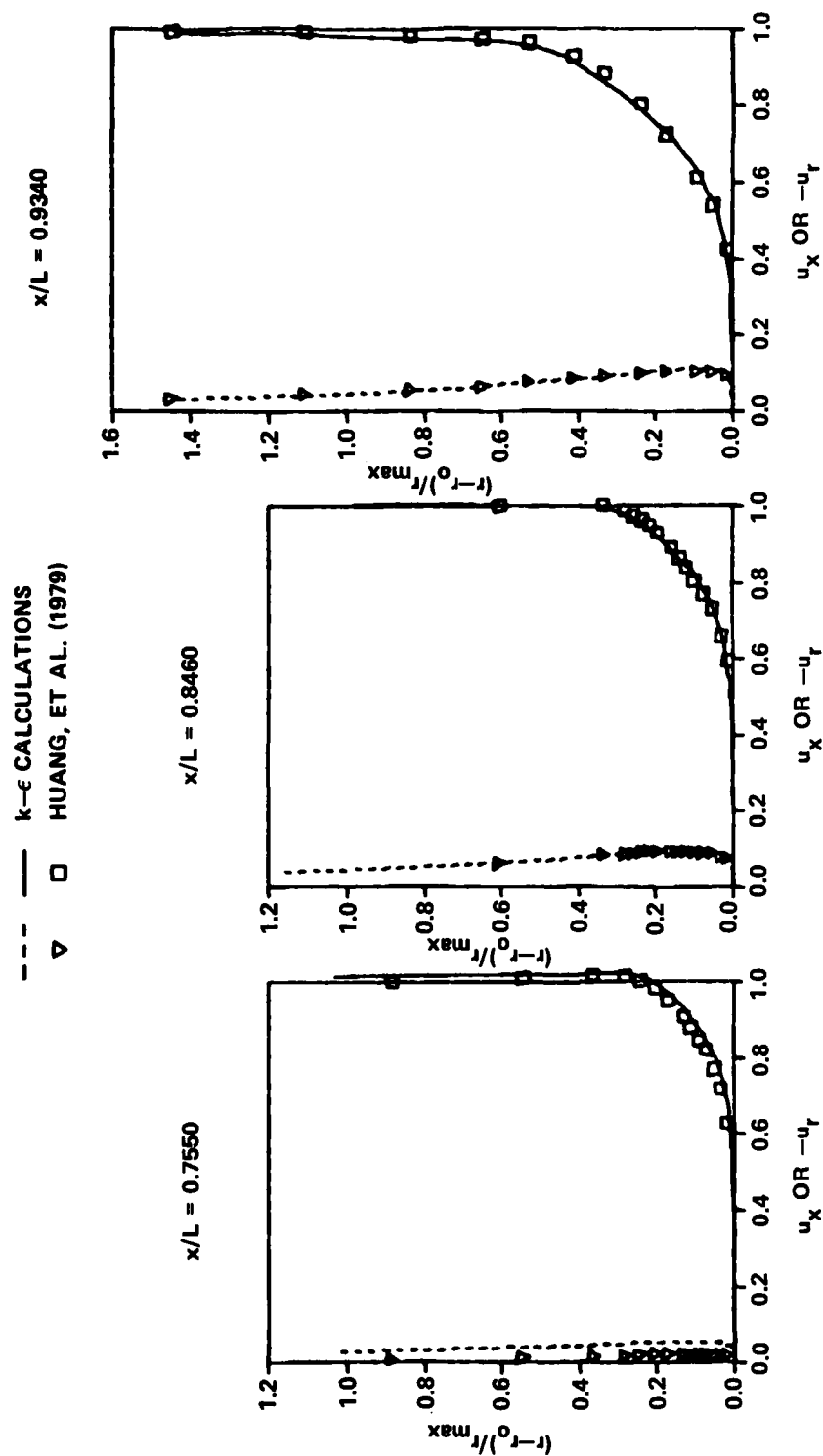
Figure 11 – The Velocity Profiles at Three x-Stations for Afterbody 1

54
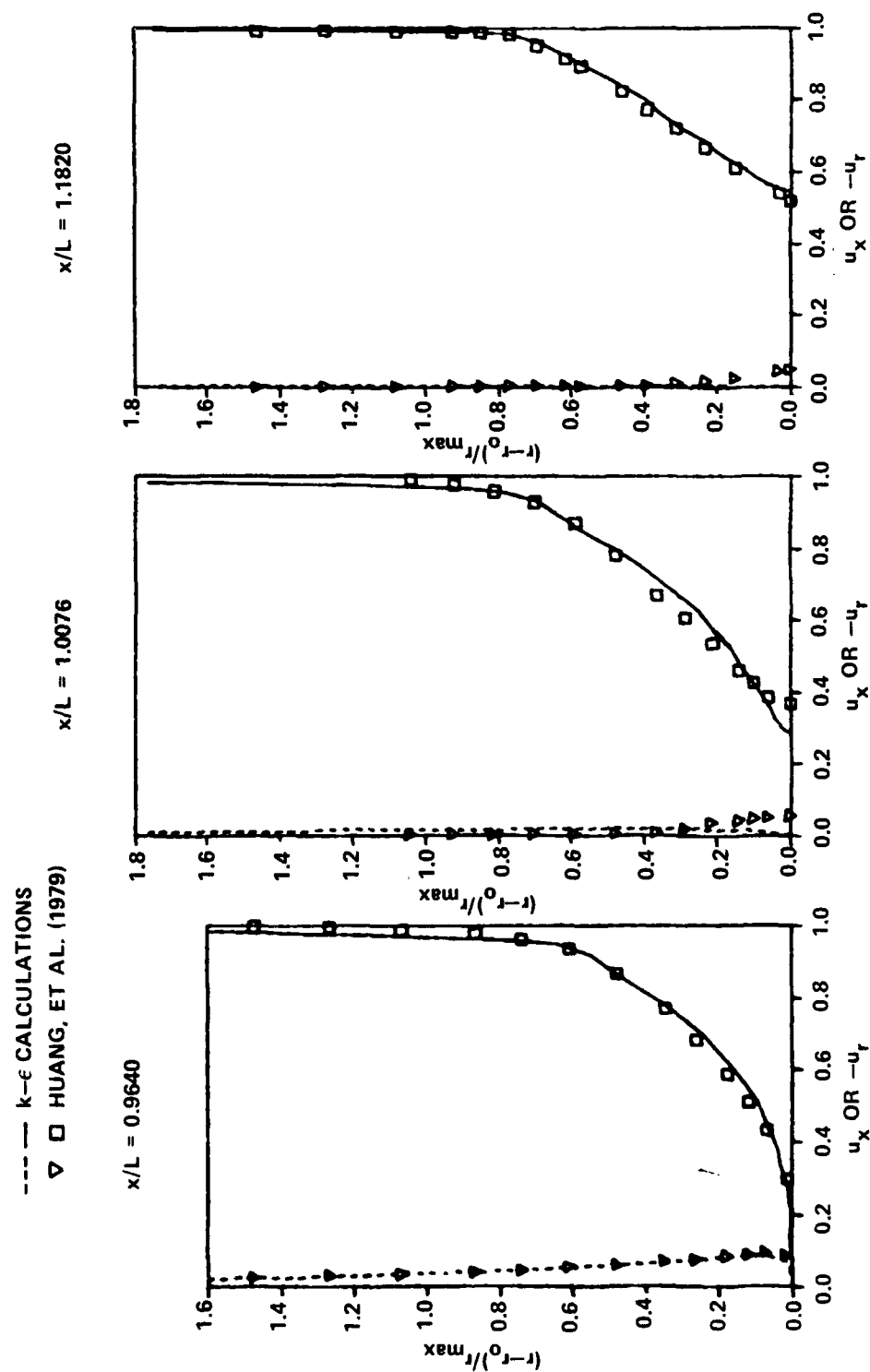
Figure 12 – The Velocity Profiles at Three x-Stations for Afterbody 1

55
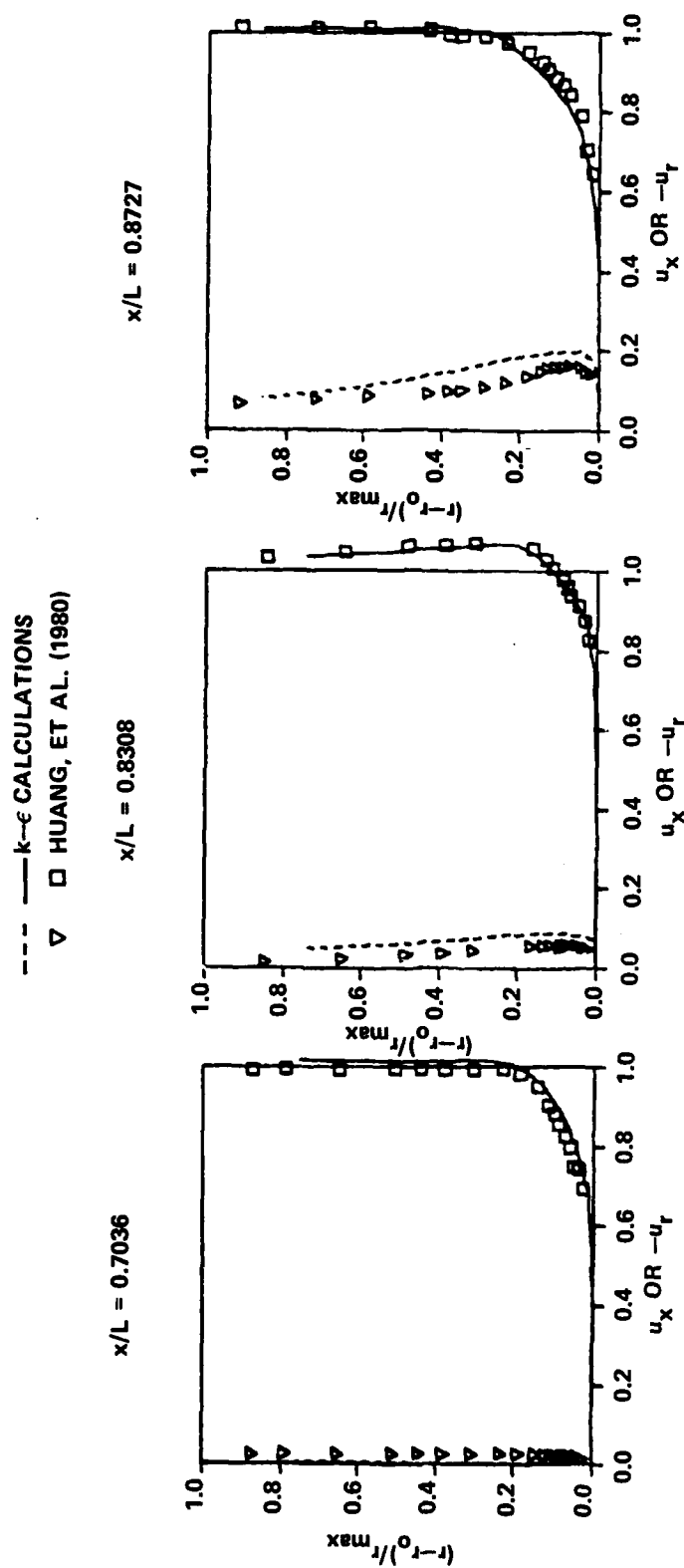
Figure 13 – The Velocity Profiles at Three x-Stations for Afterbody 5

56

Figure 14 – The Velocity Profiles at Three x-Stations for Afterbody 5

57
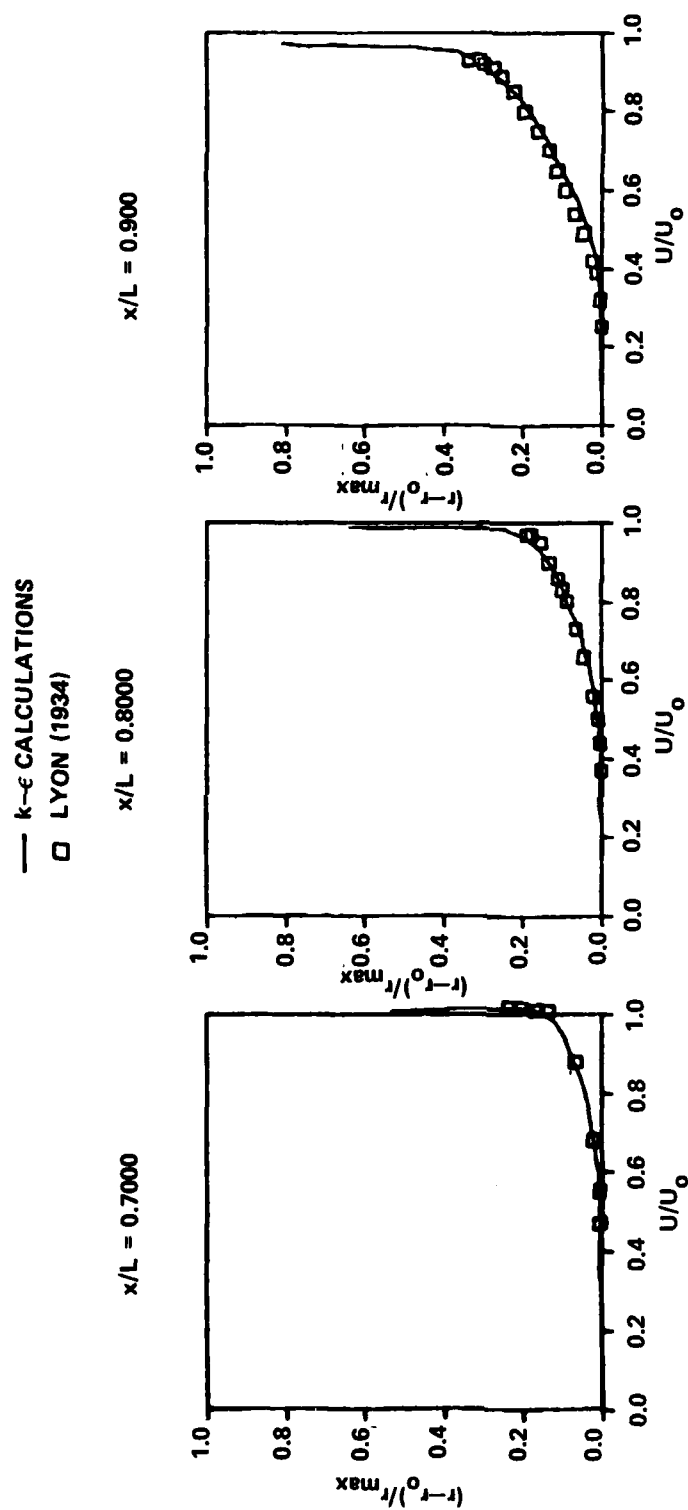
Figure 15 - The Velocity Profiles at Three x-Stations for Model A
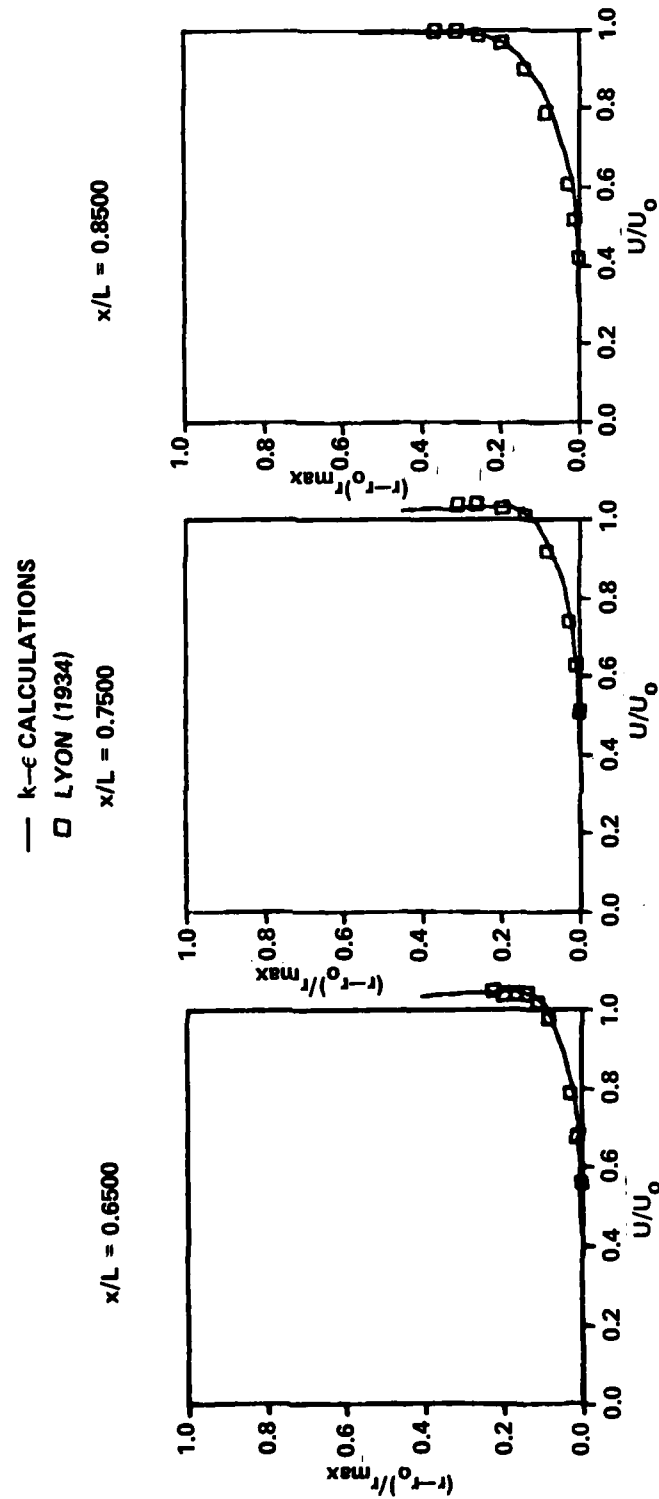
Figure 16 - The Velocity Profiles at Three x-Stations for Model B
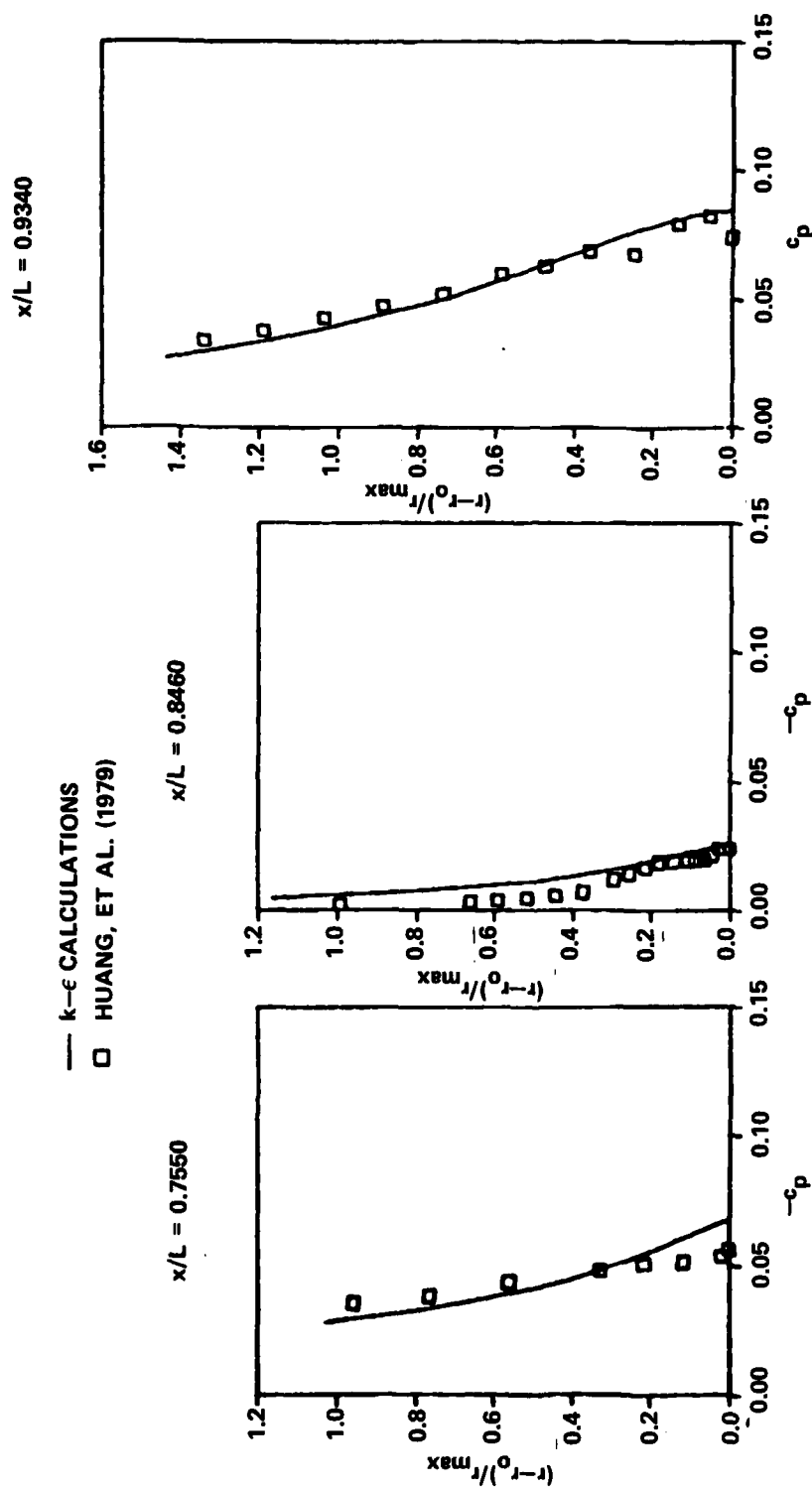
Figure 17 – The Pressure Profiles at Three x-Stations for Afterbody 1
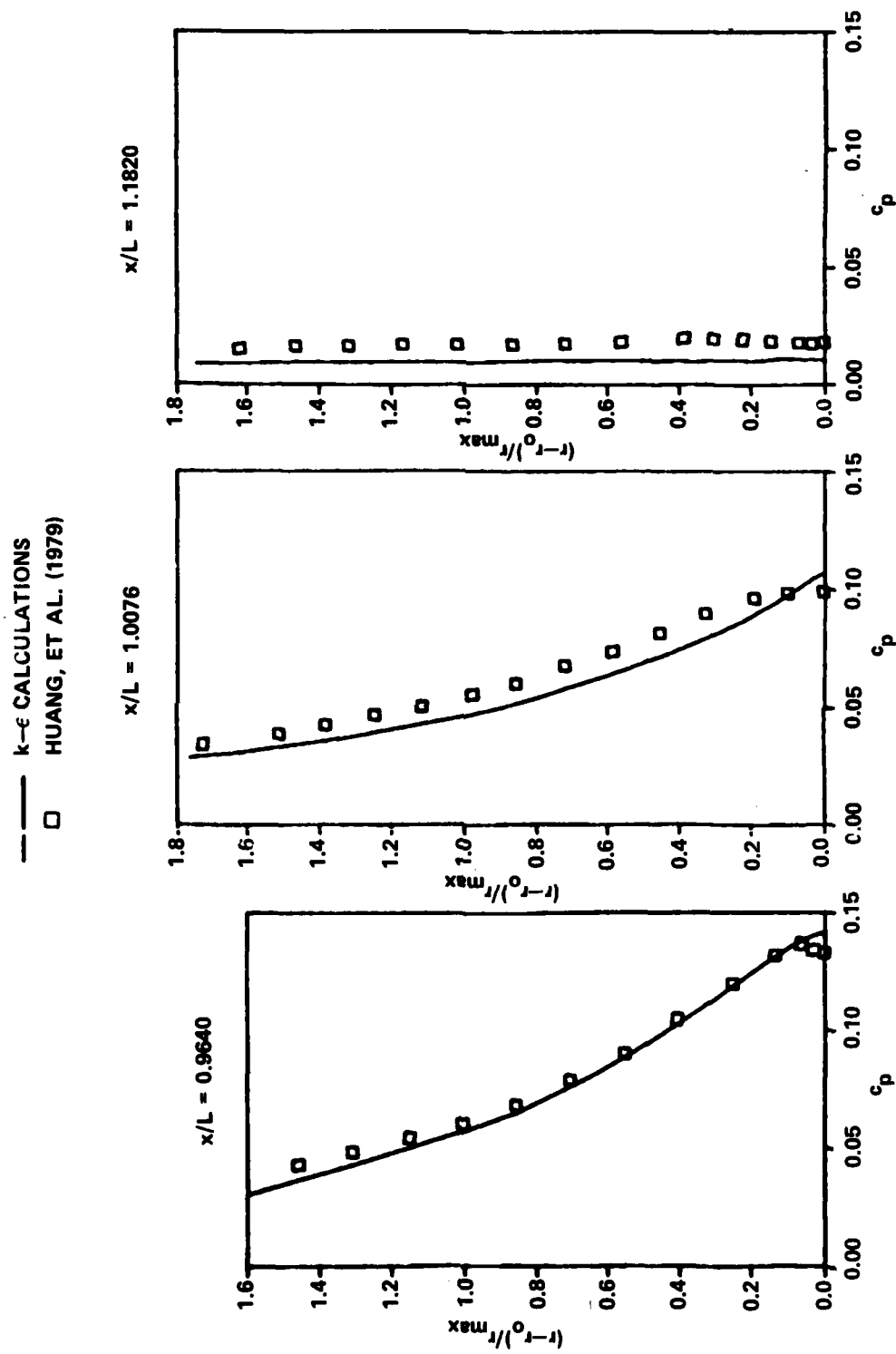
Figure 18 - The Pressure Profiles at Three x-Stations for Afterbody 1

61
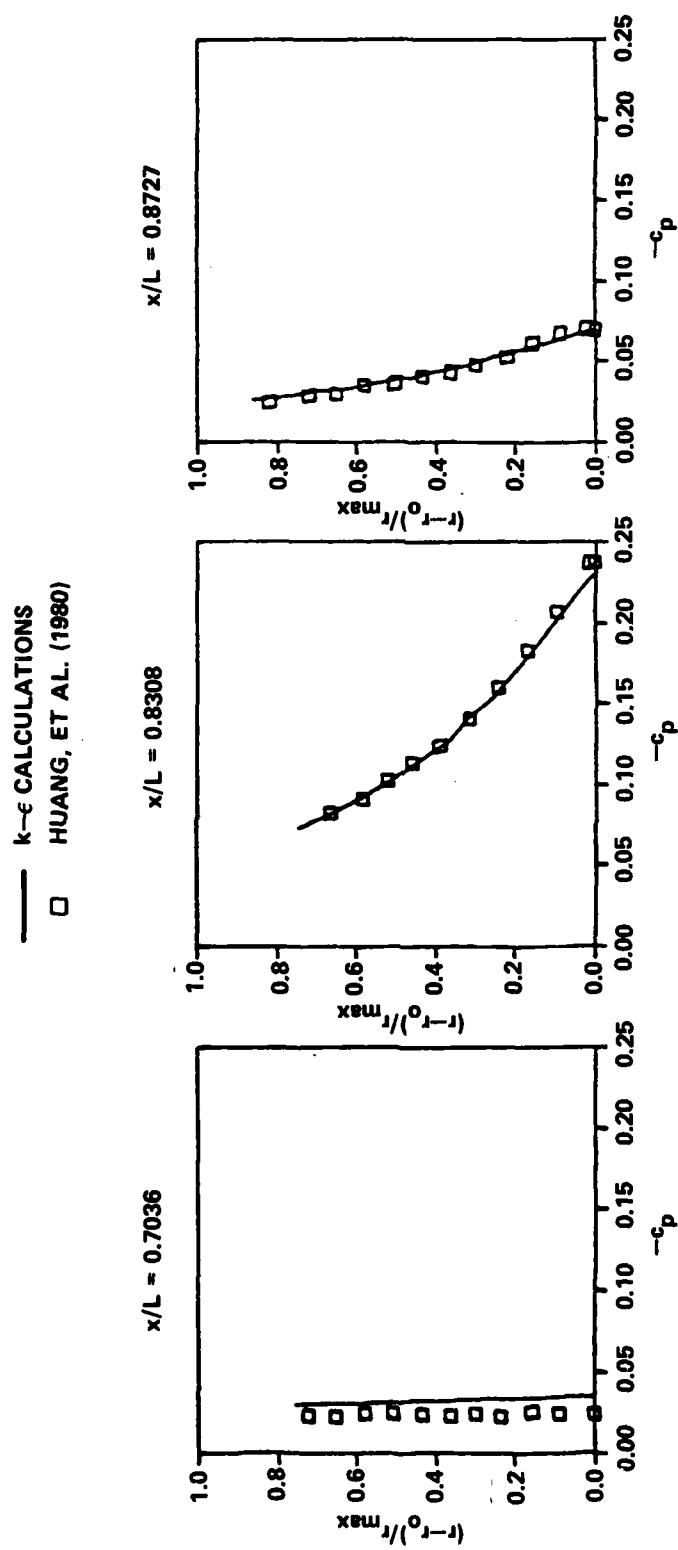
Figure 19 - The Pressure Profiles at Three x-Stations for Afterbody 5
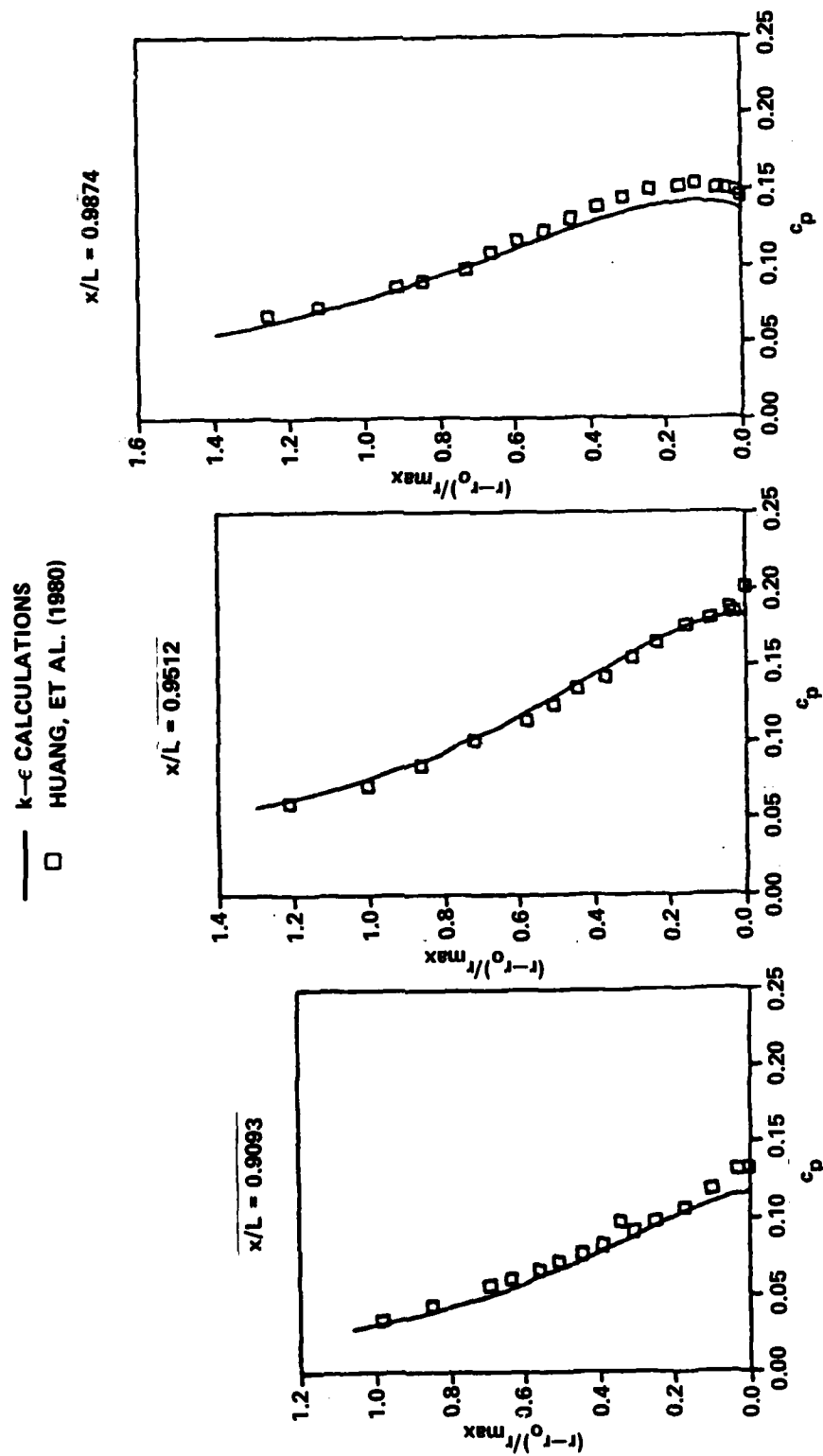
Figure 20 - The Pressure Profiles at Three x-Stations for Afterbody 5

63
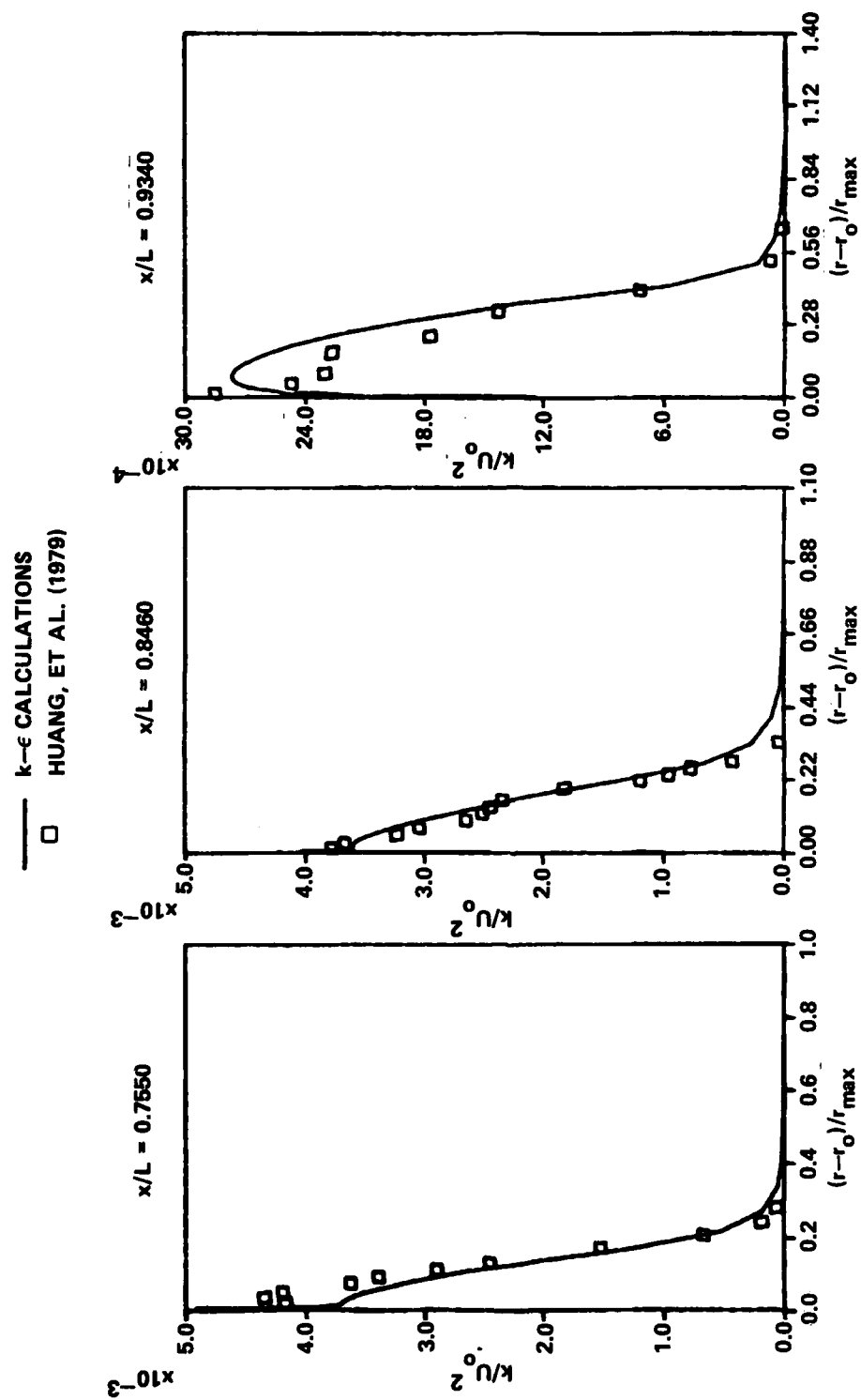
Figure 21 - The Turbulent Kinetic Energy Profiles at Three x-Stations for Afterbody 1

64
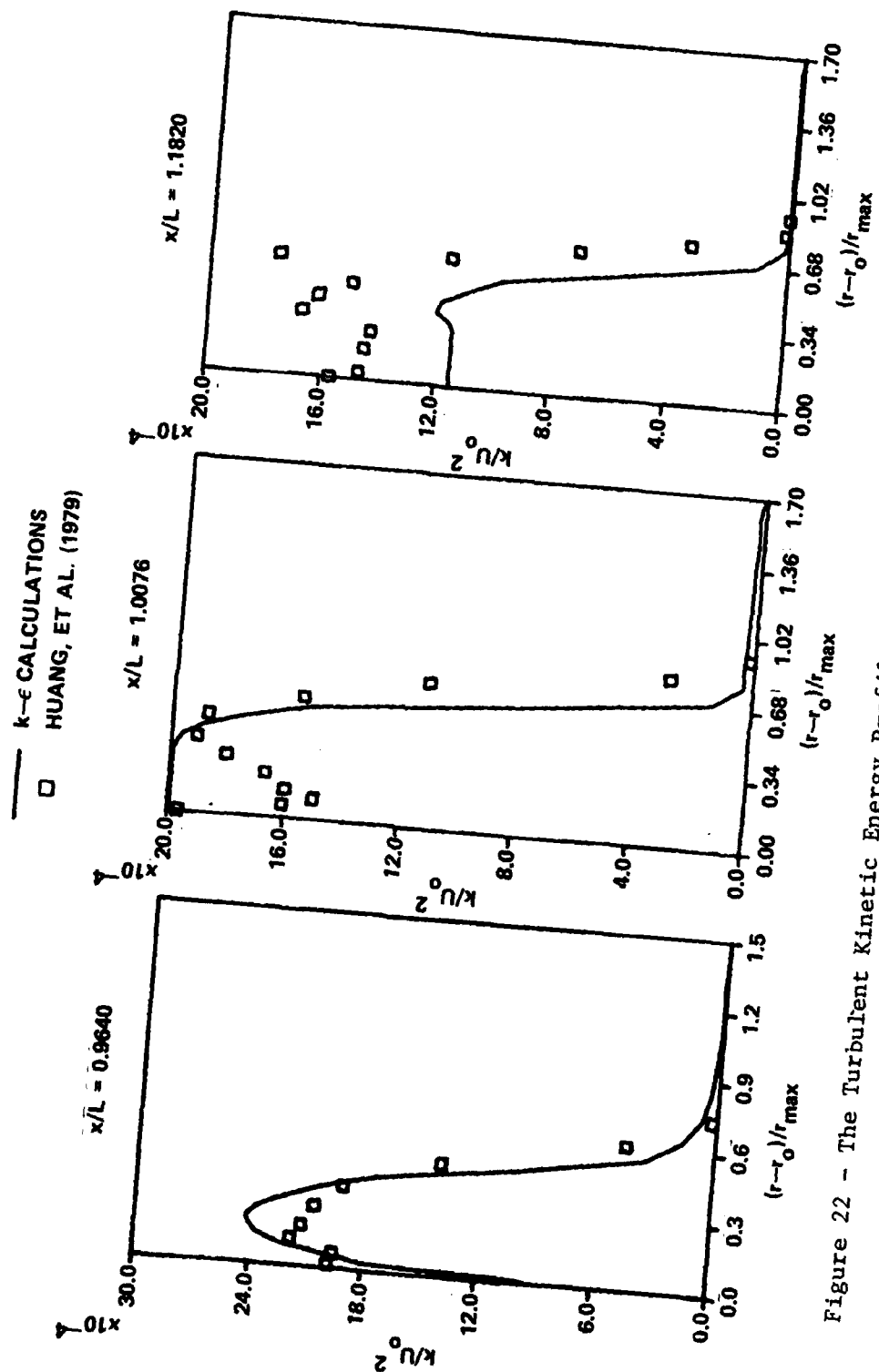
Figure 22 – The Turbulent Kinetic Energy Profiles at Three x-Stations for Afterbody 1

65
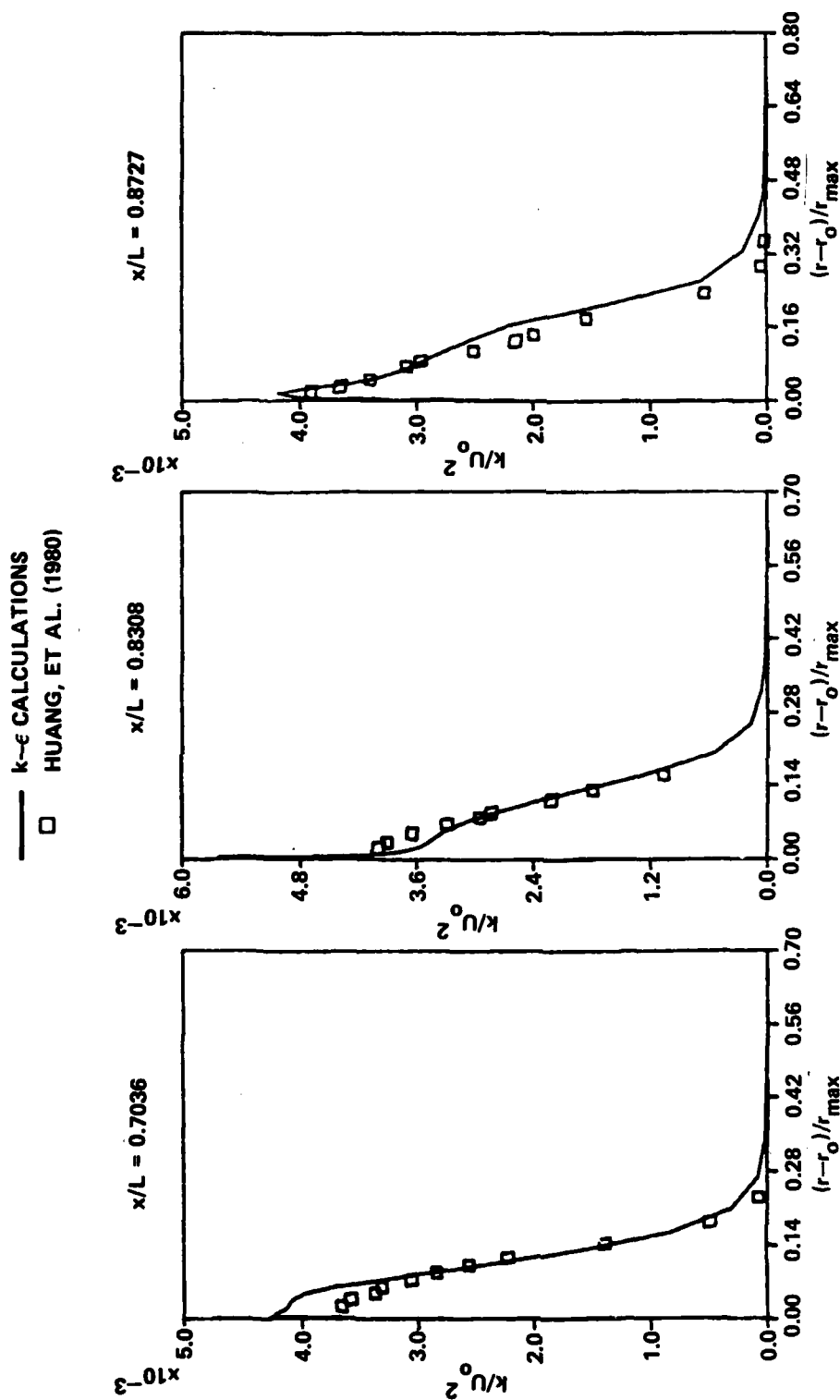
Figure 23 – The Turbulent Kinetic Energy Profiles at Three x-Stations for Afterbody 5

66
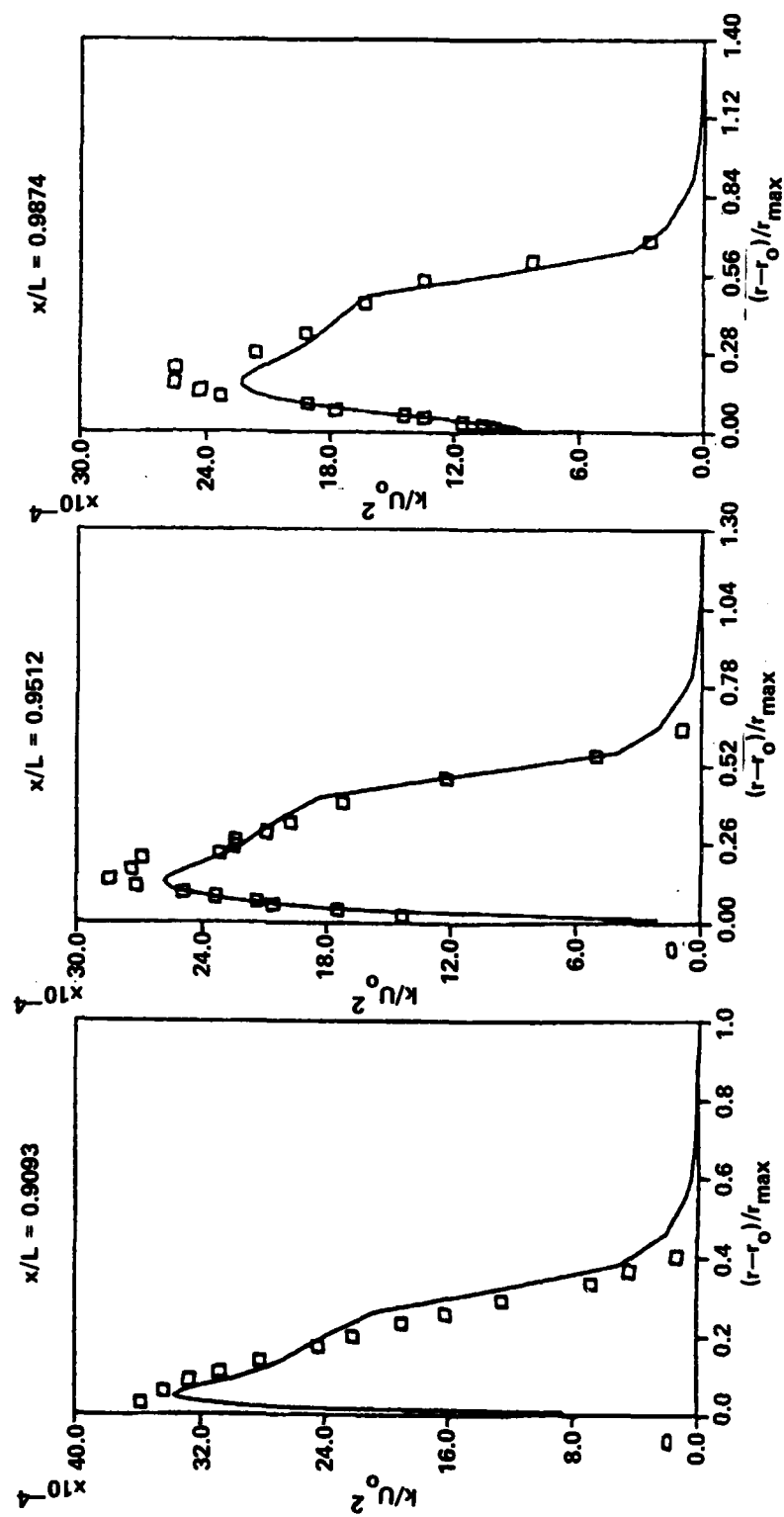
Figure 24 - The Turbulent Kinetic Energy Profiles at Three x-Stations for Afterbody 5
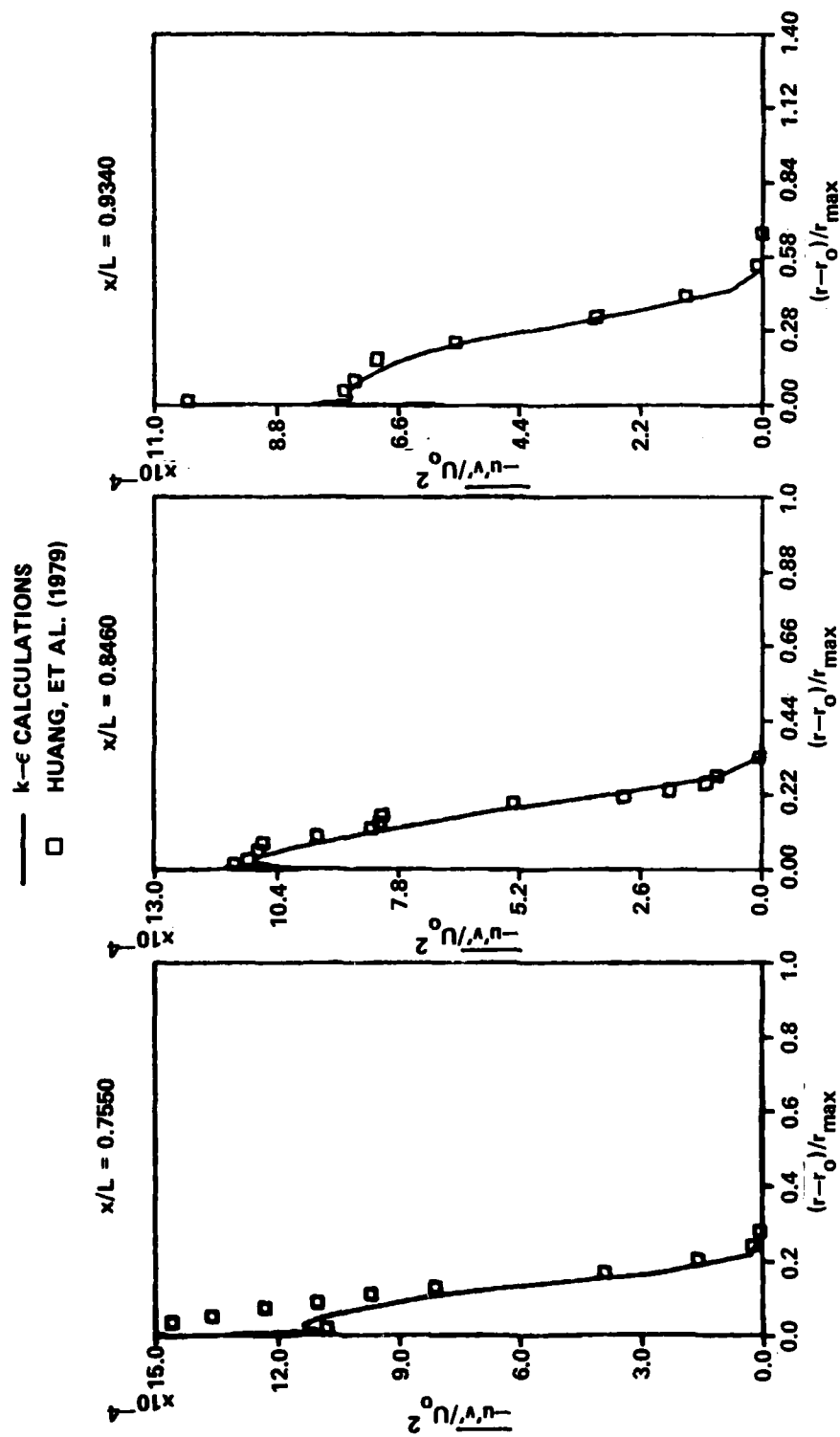
Figure 25 – The Normal Reynolds Stress Profiles at Three x-Stations for Afterbody 1
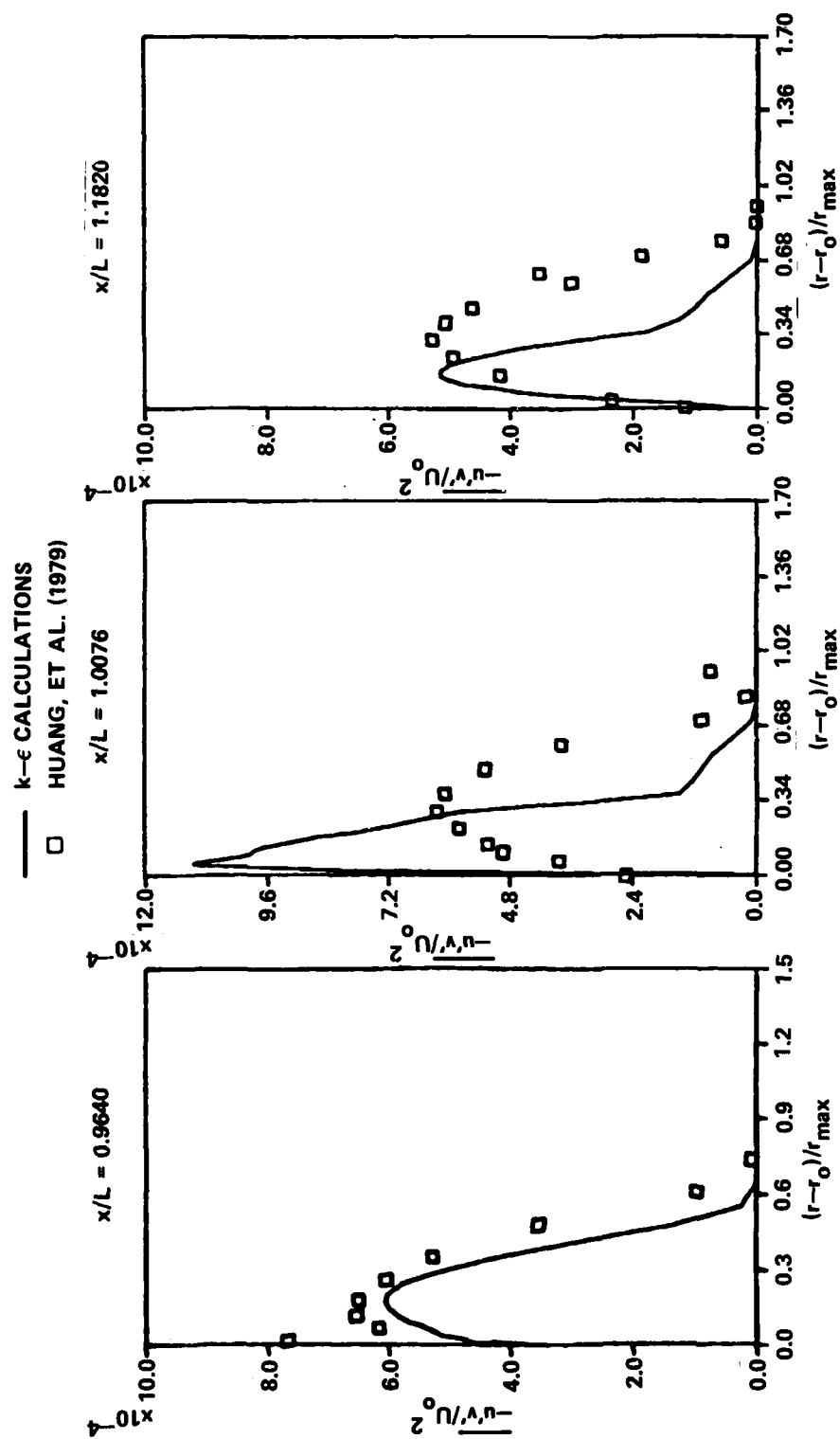
Figure 26 – The Normal Reynolds Stress Profiles at Three x-Stations for Afterbody 1
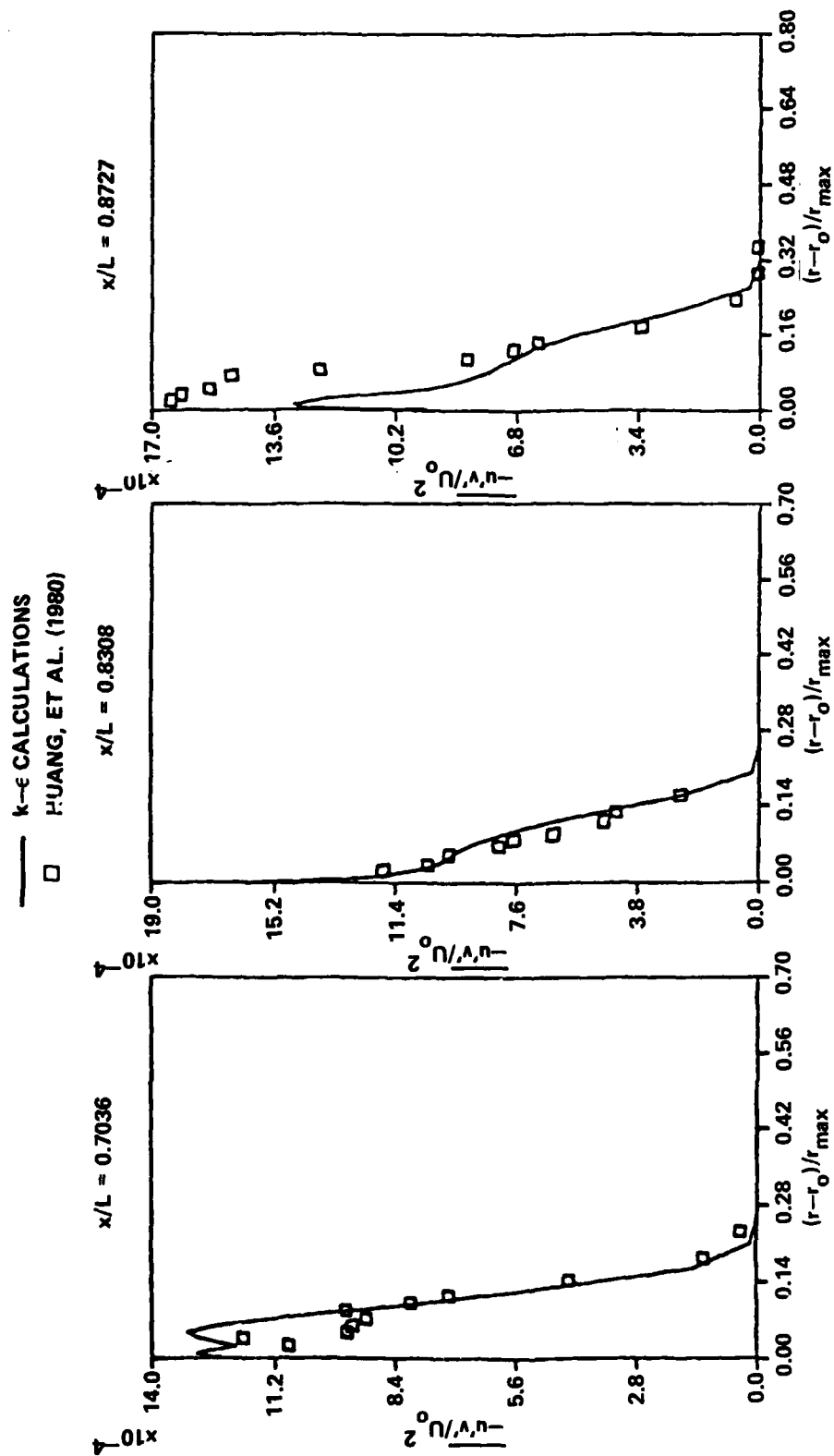
Figure 27 – The Normal Reynolds Stress Profiles at Three x-Stations for Afterbody 5
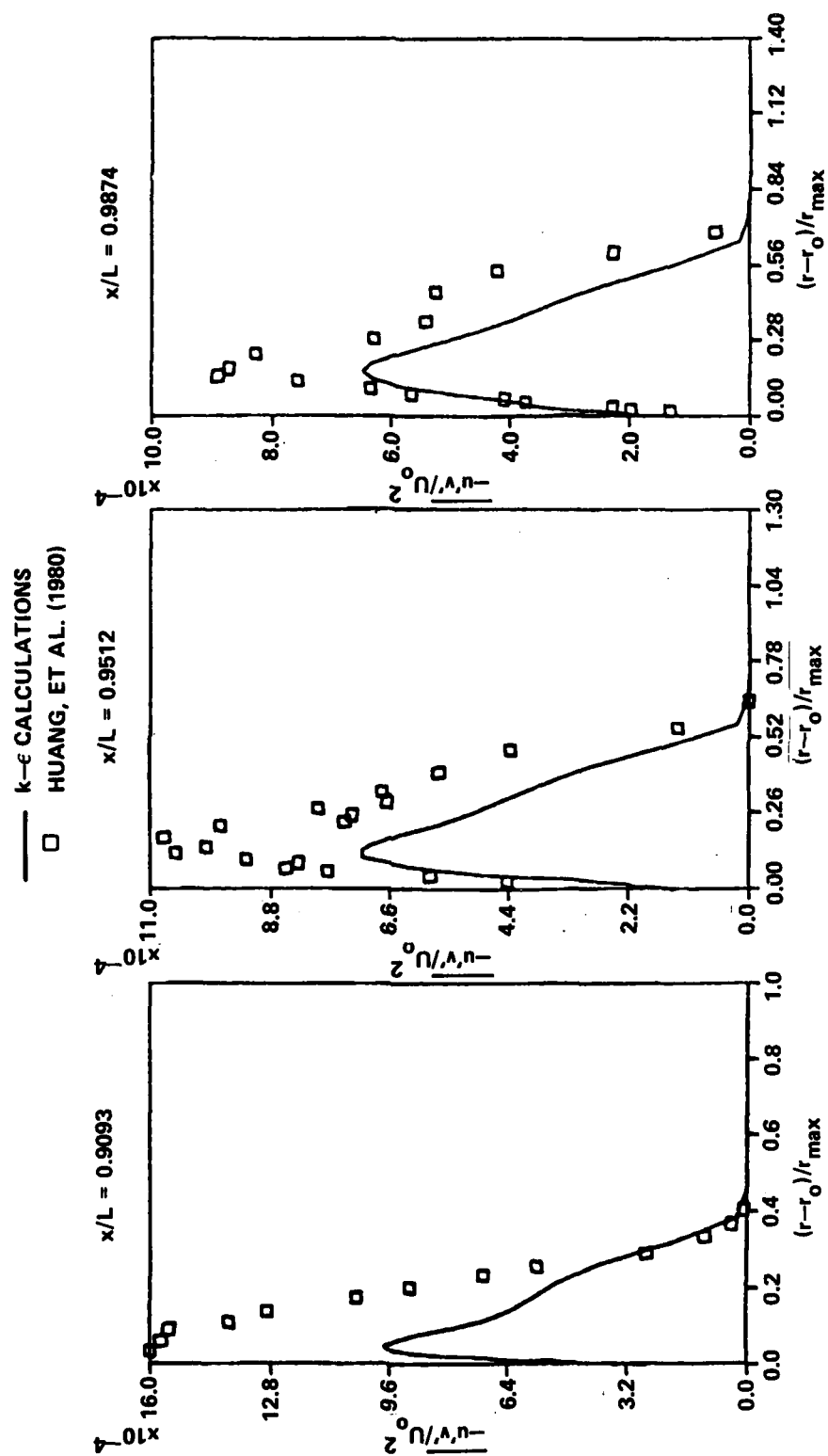
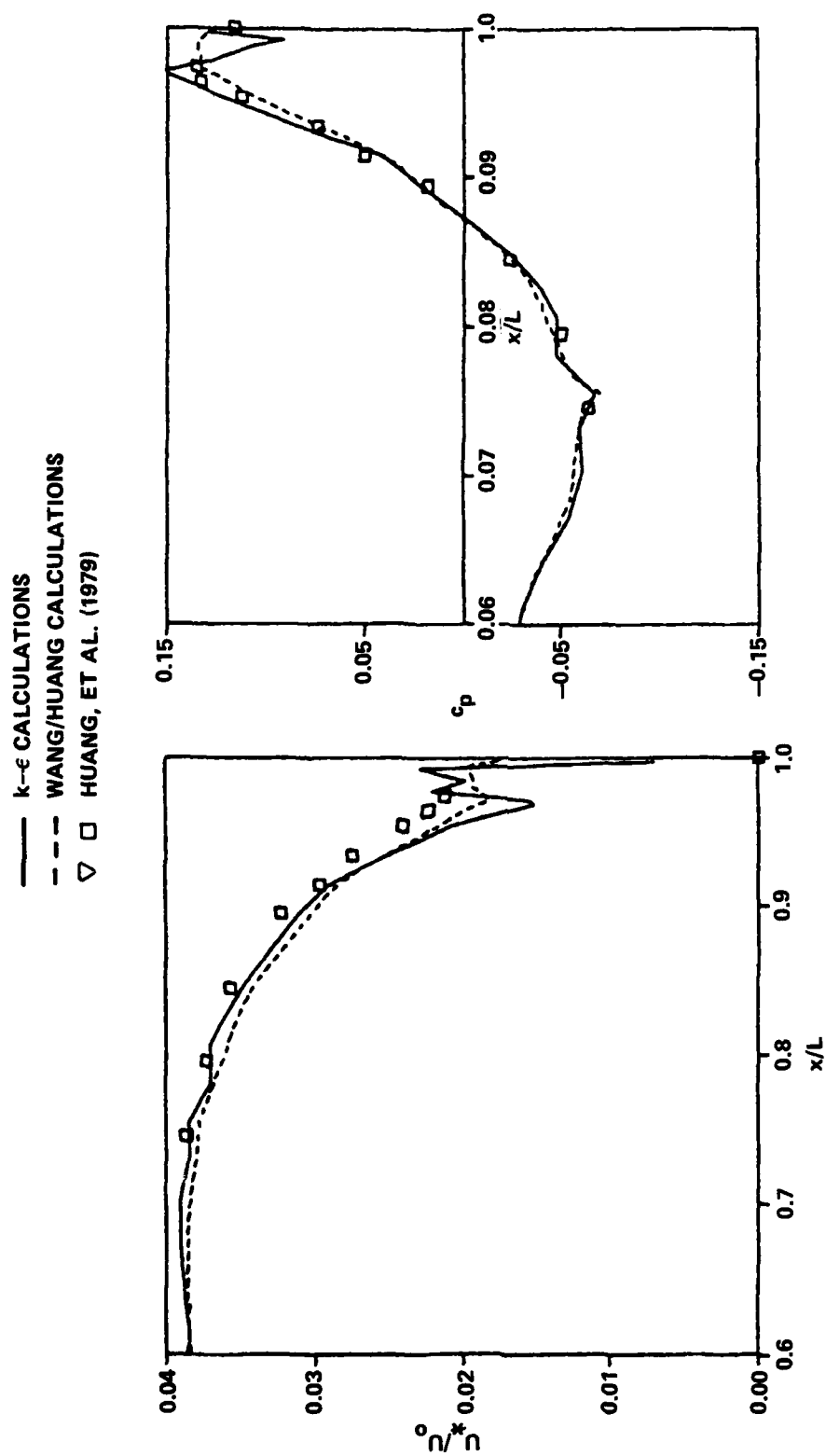Figure 28 – The Normal Reynolds Stress Profiles at Three x-Stations for Afterbody 5

Figure 29 – A Comparison of the u* and c_p Distributions for Afterbody 1
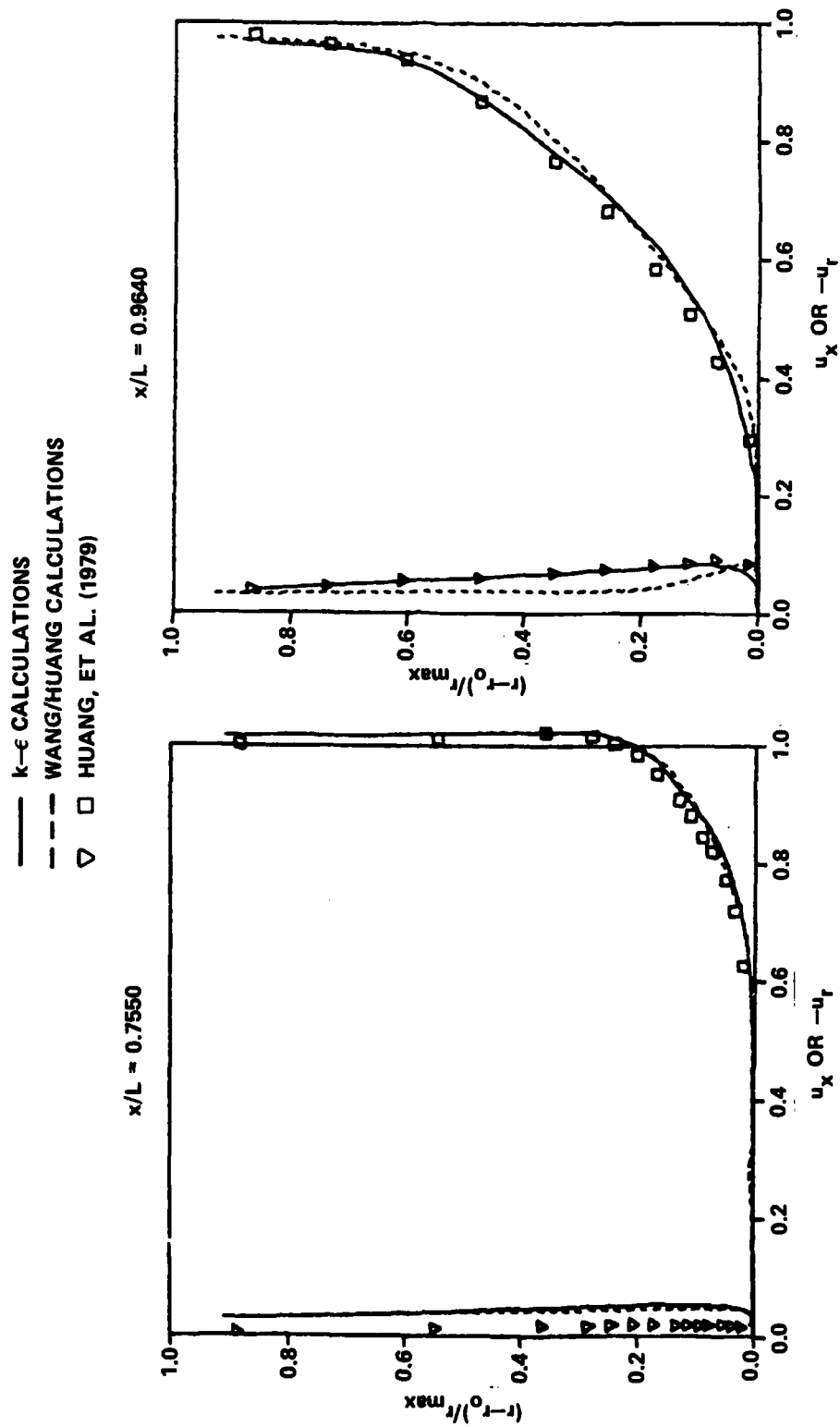
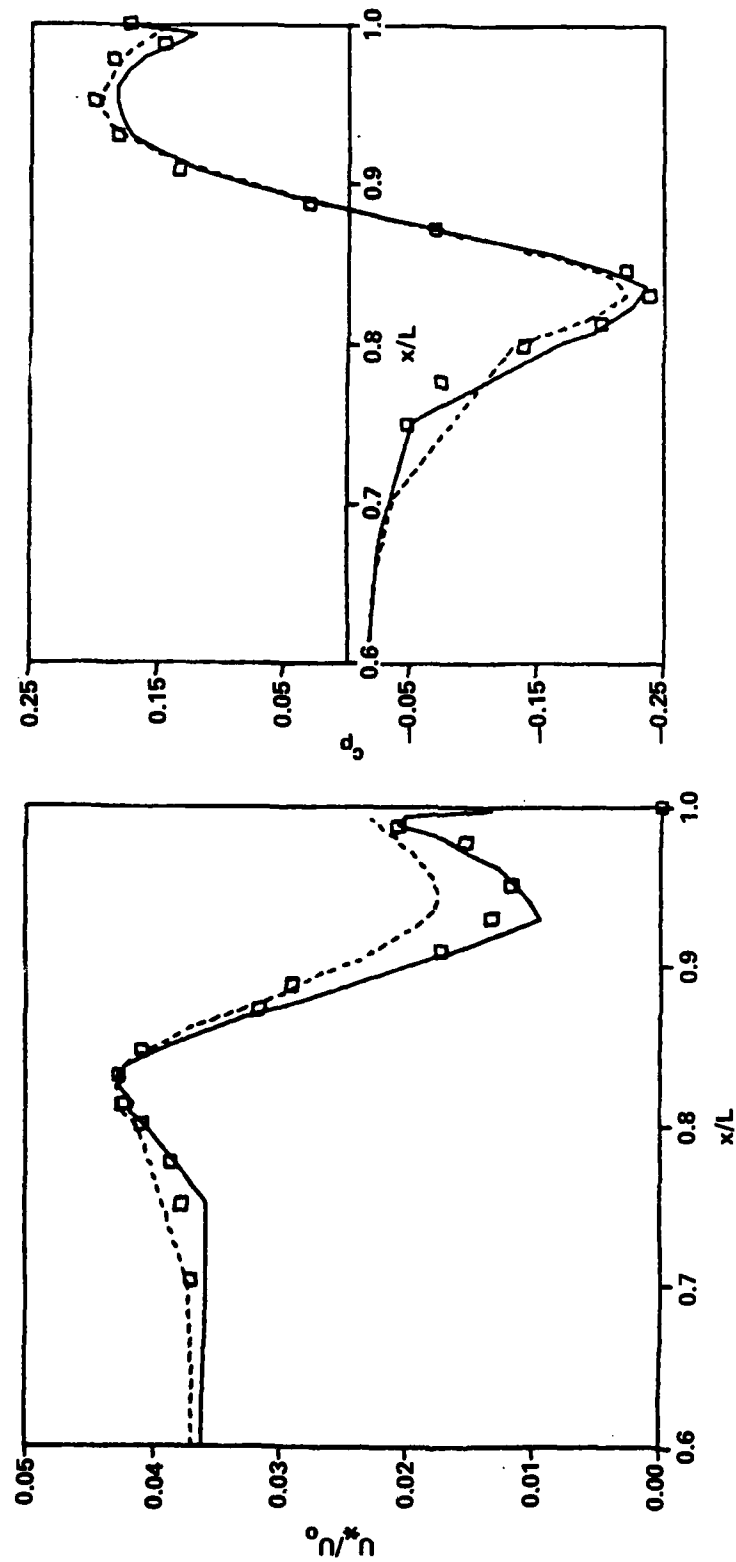Figure 30 - A comparison of Velocity Profiles at Two x-Stations for Afterbody 1

Figure 31 - A Comparison of the u* and c_p Distributions for Afterbody 5
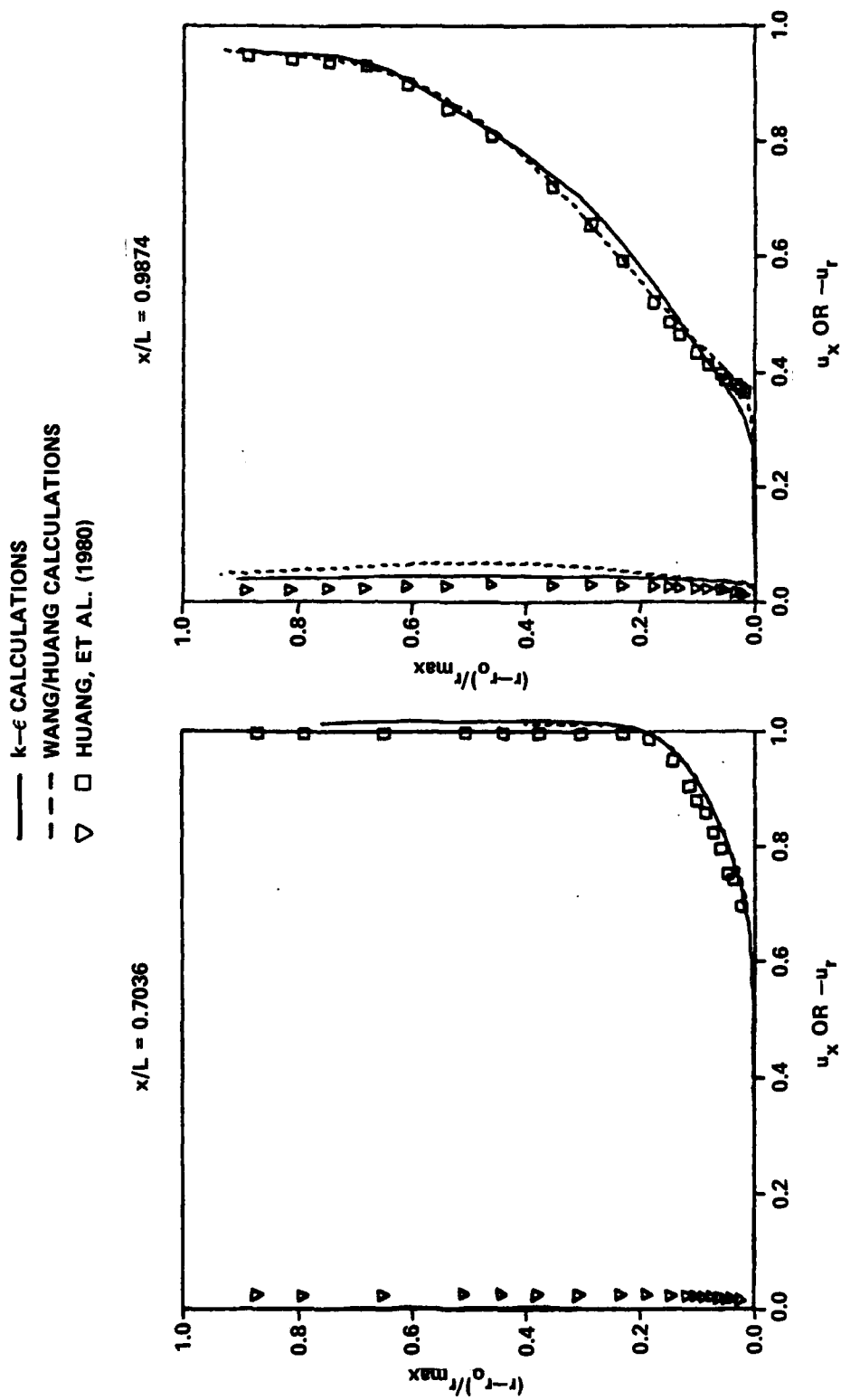
74

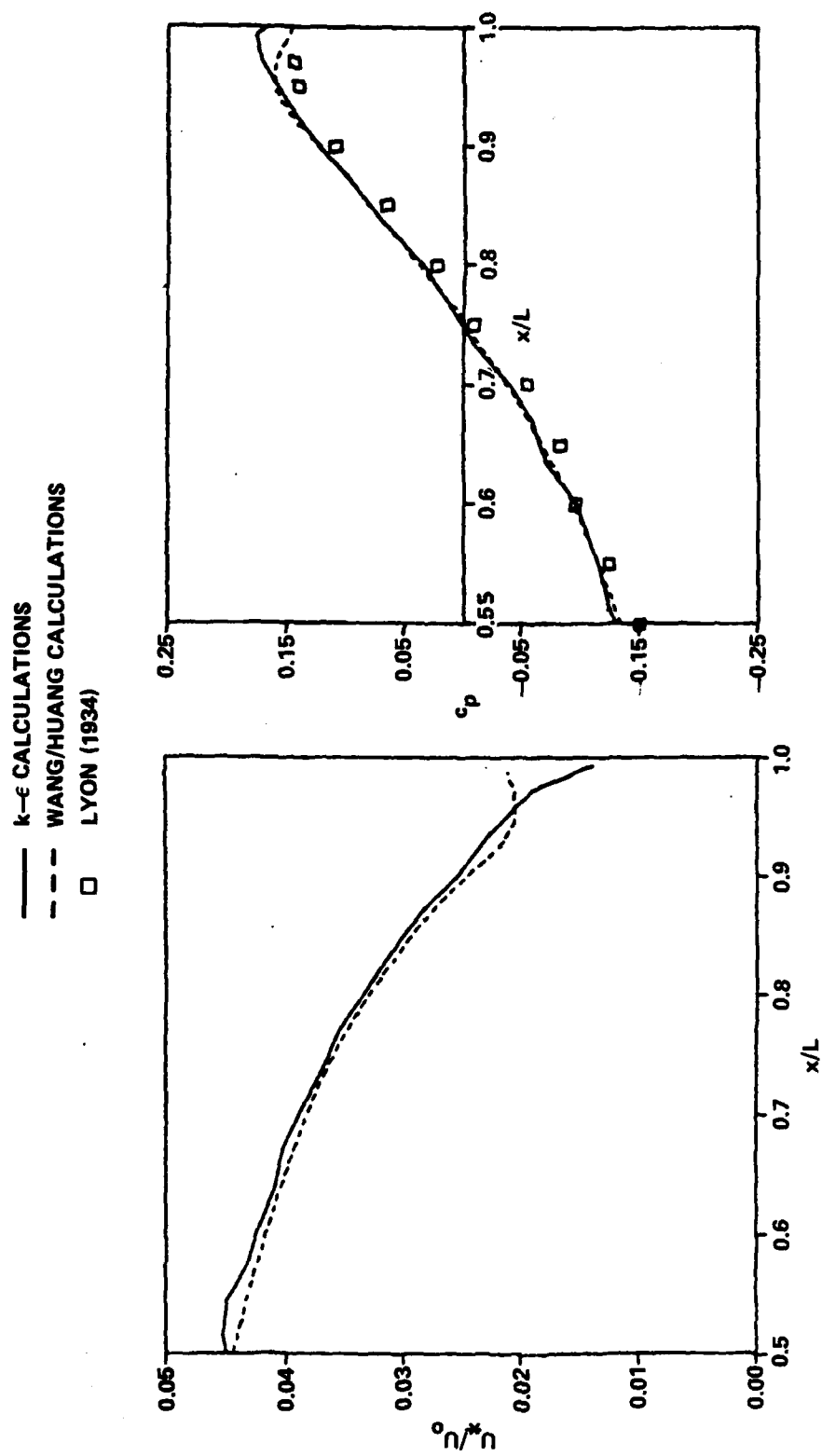Figure 32 – A Comparison of Velocity Profiles at Two x-Stations for Afterbody 5

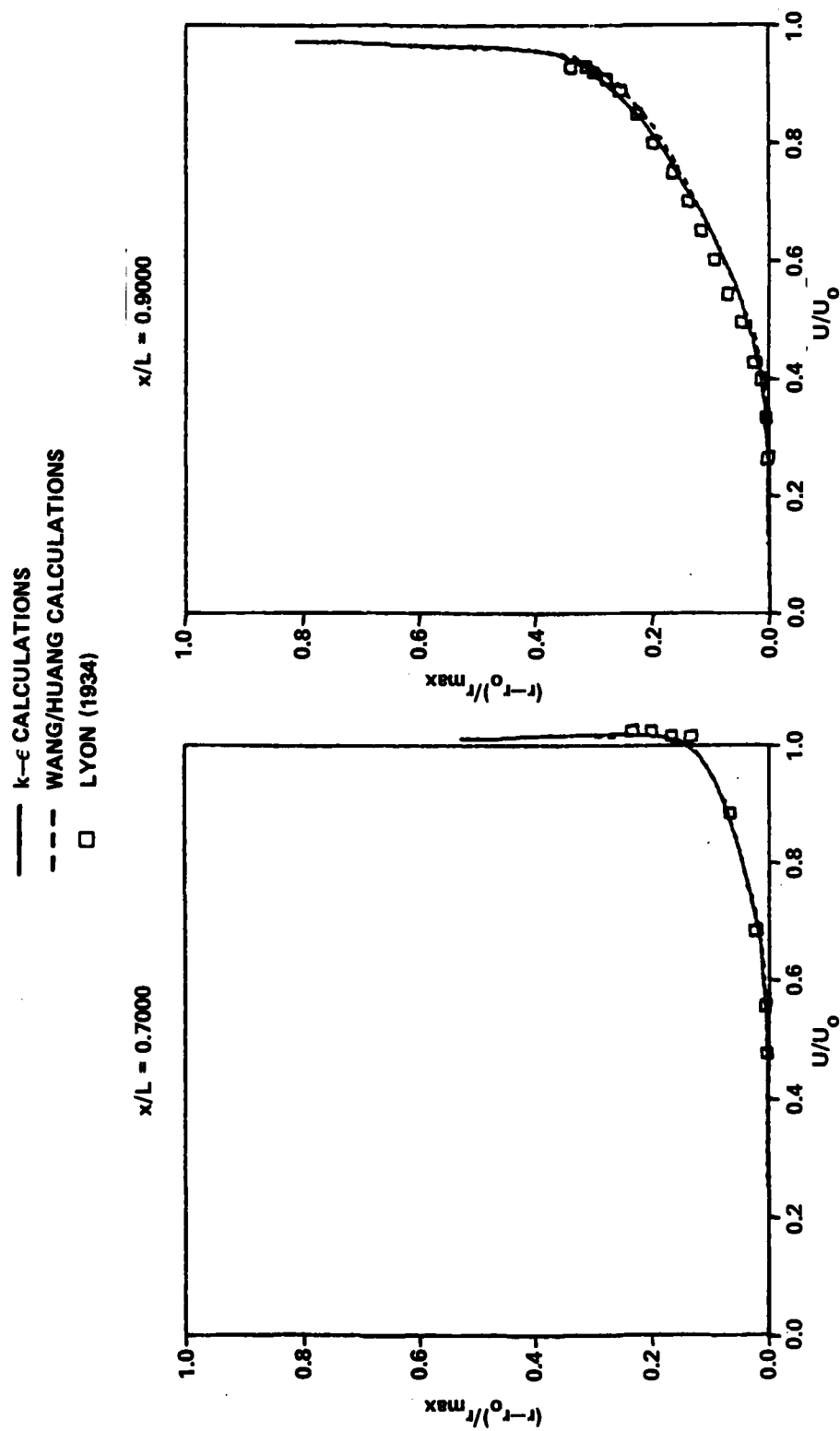Figure 33 – A Comparison of the u* and c_p Distributions for Model A

76

Figure 34 - A Comparison of the Total Velocity Profiles at Two x-Stations for Model A

Figure 35 – A Comparison of the u* and c_p Distributions for Model B

78
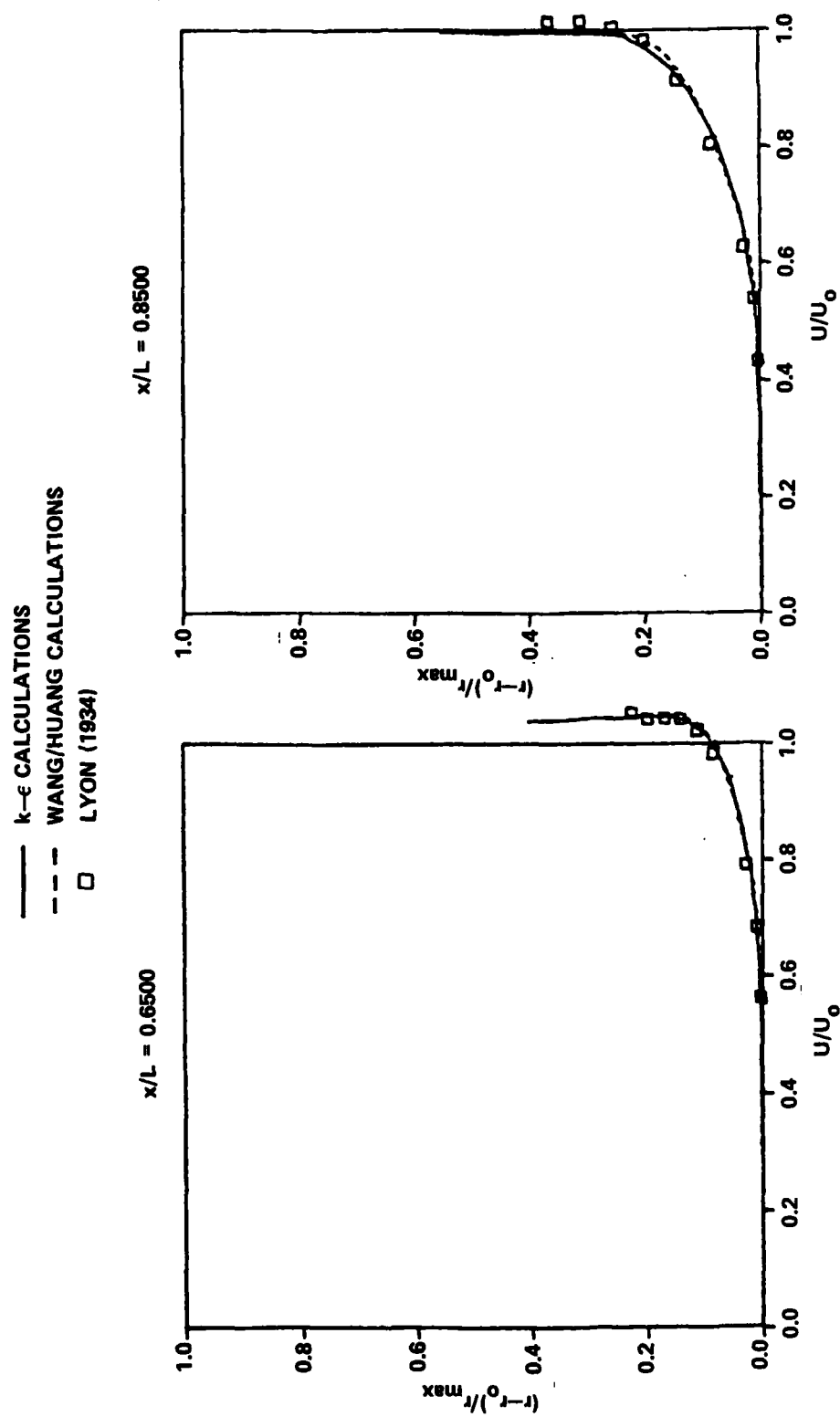
Figure 36 - A Comparison of the Total Velocity Profiles at Two x-Stations for Model B

79
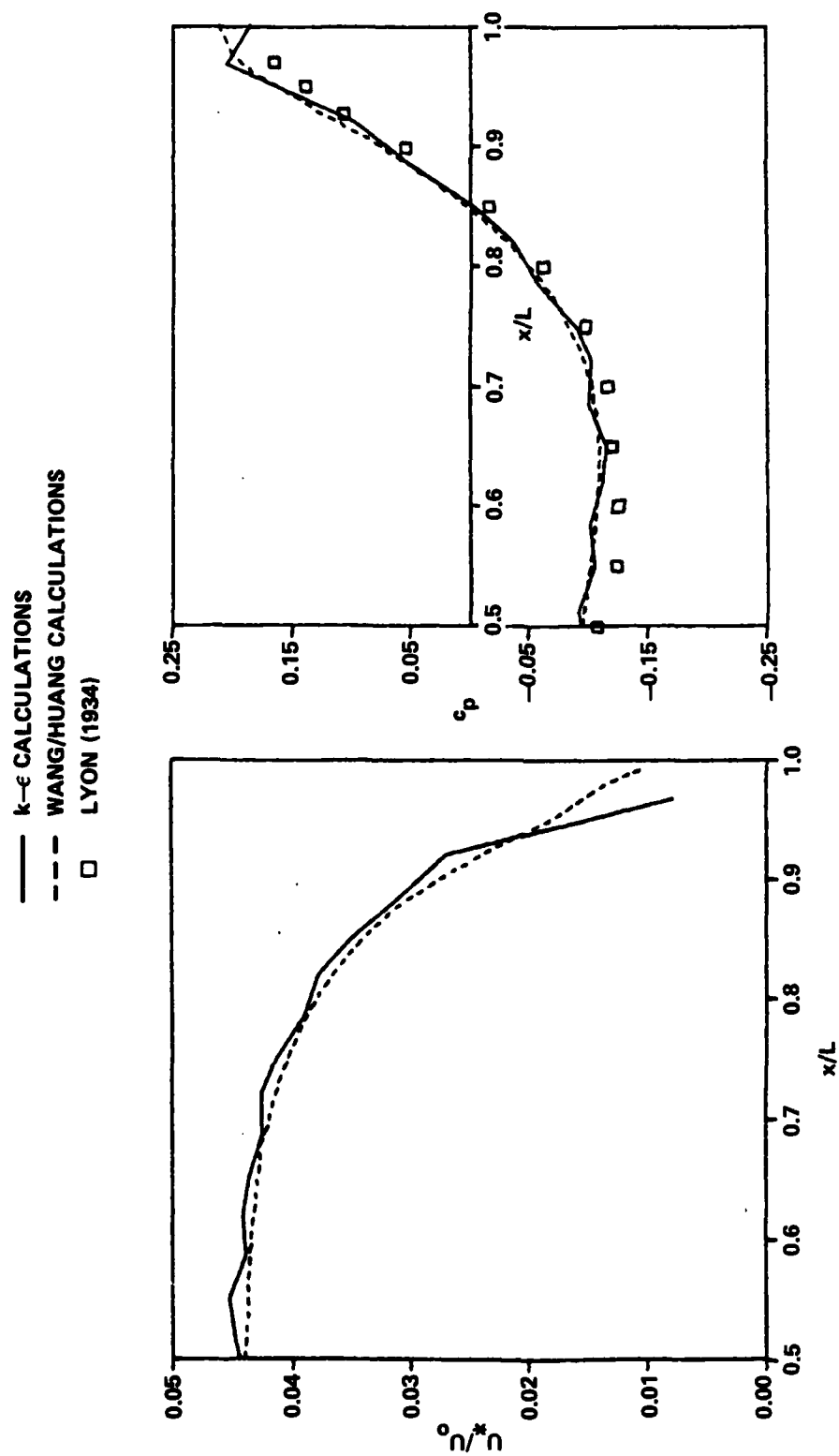
Figure 37 - The u* and c_p Distribution for Afterbody 5 with y+ = 100

Figure 38 – The Velocity Profiles at Three x-Stations for Afterbody 5 with y+ = 100

81

Figure 39 – The Pressure Profiles at Three x-Stations for Afterbody 5 with y+ = 100
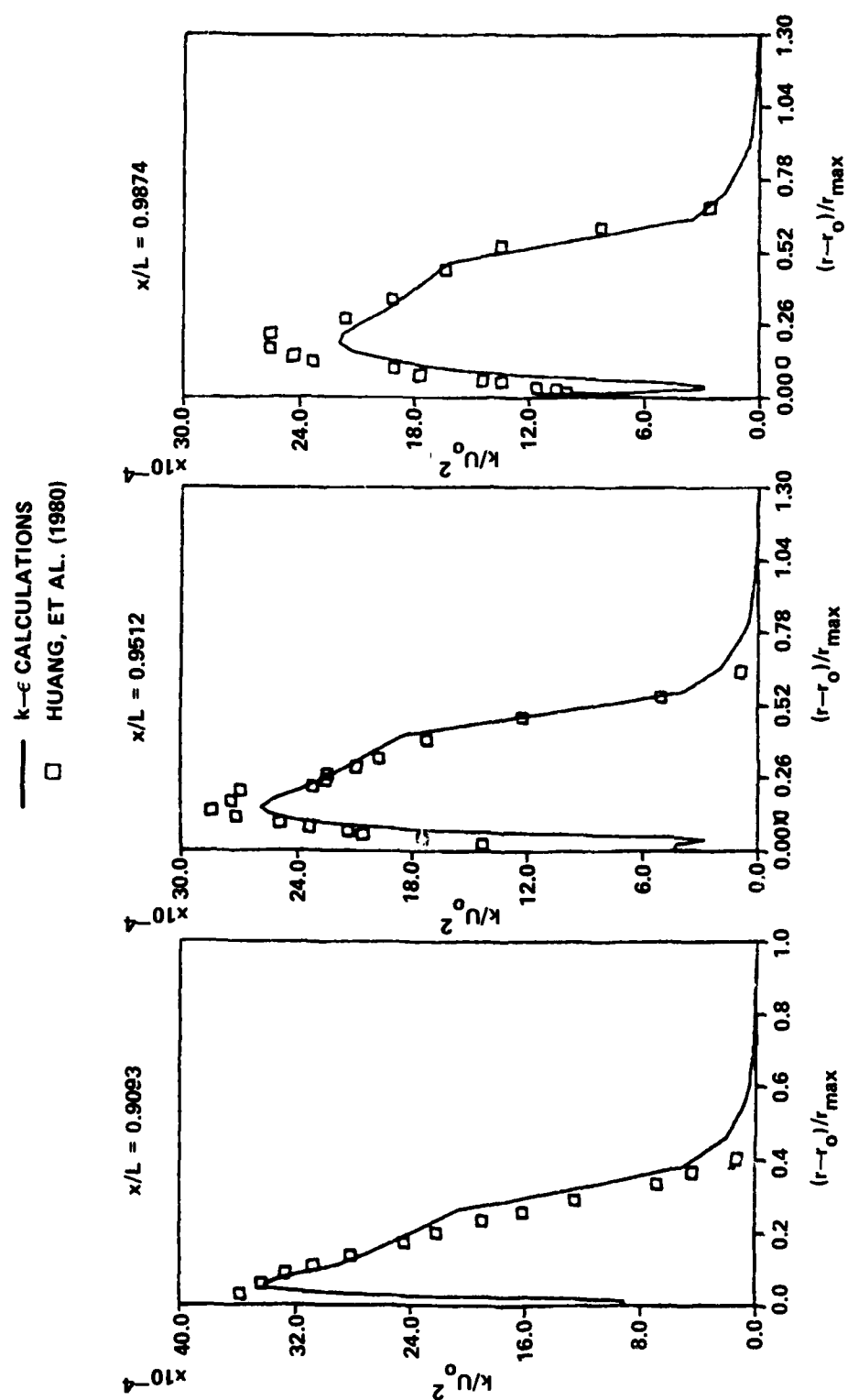
Figure 40 – The k/U_o^2 Profiles at Three x-Stations for Afterbody 5 with y+ = 100

83

A CALCULATION OF THE PARABOLIZED NAVIER-STOKES
EQUATIONS FOR TURBULENT AX.. (U) DAVID W TAYLOR NAVAL
SHIP RESEARCH AND DEVELOPMENT CENTER BET..   T F HOGAN
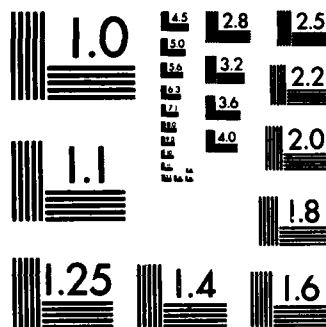
MICROCOPY RESOLUTION TEST CHART

NATIONAL BUREAU OF STANDARDS-1963-A
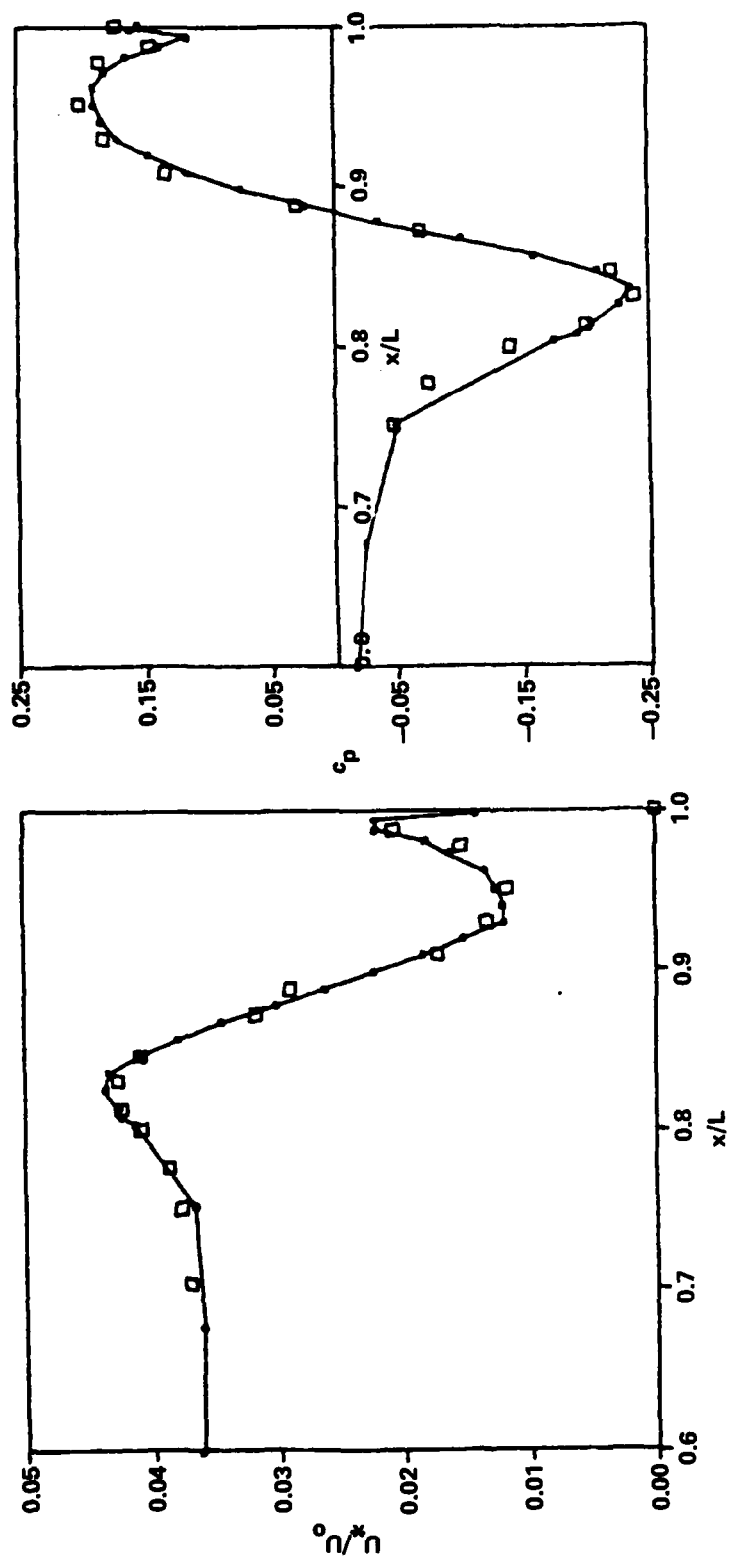
Figure 41 - The u* and c_p Distribution for Afterbody 5 with y+ = 300

84
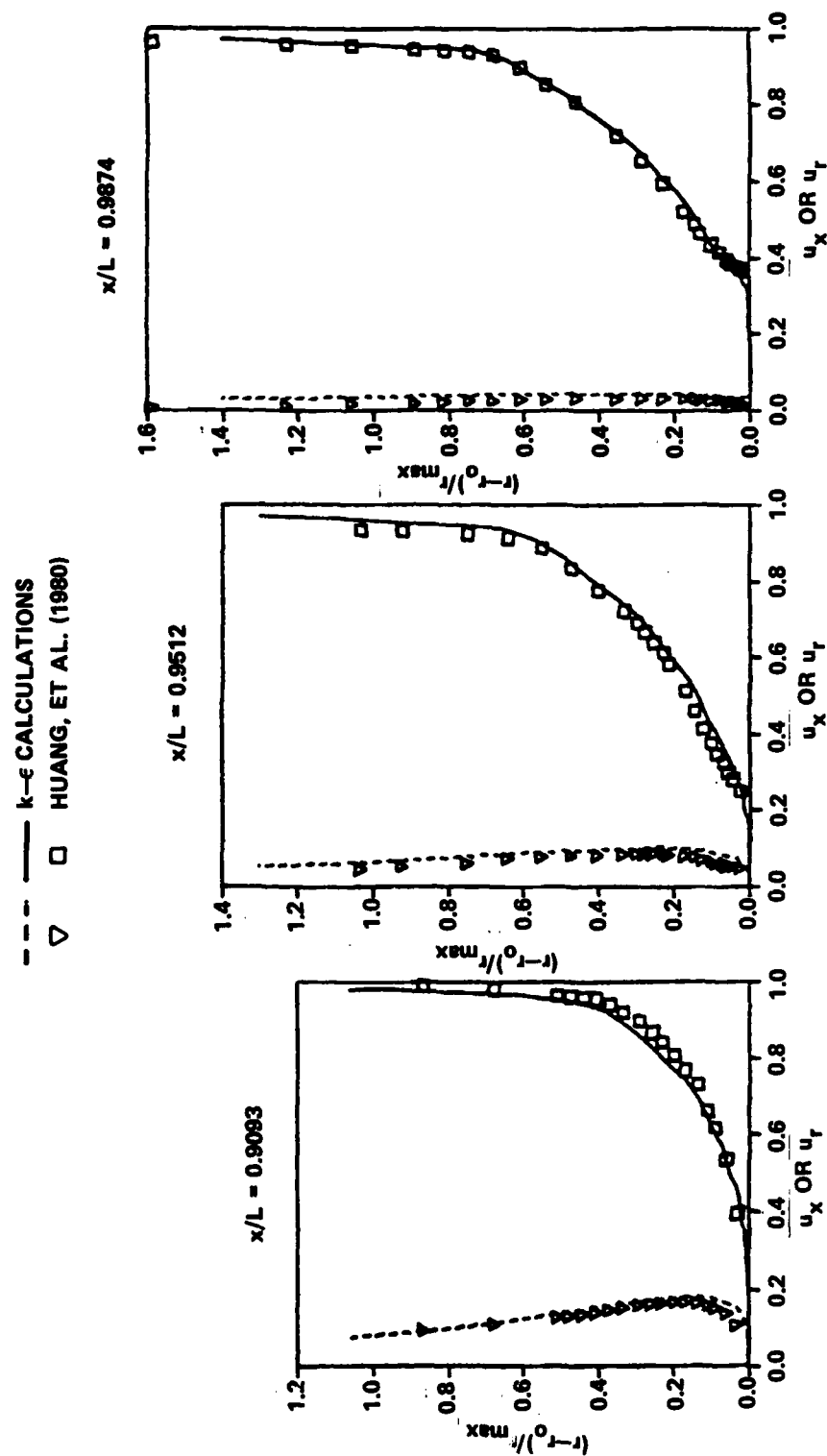
Figure 42 - The Velocity Profiles at Three x-Stations for Afterbody 5 with y+ = 300
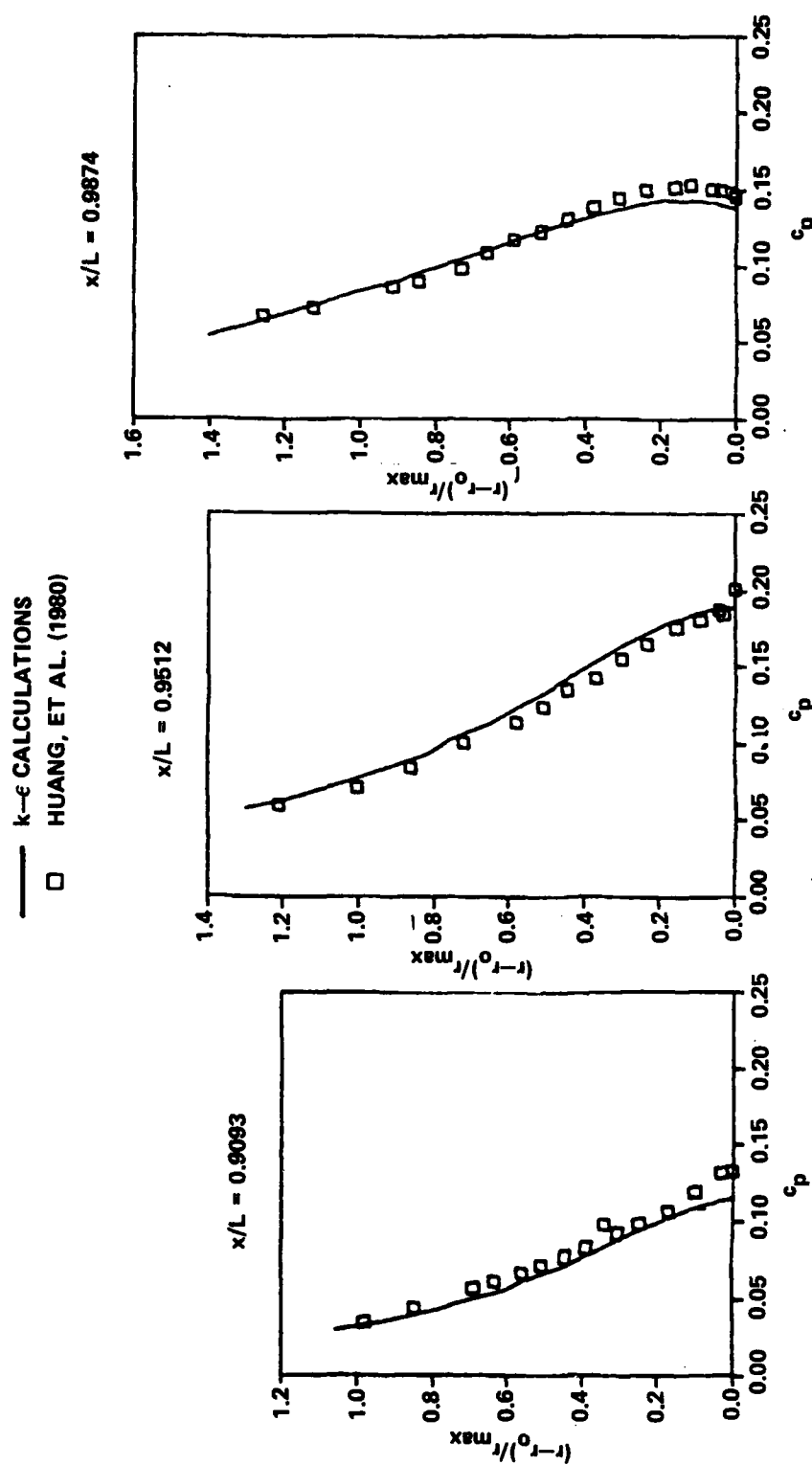
Figure 43 - The Pressure Profiles at Three x-Stations for Afterbody 5 with y+ = 300
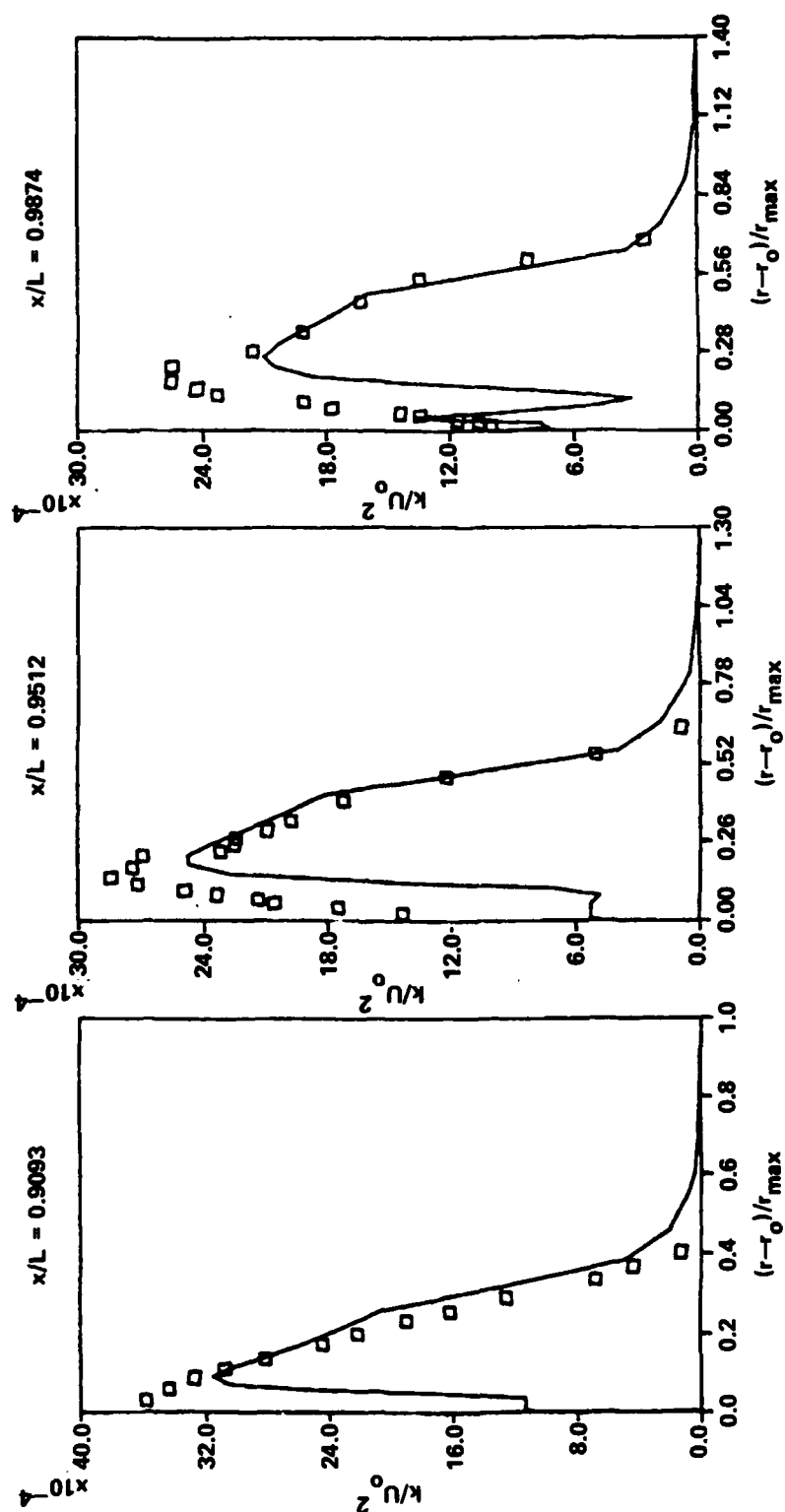
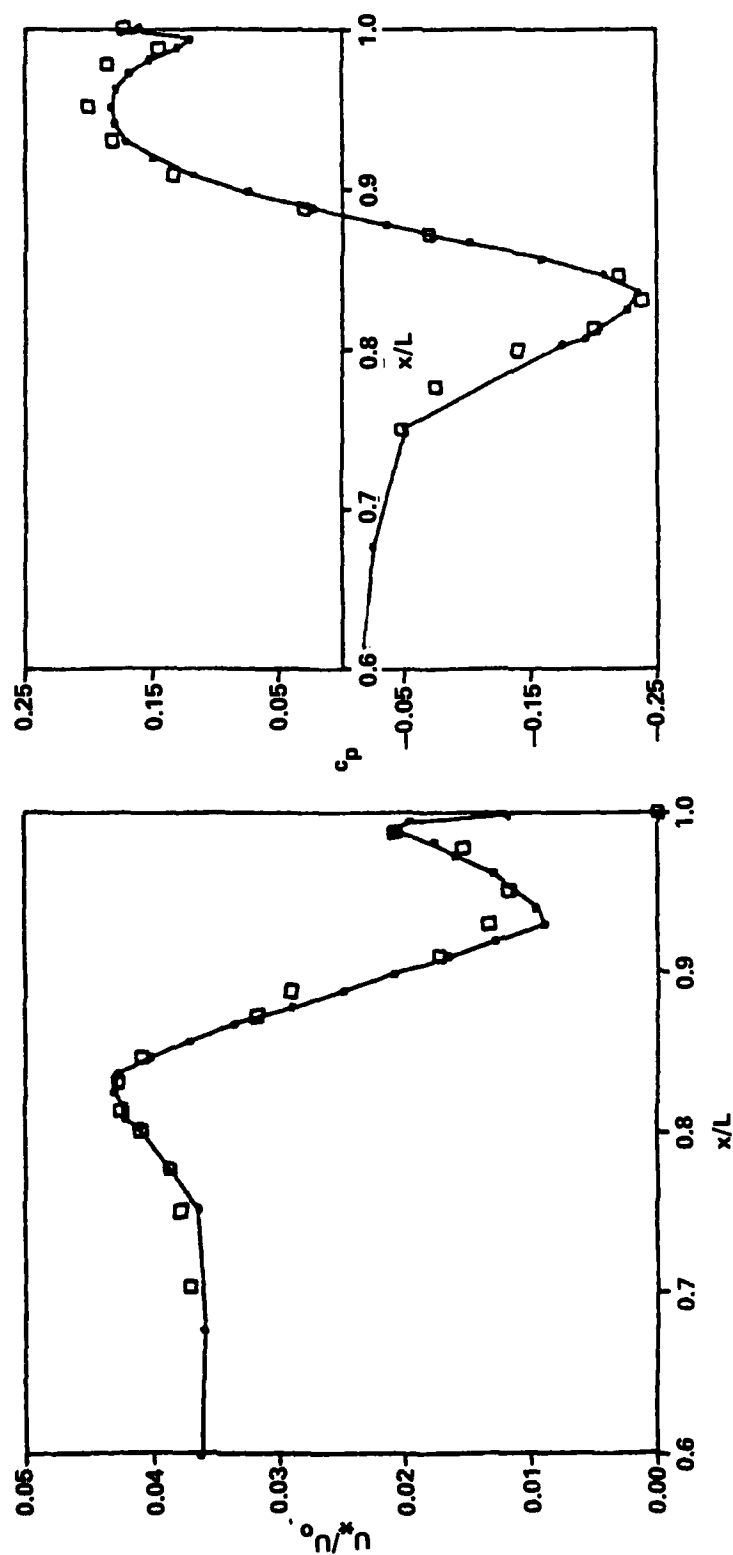Figure 44 – The k/U_o^2 Profile at Three x-Stations for Afterbody 5 with y+ = 300

87
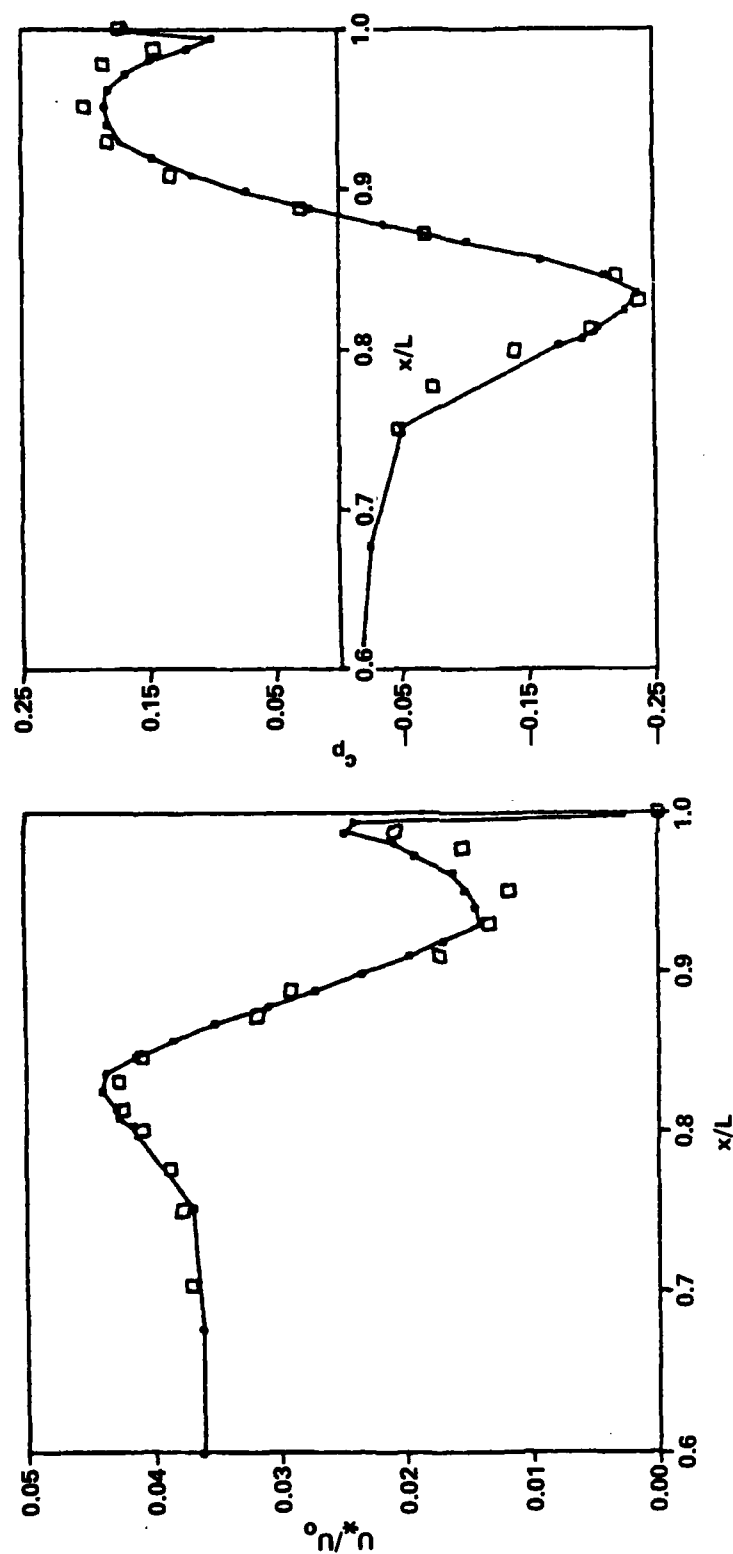
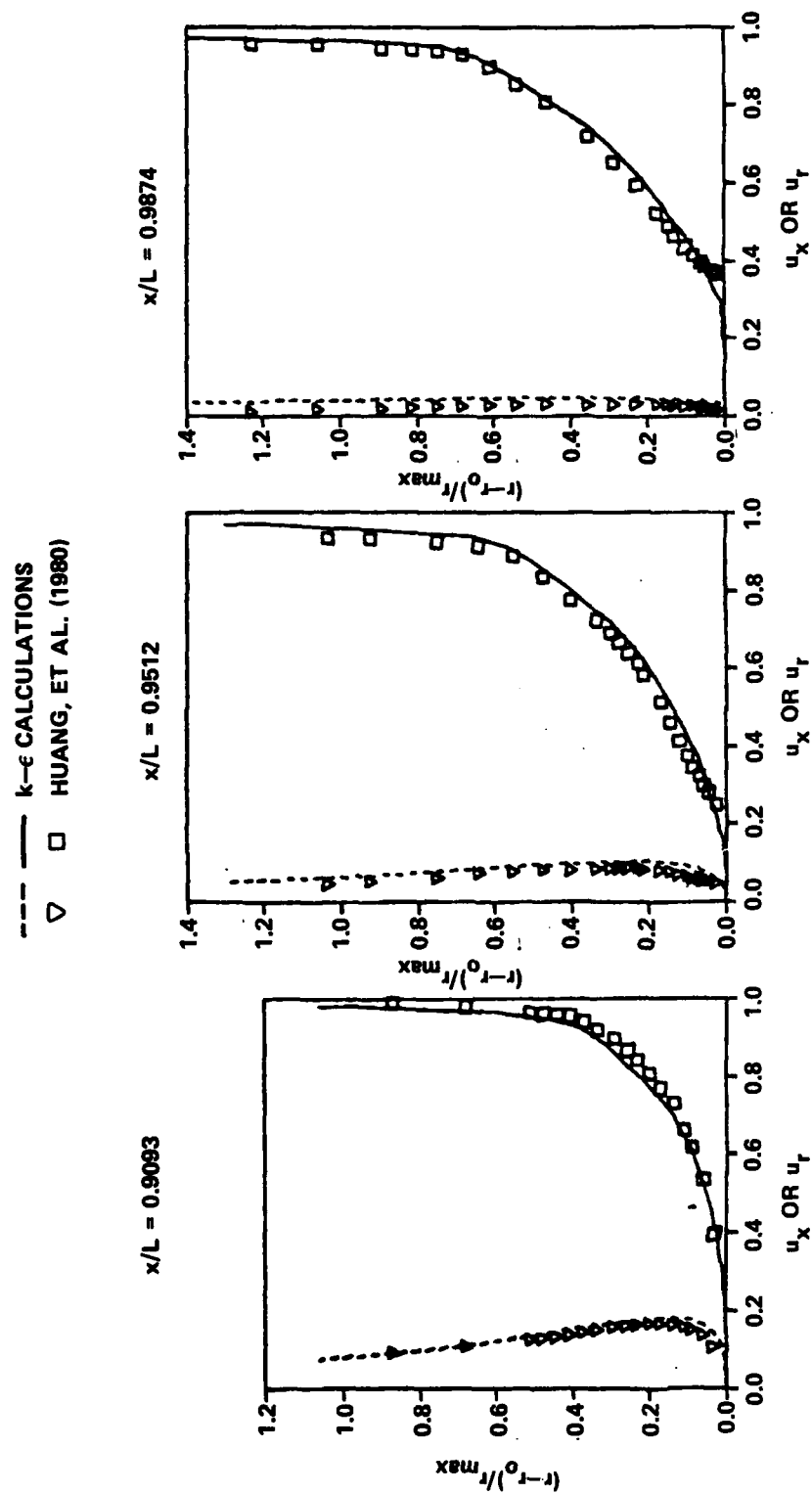Figure 45 – The u* and c_p Distribution for Afterbody 5 with y+ = 500
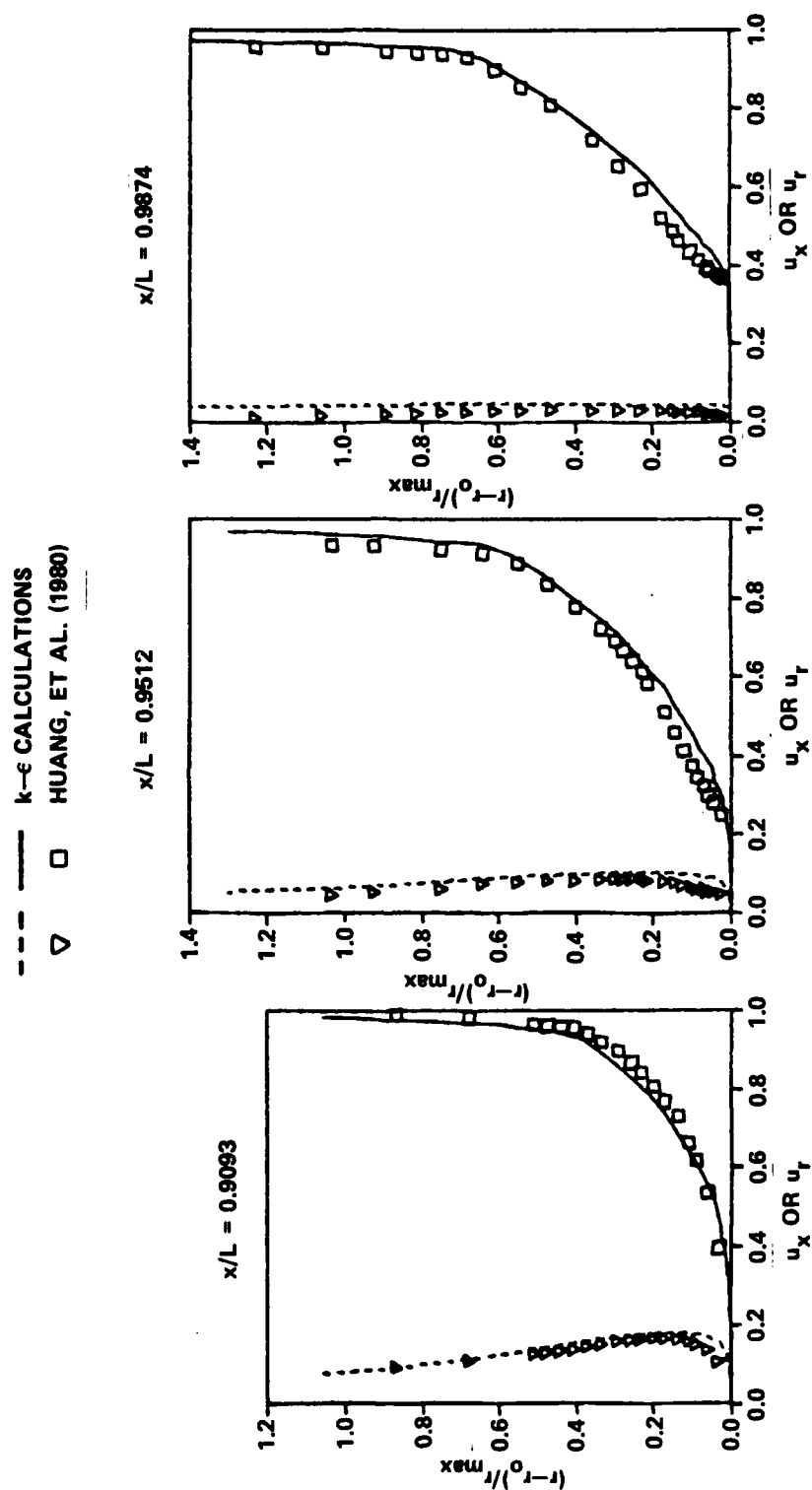
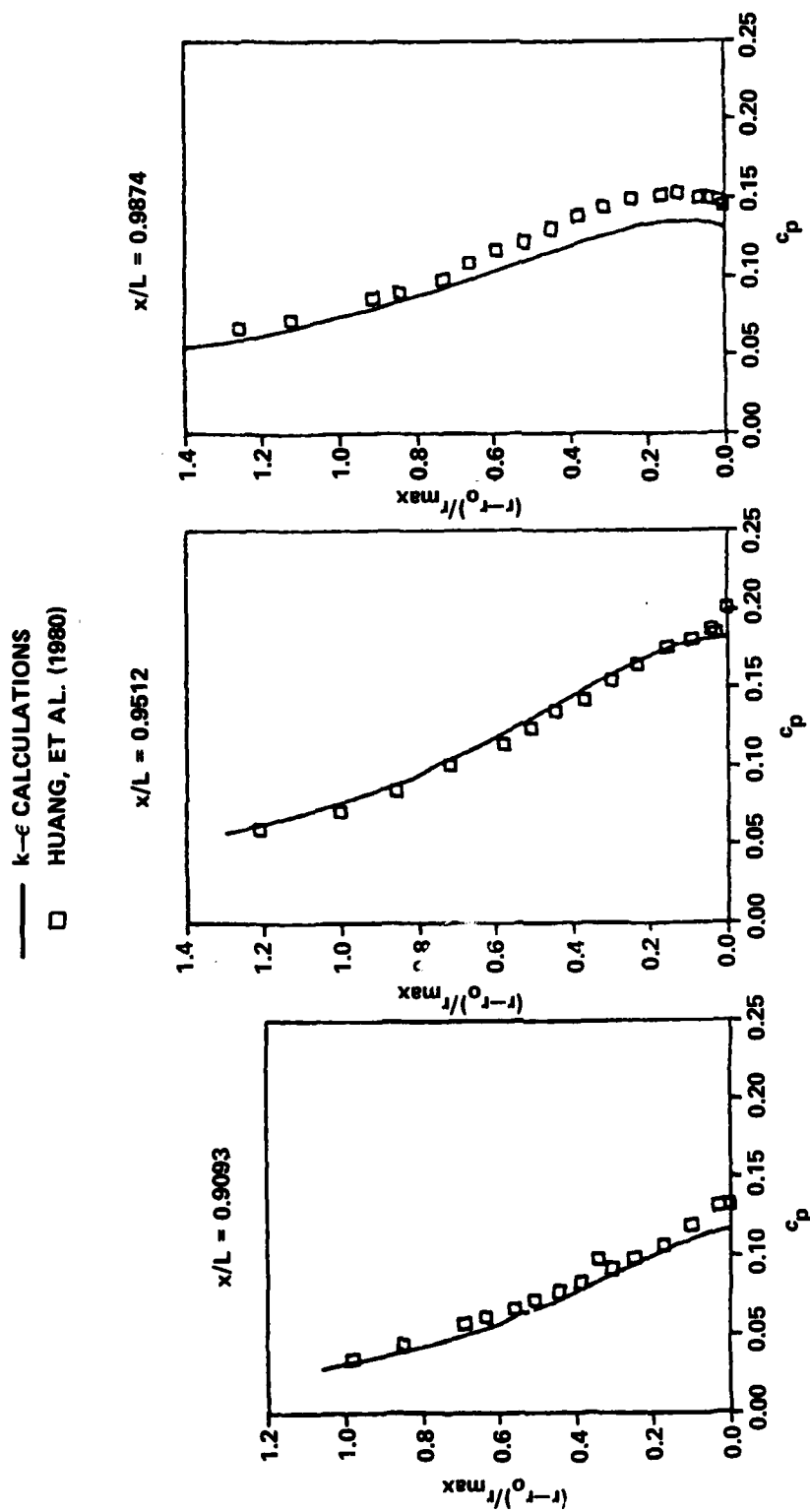Figure 46 – The Velocity Profiles at Three x-Stations for Afterbody 5 with y+ = 500
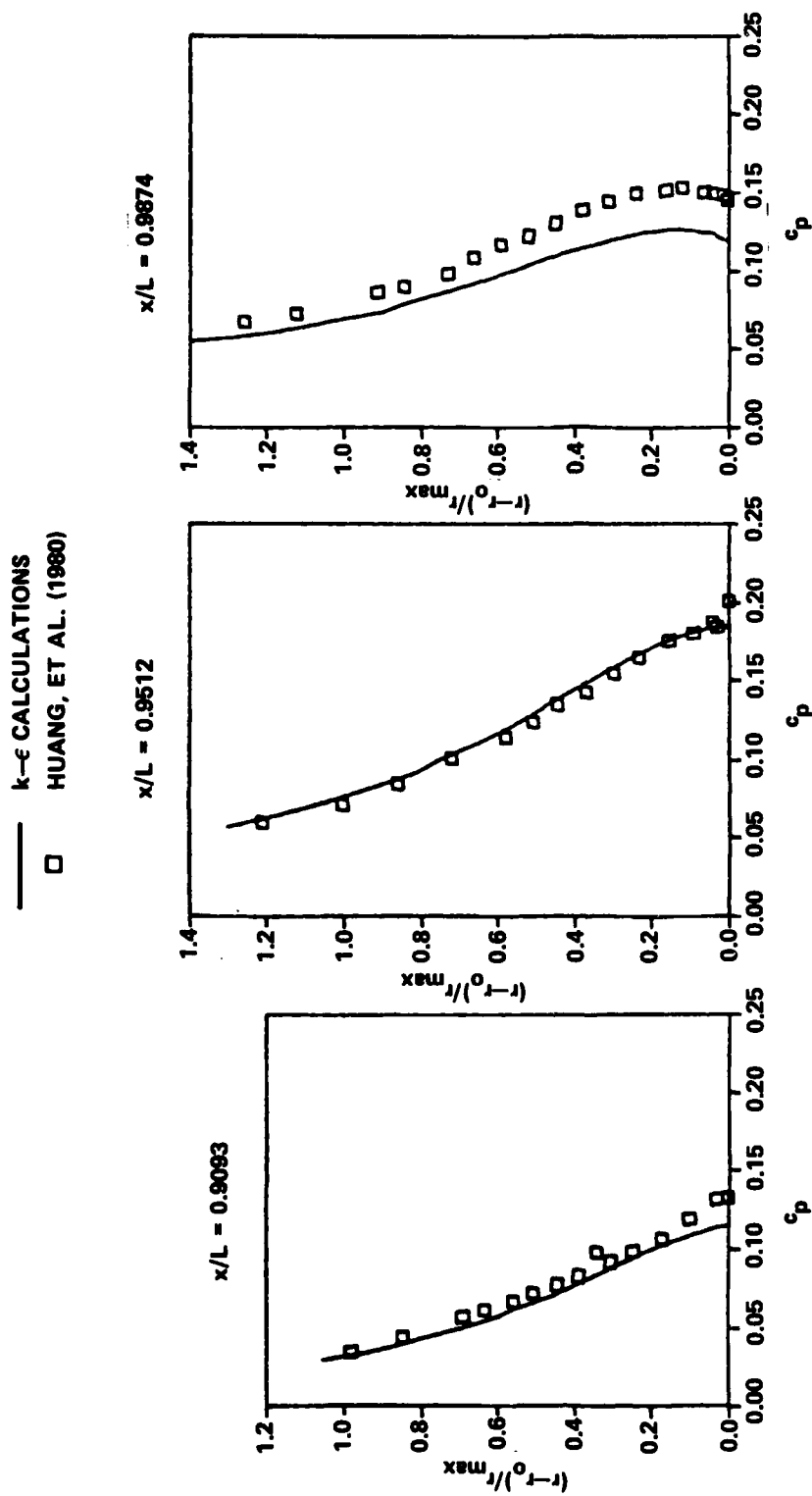
Figure 47 - The Pressure Profiles at Three x-Stations for Afterbody 5 with y+ = 500
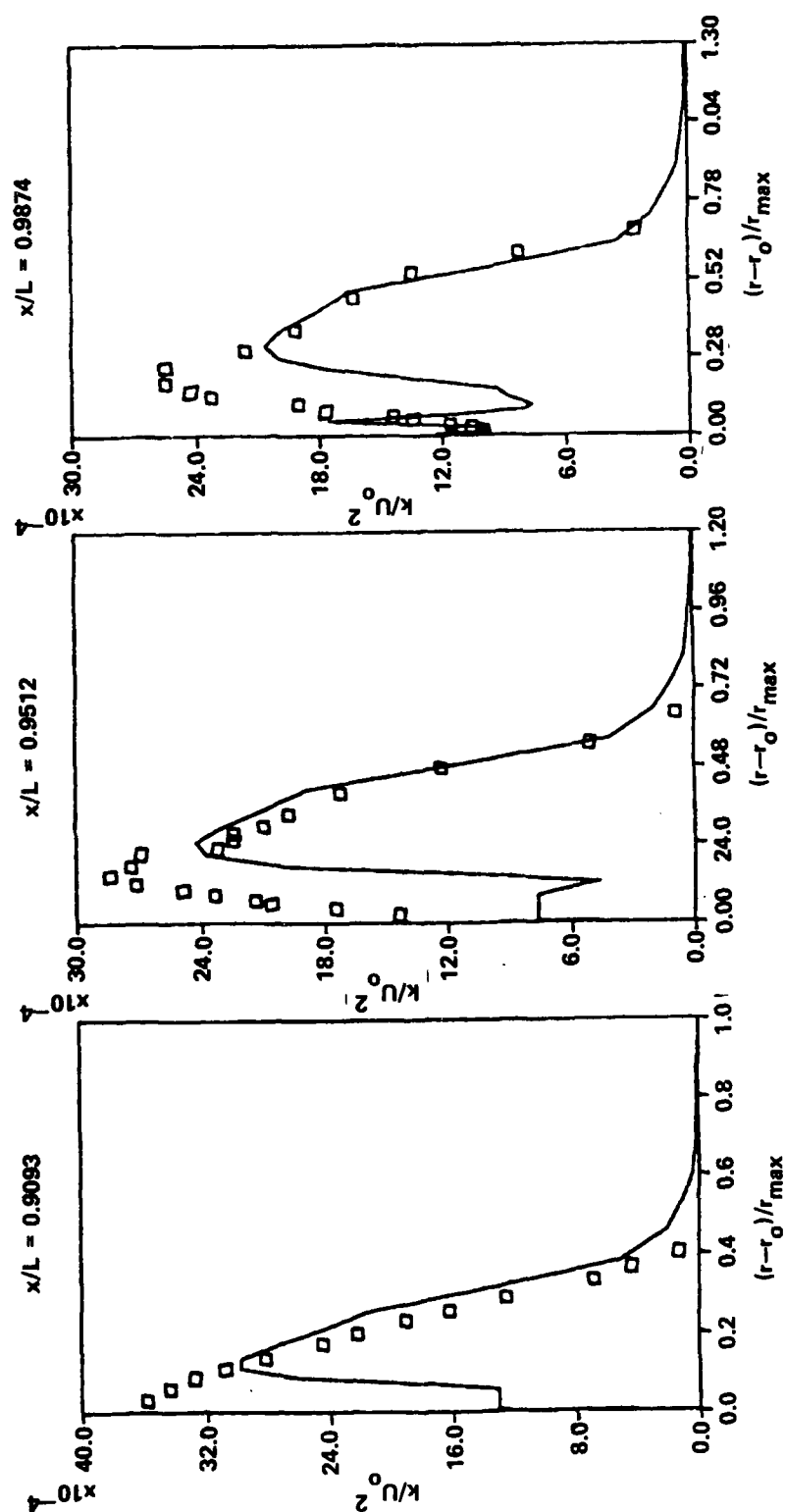
Figure 48 - The k/U_o^2 Profiles at Three x-Stations for Afterbody 5 with $y+$ = 500

91

Figure 49 - Comparison of the Computed u^* and c_p Distribution for Afterbody 5 at $Re = 1 \times 10^8$

92
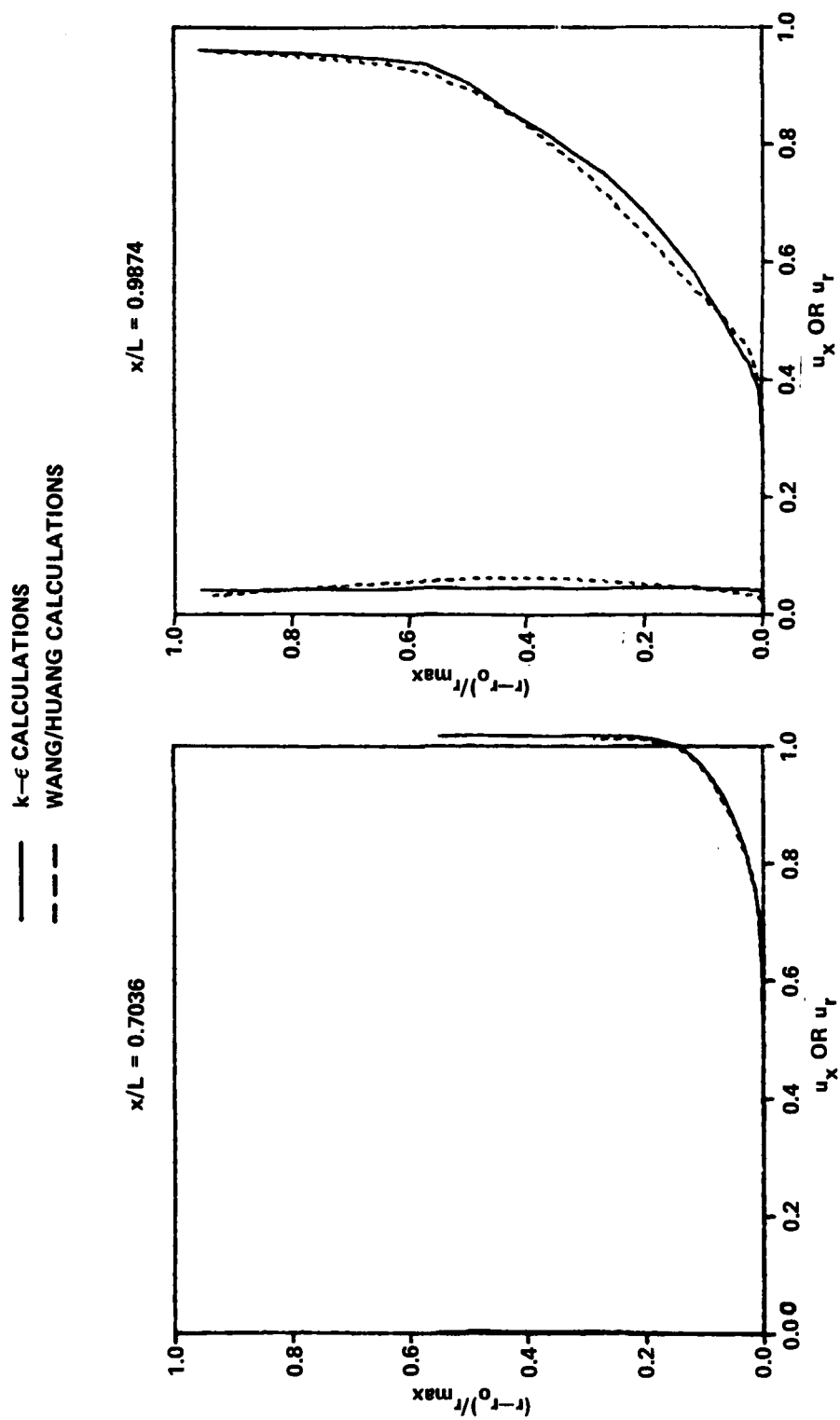
Figure 50 – A Comparison of the Computed Velocity Profiles at Two x-Stations

for Afterbody 5 at Re = 1×10^8

k-ε CALCULATIONS
- - - WANG/HUANG CALCULATIONS
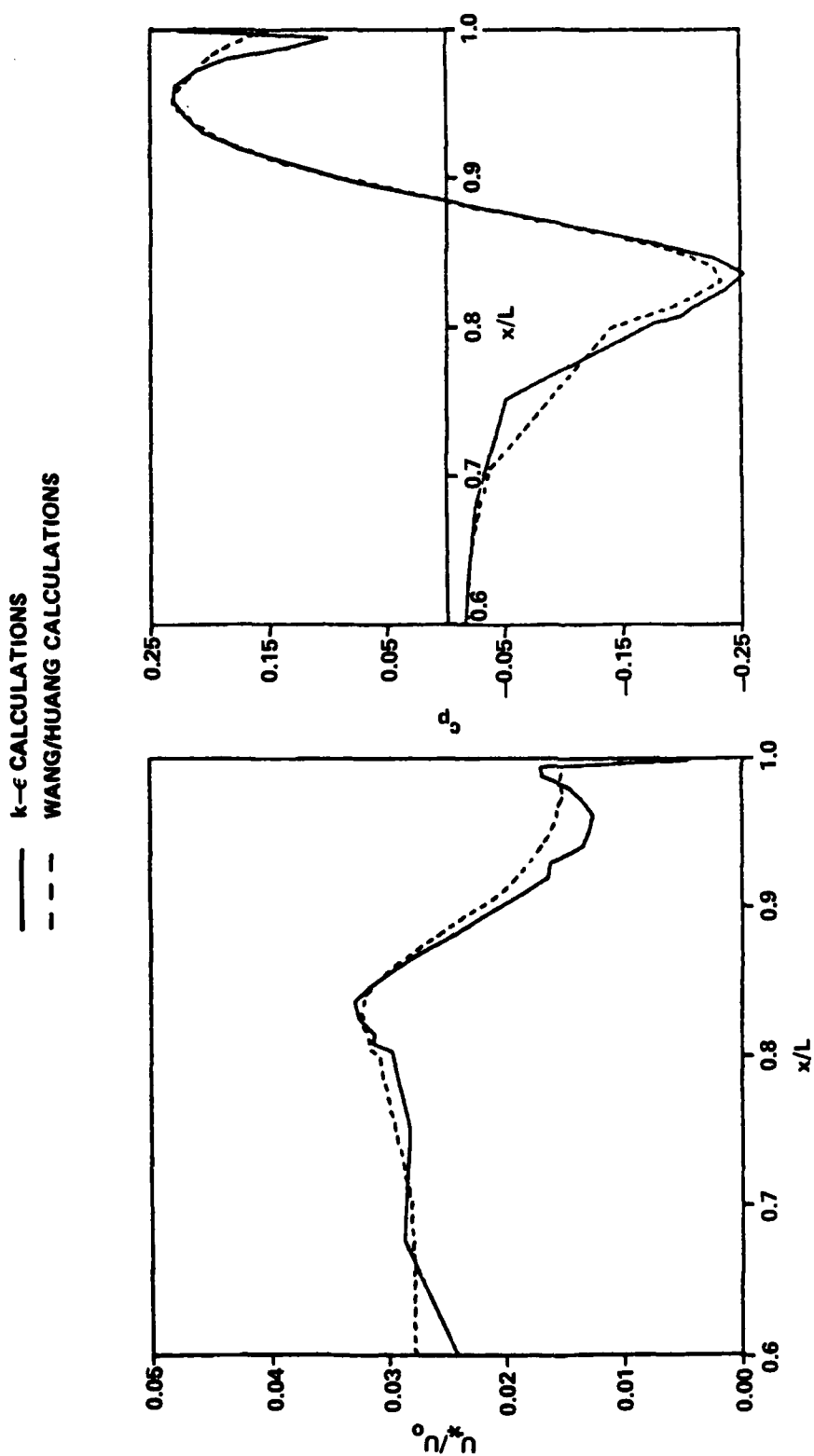
Figure 51 - Comparison of the Computed u* and c_p Distribution for Afterbody 5 at Re = 1×10^9

94
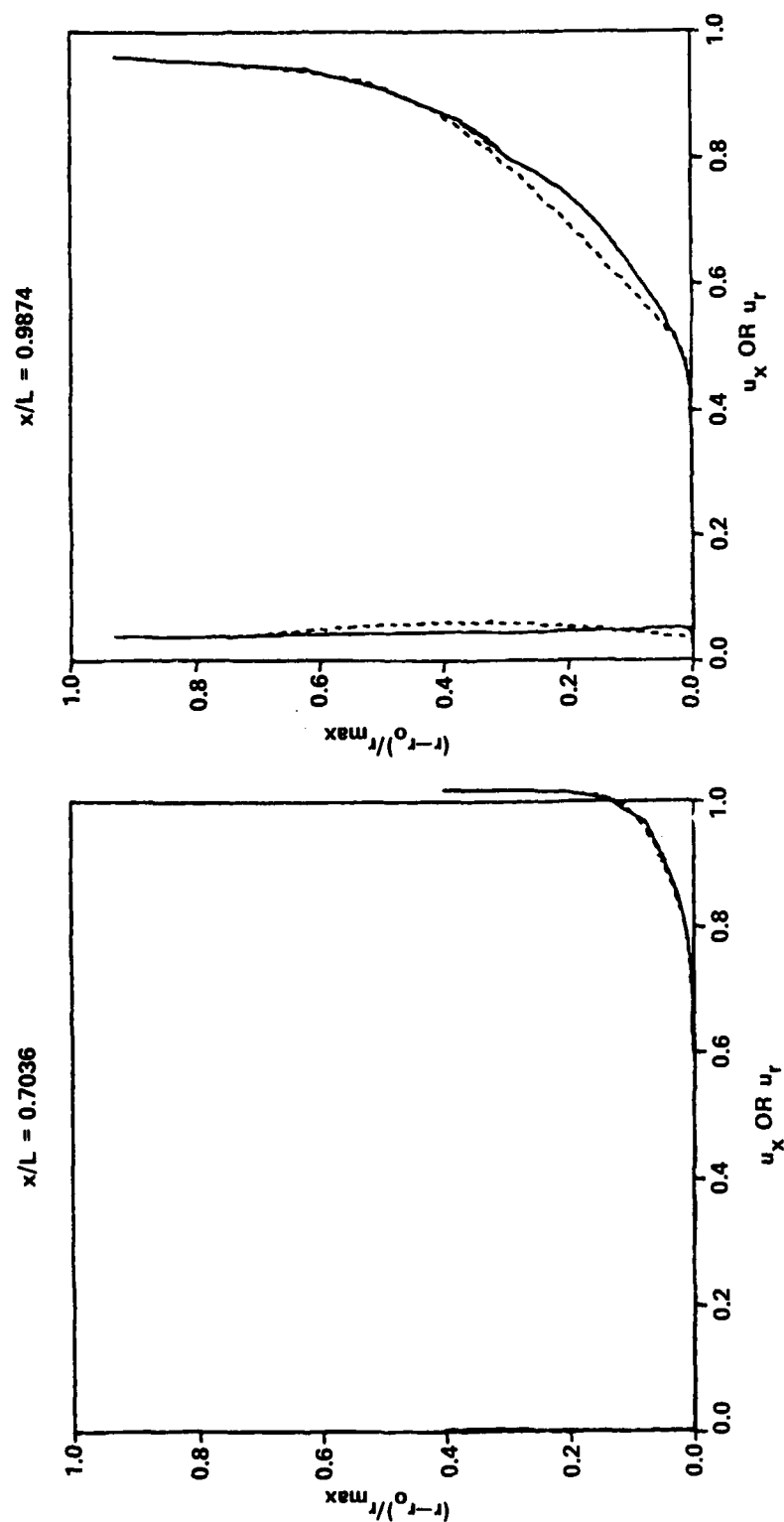
Figure 52 - A Comparison of the Computed Velocity Profiles at Two x-Stations
for Afterbody 5 at Re = 1×10^9

APPENDIX A

The equations listed under (2.46) are integrated using the finite volume method. In this approach, the values of the downstream flow variables are obtained by integrating the equations over small control volumes, as shown in Figure 2, that extend from the bottom to the top of the flow domain. For each control volume, linear interpolations of the variables are used to evaluate the integral. By way of examples: if g represents a field variable given at the staggered grid points $(x^{i+1/2}, \psi_{j+1/2})$ and denoted by $g_{j+1/2}^{i+1/2}$ (as U, p, k, ε, ν_T), and f is a variable given on the grid points (x^i, ψ_j) and denoted by f_j (as α), then, for a control volume extending from $x^{i-1/2}$ to $x^{i+1/2}$ and from ψ_{j-1} to ψ_j, three typical integrals, fg, f∂g/∂x, and g ∂f/$\partial\psi$ are evaluated as:

$$\int_{x^{i-1/2}}^{x^{i+1/2}} \int_{\psi_{j-1}}^{\psi_j} fg \, dxd\psi = (x^{i+1/2}-x^{i-1/2}) \, (\psi_j-\psi_{j-1}) \, \frac{(f_j^{\,i}+f_{j-1}^{\,i})}{2}$$

$$\frac{(g_{j-1/2}^{i+1/2}+g_{j-1/2}^{i-1/2})}{2} \tag{A.1}$$

$$\int_{x^{i-1/2}}^{x^{i+1/2}} \int_{\psi_{j-1}}^{\psi_j} f \frac{\partial g}{\partial x} \, dxd\psi = (\psi_j-\psi_{j-1}) \, \frac{(f_j+f_{j-1})}{2} \, (g_{j-1/2}^{i+1/2}-g_{j-1/2}^{i-1/2}) \tag{A.2}$$

and

$$\int_{x^{i-1/2}}^{x^{i+1/2}} \int_{\psi_{j-1}}^{\psi_j} g \frac{\partial f}{\partial x} \, dxd\psi = (x^{i+1/2}-x^{i-1/2}) \, (g_{j-1/2}^{i+1/2}+g_{j-1/2}^{i-1/2})(f_j^{\,i}-f_{j-1}^{\,i}) \tag{A.3}$$

97

For the U momentum Equation (2.46), the control volumes extend from $x^{i-1/2}$ to $x^{i+1/2}$ and from ψ_{j-1} to ψ_j. Denoting this area by ΔA_j, in Equation (3.4), the integral of each item in this equation is written as

$$I_1 = I_2 + I_3 + I_4 + I_5 + I_6 \qquad (A.4)$$

In the following integrations, the superscript (n) on the downstream variables will denote that the variable is evaluated from the previous station and that superscript (n+1) is the present iteration. For n = 0, we set the zeroth iterate equal to the upstream value of the variable, except for p, where the value of the initial guess or the pressure result from the previous total sweep. The factor $(1-\delta^i_{3/2})$, which is equal to 1 except at i = 3/2, where it is zero, is multiplied by some of the integral terms below to indicate that these integrals are zero at i = 3/2. This is done since these integrals require the two previous upstream stations. The evaluation of the individual terms in Equation (A.4) is

$$I_1 = \iint_{\Delta A_j} U \cos \alpha \frac{\partial U}{\partial x}\, dx\, d\psi = (\psi_j - \psi_{j-1})\, [(U^{i+1/2(n)}_{j-1/2} + U^{i-1/2}_{j-1/2})/2]$$

$$\cos\,[\alpha^{i(n)}_j + \alpha^{i(n)}_{j-1})/2]\, (U^{i+1/2(n+1)}_{j-1/2} - U^{i-1/2}_{j-1/2}) \qquad (A.5a)$$

$$I_2 = -\iint_{\Delta A_j} \cos \alpha \frac{\partial p}{\partial x}\, dx\, d\psi = -(\psi_j - \psi_{j-1})\, \cos\,[(\alpha^{i(n)}_j + \alpha^{i(n)}_{j-1})/2]$$

$$(p^{i+1/2}_{j-1/2} - p^{i-1/2(n)}_{j-1/2}) \qquad (A.5b)$$

98

$$I_3 = \iint_{\Delta A_j} \frac{\sin \alpha}{r} \frac{\partial}{\partial x} \left[r \nu_e \sin \alpha \ \frac{\partial U}{\partial x} \right] dx d\psi =$$

$$\{(1-\delta_{3/2}^i) \ (\psi_j - \psi_{j-1}) \ \sin \ [\alpha_j^{i(n)} + \alpha_{j-1}^{i(n)})/2]$$

$$(r_j^{i+1/2(n)} + r_{j-1}^{i+1/2(n)} + r_j^{i-1/2} + r_{j-1}^{i-1/2})/4\}$$

$$\{[r_j^{i+1/2(n)} + r_{j-1}^{i+1/2(n)})/2] \ \nu_{ej-1/2}^{i+1/2(n)} \ \sin \ [(\alpha_j^{i(n)} + \alpha_{j-1}^{i(n)})/2]$$

$$[(U_{j-1/2}^{i+1/2(n+1)} - U_{j-1/2}^{i-1/2})/(x^{i+1/2} - x^{i-1/2})]$$

$$-[(r_j^{i-1/2} + r_{j-1}^{i-1/2})/2] \ \nu_{ej-1/2}^{i-1/2} \ \sin \ [(\alpha_j^{i-1} + \alpha_{j-1}^{i-1})/2]$$

$$[(U_{j-1/2}^{i-1/2} - U_{j-1/2}^{i-3/2})/(x^{i-1/2} - x^{i-3/2})]\}$$

$$\text{(A.5c)}$$

$$I_4 = -\iint_{\Delta A_j} \frac{\sin \alpha}{r} \frac{\partial}{\partial x} \left[r^2 \nu_e \ U \ \frac{\partial U}{\partial \psi} \right] dx d\psi =$$

$$-(1-\delta_{3/2}^i)\{\sin[(\alpha_j^{i(n)} + \alpha_{j-1}^{i(n)}/2]/[r_j^{i+1/2(n)} + r_{j-1}^{i-1/2} + r_j^{i-1/2})/4]\}$$

$$\{[(r_j^{i+1/2(n)} + r_{j-1}^{i+1/2(n)})/2]^2 \ \nu_{ej-1/2}^{i+1/2(n)} U_{j-1/2}^{i+1/2(n)}$$

$$[(U_{j+1/2}^{i+1/2(n)} - U_{j-1/2}^{i+1/2(n+1)})/2] - [(r_j^{i-1/2} + r_{j-1}^{i-1/2})/2]^2$$

$$\nu_{ej-1/2}^{i-1/2} \ U_{j-1/2}^{i-1/2} \ [(U_{j+1/2}^{i-1/2} - U_{j-1/2}^{i-1/2})/2]\}$$

$$\text{(A.5d)}$$

$$I_5 = -\iint_{\Delta A_j} U \frac{\partial}{\partial \psi}\left[r\nu_e \sin\alpha \frac{\partial U}{\partial x}\right]dxd\psi =$$

$$- (1-\delta_{3/2}^{i})\ [(U_{j-1/2}^{i+1/2(n)}+U_{j-1/2}^{i-1/2})/2]\{[(r_j^{i+1/2(n)}+r_j^{i-1/2})/2]$$

$$[(\nu_{ej+1/2}^{i+1/2(n)}+\nu_{ej+1/2}^{i-1/2}+\nu_{ej-1/2}^{i+1/2(n)}+\nu_{ej-1/2}^{i-1/2})/4]\ \sin\ (\alpha_j^{i(n)})$$

$$[(U_{j+1/2}^{i+1/2(n+1)}+U_{j-1/2}^{i+1/2(n+1)}-U_{j+1/2}^{i-1/2}-U_{j-1/2}^{i-1/2})/2]$$

$$-[(r_{j-1}^{i+1/2(n)}+r_{j-1}^{i-1/2})/2]\ [\nu_{ej-1/2}^{i+1/2(n)}+\nu_{ej-1/2}^{i-1/2}+\nu_{ej-3/2}^{i+1/2(n)}+\nu_{ej-3/2}^{i-1/2})/4]$$

$$\sin\ (\alpha_{j-1}^{i(n)})\ [(U_{j-1/2}^{i+1/2(n)}+U_{j-3/2}^{i+1/2(n+1)}-U_{j-1/2}^{i-1/2}-U_{j-3/2}^{i-1/2})/2]\} \qquad \text{(A.5e)}$$

$$I_6 = \iint_{\Delta A_j} U \frac{\partial}{\partial \psi}\left[r^2\nu_e U \frac{\partial U}{\partial \psi}\right]dxd\psi =$$

$$2[(U_{j-1/2}^{i+1/2(n)}+U_{j-1/2}^{i-1/2})/2]\{[(r_j^{i(n)}+r_j^{i-1})/2]^2$$

$$[(\nu_{ej+1/2}^{i+1/2(n)}+\nu_{ej+1/2}^{i-1/2}+\nu_{ej-1/2}^{i+1/2(n)}+\nu_{ej-1/2}^{i-1/2})/4]$$

$$[(U_{j+1/2}^{i+1/2(n)}+U_{j+1/2}^{i-1/2}+U_{j-1/2}^{i+1/2(n)}+U_{j-1/2}^{i-1/2})/4]$$

$$[(U_{j+1/2}^{i+1/2(n+1)}-U_{j-1/2}^{i+1/2(n+1)})/(\psi_{j+1}^{-}-\psi_{j-1})]$$

$$-[(r_{j-1}^{i(n)}+r_{j-1}^{i-1})/2]^2[(\nu_{ej-1/2}^{i+1/2(n)}+\nu_{ej-1/2}^{i-1/2}+\nu_{ej-3/2}^{i+1/2(n)}$$

$$+\nu_{ej-3/2}^{i-1/2})/4] \qquad \text{(A.5f cont.)}$$

100

$$[(U_{j-1/2}^{i+1/2(n)}+U_{j-1/2}^{i-1/2}+U_{j-3/2}^{i+1/2(n)}+U_{j-3/2}^{i-1/2})/4]$$

$$[(U_{j-1/2}^{i-1/2(n+1)}+U_{j-3/2}^{i+1/2(n+1)})/(\psi_j-\psi_{j-1})\}$$ (A.5f)

In these integrals, upstream differencing is used for all derivatives in x, and I_6 is evaluated so that this term is implicit. In the integrals in Equation (A.5), the $U^{(n+1)}$ terms are collected and a tridiagonal system of equations results:

$$A_{j-1/2}^{U(n+1)} U_{j-3/2}^{i+1/2(n+1)} + B_{j-1/2}^{U(n+1)} U_{j-1/2}^{i+1/2(n+1)} + C_{j-1/2}^{U(n+1)} U_{j+1/2}^{i+1/2(n+1)}$$

$$= E_{j-1/2}^{u(n+1)} + F_{j-1/2}^{u(n+1)} (p_{j-1/2}^{i+1/2}-p_{j-1/2}^{i-1/2(n)})$$ (A.6)

The coefficients in Equation (A.6) depend on the known upstream values and previous iteration values of the downstream values of U, α, r, k, ϵ, and ν_e. Equation (A.6) is solved by the double sweep method presented in Appendix B, given the top and bottom boundary condition for $U^{i+1/2(n+1)}$.

For the normal momentum, Equation (2.46e), the control volumes extend from x^{i-1} to x^i, and from $(\psi_{j-1}+\psi_j)/2$ to $(\psi_j+\psi_{j+1})/2$. The three integrals needed to be evaluated in Equation (2.46e) are written

$$J_1 = J_2 + J_3$$ (A.7)

and if we denote a control volume for this equation by ΔA_j, Equation (3.6), the integral is

$$J_1 = \iint_{\Delta A_j'} U^2 \cos \alpha \frac{\partial \alpha}{\partial x} dxd\psi = [(\psi_{j+1}-\psi_{j-1})/2]$$

$$[(U_{j+1/2}^{i-1/2}+U_{j-1/2}^{i-1/2})/2]^2 \cos [(\alpha_j^{i-1}+\alpha_j^{i(n)})/2] (\alpha_j^{i(n+1)}-\alpha_j^{i-1})$$ (A.8a)

$$J_2 = -\iint_{\Delta A'_j} rU \frac{\partial p}{\partial \psi}\, dx d\psi = -(x^i - x^{i-1}) r_j^{i-1/2} [(U_{j-1/2}^{i-1/2} + U_{j+1/2}^{i-1/2})/2]$$

$$(p_{j+1/2}^{i-1/2(n)} - p_{j-1/2}^{i-1/2(n)}) \qquad (A.8b)$$

and

$$J_3 = \iint_{\Delta A'_j} \sin \alpha \frac{\partial p}{\partial x}\, dx d\psi = [(\psi_{j+1} - \psi_{j-1})/2] \sin [(\alpha_j^{i-1} + \alpha_j^{i(n)})/2]$$

$$(q_j^{i(n)} - q_j^{i-1(n)}) \qquad (A.8c)$$

where

$$q_j^{i(n)} = (p_{j+1/2}^{i+1/2} + p_{j-1/2}^{i+1/2} + p_{j+1/2}^{i-1/2(n)} + p_{j-1/2}^{i-1/2(n)})/4 \qquad (A.9)$$

The terms in Equation (A.8) are collected and the equation for $\alpha_j^{i(n+1)}$ is written for $j = 2, 3, 4, \ldots J$ as:

$$\alpha_j^{i(n+1)} = A_j^{\alpha(n+1)} + B_j^{\alpha(n+1)}\, p_{j+1/2}^{i-1/2(n)} + C_j^{\alpha(n+1)}\, p_{j-1/2}^{i-1/2(n)} \qquad (A.10)$$

The coefficients in Equation (A.10) depend on known quantities, and, because of the nature of the integration, are independent of the downstream values of U.

The equation for the downstream radial position of the streamlines Equation (2.46b) is integrated along the $x^{i+1/2}$ line. But, first this equation is multiplied by r to obtain the form:

$$\frac{\partial r^2}{\partial \psi} = \frac{2}{U \cos \alpha}$$

102

Integrating this equation from ψ_{j-1} to ψ_j along the $x^{i+1/2}$ yields

$$r_j^{i+1/2(n+1)} = \{(r_j^{i+1/2(n+1)})^2 + 2\ (\psi_j - \psi_{j-1})/[U_{j-1/2}^{i+1/2(n+1)}$$

$$\cos\ [(\alpha_j^{i(n)} + \alpha_{j-1}^{i(n)})/2]\} \tag{A.11}$$

Since the r position of $\psi = 0$ is known, the values of all $r_j^{i+1/2(n+1)}$ are obtained by summing Equation (A.11).

The k and ε Equations (2.46f, g) are solved simultaneously as follows:

$$U \cos \alpha \frac{\partial k}{\partial x} = \frac{\sin \alpha}{r} \frac{\partial}{\partial x}\left[\frac{r\nu_e}{\sigma_k} \sin \alpha \frac{\partial k}{\partial x}\right] - \frac{\sin \alpha}{r} \frac{\partial}{\partial x}\left[\frac{r^2\nu_e}{\sigma_k} U \frac{\partial k}{\partial \psi}\right]$$

$$- U \frac{\partial}{\partial \psi}\left[\frac{r\nu_e}{\sigma_k} \sin \alpha \frac{\partial k}{\partial x}\right] + U \frac{\partial}{\partial \psi}\left[\frac{r^2\nu_e}{\sigma_k} U \frac{\partial k}{\partial \psi}\right]$$

$$-0.33\ C_3\ \varepsilon \cos \alpha \frac{\partial U}{\partial x} + C_\mu \gamma \frac{k^2}{\varepsilon}\left[rU \frac{\partial U}{\partial \psi} - \sin \alpha \frac{\partial U}{\partial x}\right]^2 - \varepsilon$$

$$\tag{A.12a}$$

and

$$U \cos \alpha \frac{\partial \varepsilon}{\partial x} = \frac{\sin \alpha}{r} \frac{\partial}{\partial x}\left[\frac{r\nu_e}{\sigma_\varepsilon} \sin \alpha \frac{\partial \varepsilon}{\partial x}\right] - \frac{\sin \alpha}{r} \frac{\partial}{\partial x}\left[\frac{r^2\nu_e}{\sigma_\varepsilon} U \frac{\partial \varepsilon}{\partial \psi}\right]$$

$$- U \frac{\partial}{\partial \psi}\left[\frac{r\nu_e}{\sigma_\varepsilon} \sin \alpha \frac{\partial \varepsilon}{\partial x}\right] + U \frac{\partial}{\partial \psi}\left[\frac{r^2\nu_e}{\sigma_\varepsilon} -U \frac{\partial \varepsilon}{\partial \psi}\right]$$

$$-0.33\ C_\mu\ k \cos \alpha \frac{\partial U}{\partial x} + C_1 C_\mu\ \gamma k\left[rU \frac{\partial U}{\partial \psi} - \sin \alpha \frac{\partial U}{\partial x}\right]^2 - \frac{c_2 \varepsilon^2}{k}$$

$$\tag{A.12b}$$

The control volumes for Equations (A.12) are the same as those for the U equation. The integrals are written for Equations (A.12a and b) respectively as:

$$L_1 = L_2 + L_3 + L_4 + L_5 + L_6 + L_7 + L_8 \qquad \text{(A.13a)}$$

$$M_1 = M_2 + M_3 + M_4 + M_5 + M_6 + M_7 + M_8 \qquad \text{(A.13b)}$$

A term in Equation (A.13) corresponds to a term in Equation (A.12) in the order that it is written. The procedure to determine L_1 through L_5 and M_1 through M_5 is the same as that performed to determine I_1 through I_6 in Equation (A.5). The only difference is that since the U, α, and r equation integrations are performed before the k and ε equation integrations, the values of $U^{i+1/2(n+1)}$, $\alpha^{i(n+1)}$ and $r^{i+1/2(n+1)}$ are known. These values are used to determine the coefficients in L_1 through L_5 and M_1 through M_5. The ν_e terms, however, are given from the previous iteration. The last three terms in Equations (A.13a) and (A.13b) are determined by taking downstream values of k, ε, (k^2/ε) and (ε^2/k). To determine the downstream values of the nonlinear terms (k^2/ε) and (ε^2/k), a Taylor series in k and ε are taken to first order:

$$(k^2/\varepsilon)^{i+1/2} = (k^2/\varepsilon)^{i-1/2} + 2(k/\varepsilon)^{i-1/2}\,(k^{i+1/2}-k^{i-1/2})$$

$$- (k^2/\varepsilon^2)^{i-1/2}\,(\varepsilon^{i+1/2}-\varepsilon^{i-1/2}) = 2(k/\varepsilon)^{i-1/2}\,k^{i+1/2}$$

$$- (k^2/\varepsilon^2)^{i-1/2}\,\varepsilon^{i+1/2} \qquad \text{(A.14a)}$$

$$(\varepsilon^2/k)^{i+1/2} = (\varepsilon^2/k)^{i-1/2} + 2(\varepsilon/k)^{i-1/2}\,(\varepsilon^{i+1/2}-\varepsilon^{i-1/2})$$

$$- (\varepsilon^2/k^2)^{i-1/2}\,(k^{i+1/2}-k^{i-1/2}) = 2(\varepsilon/k)\,\varepsilon^{i+1/2}$$

$$- (\varepsilon^2/k^2)^{i-1/2}\,k^{i+1/2} \qquad \text{(A.14b)}$$

104

With these two approximations, the integral terms L_6, L_7, L_8, M_6, M_7, and M_8 are given by:

$$L_6 = - \iint_{\Delta v} 0.33 \ C_3 \ \epsilon \ \cos \alpha \ \frac{\partial U}{\partial x} \ dxd\psi = - (\psi_j - \psi_{j-1}) \ 0.33 \ C_3 \ \epsilon_{j-1/2}^{i+1/2(n+1)}$$

$$\cos \ [(\alpha_j^{i(n+1)} + \alpha_{j-1}^{i(n+1)})/2] \ (U_{j-1/2}^{i+1/2(n+1)} - U_{j-1/2}^{i-1/2}) \tag{A.15a}$$

$$L_7 = \iint_{\Delta v} C_\mu \gamma \ (k^2/\epsilon)(rU\partial U/\partial \psi - \sin \alpha \ \partial U/\partial x)^2 \ dxd\psi =$$

$$(\psi_j - \psi_{j-1})(x^{i+1/2} - x^{i-1/2}) \ C_\mu \ \gamma_{j-1/2}^{i+1/2(n+1)} [2(k/\epsilon)_{j-1/2}^{i-1/2} \ k_{j-1/2}^{i+1/2(n+1)}$$

$$-2(k^2/\epsilon^2)_{j-1/2}^{i-1/2} \epsilon_{j-1/2}^{i+1/2(n+1)}] \ \{[(r_j^{i+1/2(n+1)} + r_{j-1}^{i+1/2(n+1)})/2] \ U_{j-1/2}^{i+1/2(n+1)}$$

$$[(U_{j+1/2}^{i+1/2(n+1)} - U_{j-3/2}^{i+1/2(n+1)}/(\psi_{j+1} - \psi_{j-1})] - \sin \ [(\alpha_j^{i(n+1)} + \alpha_j^{i-1})/2]$$

$$(U_{j-1/2}^{i+1/2(n+1)} - U_{j-1/2}^{i-1/2})/(x^{i+1/2} - x^{i-1/2})\}^2 \tag{A.15b}$$

$$L_8 = - \iint_{\Delta v} \epsilon dxd\psi = - (\psi_j - \psi_{j-1})(x^{i+1/2} - x^{i-1/2})\epsilon_{j-1/2}^{i+1/2(n+1)} \tag{A.15c}$$

$$M_6 = - \iint_{\Delta v} 0.33 \ C_\mu \ k \ \cos \alpha \ \frac{\partial U}{\partial x} \ dxd\psi = -(\psi_j - \psi_{j-1}) \ 0.33 \ C_\mu \ k_{j-1/2}^{i+1/2(n+1)}$$

$$\cos \ [(\alpha_j^{i(n+1)} + \alpha_{j-1}^{i(n+1)})/2](U_{j-1/2}^{i+1/2(n+1)} - U_{j-1/2}^{i-1/2}) \tag{A.15d}$$

$$M_7 = \iint_{\Delta v} C_1 \, C_\mu \, \gamma \, k(r \, U \, \partial U/\partial \psi - \sin \alpha \, \partial U/\partial x)^2 \, dx d\psi =$$

$$(\psi_j - \psi_{j-1})(x^{i+1/2} - x^{i-1/2}) \, C_1 \, C_\mu \, \gamma_{j-1/2}^{i+1/2(n+1)} \, k_{j-1/2}^{i+1/2(n+1)}$$

$$\{[(r_j^{i+1/2(n+1)} = r_{j-1}^{i+1/2(n+1)})/2] \, U_{j-1/2}^{i+1/2(n+1)} \, 2[(U_{j+1/2}^{i+1/2(n+1)}$$

$$-U_{j-3/2}^{i+1/2(n+1)}/(\psi_{j+1} - \psi_{j-1}) - \sin [(\alpha_j^{i(n+1)} + \alpha_j^{i-1})/2] \, (U_{j-1/2}^{i+1/2(n+1)}$$

$$-U_{j-1/2}^{i-1/2}/(x^{i+1/2} - x^{i-1/2})\}^2 \hspace{3cm} \text{(A.15e)}$$

and

$$M_8 = -\iint_{\Delta v} C_2 \, \varepsilon^2/k \, dx d\psi = -(\psi_j - \psi_{j-1})(x^{i+1/2} - x^{i-1/2})c_2$$

$$[2(\varepsilon/k)_{j-1/2}^{i-1/2} \, \varepsilon_{j-1/2}^{i+1/2(n+1)} - (\varepsilon^2/k^2)_{j-1/2}^{i-1/2} \, k_{j-1/2}^{i+1/2(n+1)}] \quad \text{(A.15f)}$$

If all the $k^{i+1/2(n+1)}$ and $\varepsilon^{i+1/2(n+1)}$ terms are collected from L_1 through L_8 and M_1 through M_8, a tridiagonal matrix system results, and is given by:

$$A_{j-1/2}^{(n+1)} \cdot \begin{bmatrix} k_{j-3/2}^{i+1/2(n+1)} \\ \\ \varepsilon_{j-3/2}^{i+1/2(n+1)} \end{bmatrix} + B_{j-1/2}^{(n+1)} \cdot \begin{bmatrix} k_{j-1/2}^{i+1/2(n+1)} \\ \\ \varepsilon_{j-1/2}^{i+1/2(n+1)} \end{bmatrix}$$

$$\text{(A.16)}$$

$$C_{j-1/2}^{(n+1)} \cdot \begin{bmatrix} k_{j+3/2}^{i+1/2(n+1)} \\ \\ \varepsilon_{j+3/2}^{i+1/2(n+1)} \end{bmatrix} = D_{j-1/2}^{(n+1)}$$

where $A_{j-1/2}^{(n+1)}$, $B_{j-1/2}^{(n+1)}$ and $C_{j-1/2}^{(n+1)}$ are 2×2 matrices, and $D_{j-1/2}^{(n+1)}$ is a 1×2 matrix. Given the top and bottom boundary conditions described in the text, Equation (A.16) is solved using the method presented in Appendix B.

APPENDIX B

In the numerical integration procedure, equations are encountered of the form

$$B_1 \underline{v}_1 + C_1 \underline{v}_2 = d_1$$

$$A_j \underline{v}_j{-1} + B_j \underline{v}_j + C_j \underline{v}_{j+1} = \underline{d}_j, \quad j = 2, 3,\ldots, N-1 \qquad (B.1)$$

$$A_N \underline{v}_{N-1} + B_{N\underline{v}_N} = d_N$$

where A_j, B_j, and C_j are n, x, n matrices and $\underline{d}_j$ is a column vector of length n, all independent of the unknown column vectors, $\underline{v}_j$'s. To solve Equation (B.1), solutions of the form (Carnaham, Luther, and Wilkes, 1969)[26]

$$\underline{v}_i = \underline{Y}_i - \beta_i^{-1} C_i \underline{v}_{i+1} \qquad (B.2)$$

are sought where $\underline{Y}_i$ is a column vector, β_i is an n, x, n matrix (both are to be determined) and β_i^{-1} is the matrix inverse of β_i. The product $\beta_i^{-1}C_i$ is the normal matrix multiplication. Substitution of Equation (B.2) into (B.1) gives the recurrence relations for γ_i and β_j:

$$\beta_i = \beta_i - A_i \beta_{i-1}^{-1} C_{i-1} \qquad (B.3)$$

$$\underline{Y}_i = \beta_i^{-1} (\underline{d}_i - A_i \underline{Y}_{i-1}) \qquad (B.4)$$

Rewriting the first equation of (B.1) as

$$\underline{v}_1 = B_1^{-1} \underline{d}_1 - B_1^{-1} C_1 \underline{v}_2 \qquad (B.5)$$

and comparing this to the case $c = 1$ in Equation (B.2) results in:

$$\beta_1 = B_1$$

$$\underline{\gamma}_1 = \beta_1^{-1} \underline{d}_1 \qquad (B.6)$$

Rewriting the Nth equation of (B.1) as

$$B_N \underline{v}_N = \underline{d}_N - A_N \underline{\gamma}_{N-1} + A_N \beta_{N-1}^{-1} C_{N-1} \underline{v}_N$$

and combining the v_N terms yields:

$$\underline{v}_N + [B_N - A_N \beta_{N-1}^{-1} C_{N-1}]^{-1} (\underline{d}_N - A_N \underline{\gamma}_{N-1}) = \underline{\gamma}_N \qquad (B.7)$$

which holds if we set $\underline{v}_{N+1} = 0$. Once the $\underline{\gamma}_i$'s and β_i's are known, the $\underline{v}_N$ is determined from Equation (B.7) and $\underline{v}_{N-j}$ for $j \geq 1$ from Equation (B.2).

REFERENCES

1. Briley, W.R., "Numerical Method for Predicting Three-Dimensional Steady Viscous Flows in Ducts," Journal of Computational Physics, 14, pp. 8-28 (1974).

2. Patankar, S.V., V.S. Pratap, and D.B. Spalding, "Predictions of Laminar Flow and Heat Transfer in Helically Coiled Pipes," Journal of Fluid Mechanics, 62, pp. 539-551 (1974).

3. Roberts, D.W. and C.K. Forester, "Parabolic Procedure for Flows in Ducts with Arbitrary Cross Sections," American Institute of Aeronautics and Astronautics Journal, 17, pp. 33-40 (1979).

4. Markatos, N.C.G. and C.B. Wills, "Prediction of Viscous Flow Around a Fully Submerged Appended Body," 13th Symposium on Naval Hydrodynamics, Tokyo, Japan, pp. 631-647 (1980).

5. Muraoka, K., "Calculation of Thick Boundary Layer and Wake of Ships by a Partially Parabolic Method," 13th Symposium on Naval Hydrodynamics, Tokyo, Japan, pp. 601-614 (1980).

6. Abdelmeguid, A.M., N.C.G. Markatos, and D.B. Spalding, "A Method of Predicting Three-Dimensional Turbulent Flows Around Ships' Hulls," International Symposium on Ship Viscous Resistance, SSPA, Goteborg, Sweden (1978).

7. Muraoka, K., "Calculation of Viscous Flow Around Ship Stern," Transactions of the West-Japan Society of Naval Architects, 58, pp. 235-257 (1978).

8. Pratap, V.S. and D.B. Spalding, "Numerical Computation of the Flow in Curved Ducts," Aeronautical Quarterly, 26, pp. 219-228 (1975).

9. Patankar, S.V. and D.B. Spalding, "A Calculation Procedure for Heat, Mass, and Momentum Transfer in Three-Dimensional Parabolic Flows," International Journal of Heat and Mass Transfer, 15, pp. 1787-1806 (1972).

10. Lighthill, M.J., "On Displacement Thickness," Journal of Fluid Mechanics, 4, pp. 383-392 (1958).

11. Launder, B.E. and D.B. Spalding, "The Numerical Computation of Turbulent Flows," Computer Methods in Applied Mechanics and Engineering, 3, pp. 269-289 (1974).

12. Jones, W.P. and B.E. Launder, "The Prediction of Laminarization with a 2-Equation Model of Turbulence," International Journal of Heat and Mass Transfer, 15, pp. 301-311 (1972).

13. Jones, W.P. and B.E. Launder, "Prediction of Low Reynolds-Number Phenomena with a 2-Equation Model of Turbulence," International Journal of Heat and Mass Transfer, 16, pp. 1119-1129 (1973).

14. Hanjalic, K. and B.E. Launder, "Sensitizing the Dissipation Equation to Irrotational Strains," Journal of Fluids Engineering, 102, pp. 34-40 (1980).

15. Liepmann, H.W. and A. Roshko, Elements of Gasdynamics, John Wiley and Sons, Inc., New York (1957).

16. Tennekes, H. and J.L. Lumley, A First Course in Turbulence, MIT Press, Cambridge, Massachusetts (1972).

17. Patel, V.C., A Nakayama, and R. Damian, "An Experimental Study of the Thick Turbulent Boundary Layer Near the Tail of a Body of Revolution," Iowa Institute of Hydraulic Research Report No. 142 (1973).

18. Dyne, G., "A Streamline Curvature Method for Calculating the Viscous Flow Around Bodies of Revolution," International Symposium on Ship Viscous Resistance, SSPA, Gotenborg, Sweden (1978).

19. Patankar, S.V. and D.B. Spalding, "A Finite-Difference Procedure for Solving the Equations of the Two-Dimensional Boundary Layer," International Journal of Heat and Mass Transfer, 10, pp. 1389-1411 (1967).

20. Wang, H.T. and T.T. Huang, "Calculation of Potential Flow/Boundary Layer Interaction on Axisymmetric Bodies," The American Society of Mechanical Engineers Symposium on Turbulent Boundary Layers, Niagara Falls, New York, pp. 47-57 (1979).

21. Hess, J.L. and A.M.O. Smith, "Calculation of Potential Flow About Arbitrary Bodies," Progress in Aeronautical Sciences, 8, Pergamon Press, New York, Chapter 1 (1966).

22. Huang, T.T., N. Santelli, and G. Belt, "Stern Boundary-Layer Flow on Axisymmetric Bodies," 12th Symposium on Naval Hydrodynamics, Washington, D.C., pp. 127-147 (1979).

23. Huang, T.T., N.C. Groves, and G. Belt, "Boundary Layer Flow on an Axisymmetric Body with an Inflected Stern," DTNSRDC Report 80/064 (1980).

24. Lyon, H.M., "The Effect of Turbulence on the Drag of Airship Models," Report and Memoranda No. 1511, Aeronautical Research Committee, London, England, pp. 123-148 (1932).

25. Lyon, H.M., "A Study of the Flow in the Boundary Layer of Streamline Bodies," Report and Memoranda No. 1622, Aeronautical Research Committee, London, England, pp. 266-318 (1934).

26. Carnaham, B., H.A. Luther, and J.O. Wilkes, Applied Numerical Methods, John Wiley and Sons, Inc., New York (1969).

INITIAL DISTRIBUTION

Copies		Copies	
1	WES	16	NAVSEA
			1 SEA 033
1	U.S. ARMY TRAS R&D		1 SEA 03D
	Marine Trans Div		1 SEA 05R
			1 SEA 05T
1	CHONR/438 Lee		1 SEA 32R
			1 SEA 312
2	NRL		1 SEA 55
	1 Code 2027		1 SEA 55N
	1 Code 2629		1 SEA 55W
			1 SEA 55W3
1	ONR/Boston		1 SEA 56X1
			1 SEA 56X4
1	ONR/Chicago		1 SEA 62P
			3 SEA 996
1	ONR/New York		
		1	NAVFAC/032C
1	ONR/Pasadena		
		1	NADC
1	ONR/San Francisco		
		1	NAVENPREDRSCHFAC/
1	NORDA		Tim Hogan
3	USNA	1	NAVSHIPYD PTSMH/Lib
	1 Tech Lib		
	1 Nav Sys Eng Dept	1	NAVSHIPYD PHILA/Lib
	1 B. Johnson		
		1	NAVSHIPYD NORVA/Lib
3	NAVPGSCOL		
	1 Lib	1	NAVSHIPYD CHASN/Lib
	1 T. Sarpkaya		
	1 J. Miller	1	NAVSHIPYD LBEACH/Lib
1	NOSC/Lib	2	NAVSHIPYD MARE
			1 Lib
1	NCSC/712		1 Code 250
1	NCEL/131	1	NAVSHIPYD PUGET/Lib
1	NSWC, White Oak/Lib	1	NAVSHIPYD PEARL/Code 202.32
1	NSWC, Dahlgren/Lib	1	NAVSEC, NORVA/6660.03, Blount
1	NUSC/Lib	12	DTIC
		1	AFOSR/NAM
		1	AFFOL/FYS, J. Olsen

115

Copies		Copies	
2	MARAD	1	U of Connecticut/Scottron
	1 Div of Ship R&D		
	1 Lib	1	Cornell U/Shen
1	NASA/HQ/Lib	1	Florida Atlantic U/Tech Lib
1	NASA/Ames Res Ctr, Lib	2	Harvard U
			1 G. Carrier
2	NASA/Langley Res Ctr		1 Gordon McKay Lib
	1 Lib		
	1 D. Bushnell	1	U of Hawaii/Bretschneider
1	NBS/Lib	1	U of Illinois/J. Robertson
1	NSF/Eng Lib	4	U of Iowa
			1 Lib
1	LC/Sci & Tech		1 L. Landweber
			1 J. Kennedy
1	DOT/Lib TAD-491.1		1 V.C. Patel
2	MMA	1	Johns Hopkins U/Lib
	1 National Maritime Res Ctr		
	1 Lib	1	Kansas State U/Nesmith
1	U of Bridgeport/E. Uram	1	U of Kansas/Civil Eng Lib
1	Brown Univ/J.T.C. Liu	1	Lehigh U/Fritz Eng Lab Lib
2	U of Cal/Dept Naval Arch, Berkeley	4	MIT
	1 Lib		1 Lib
	1 W. Webster		1 J.R. Kerwin
			1 P. Leehey
2	U of Cal., San Diego		1 J.N. Newman
	1 A.T. Ellis		
	1 Scripps Inst Lib	2	U of Minn/St. Anthony Falls
			1 Lib
5	CIT		1 R. Arndt
	1 Aero Lib		
	1 T.Y. Wu	1	U of Mich/NAME/Lib
	1 A.J. Acosta		
	1 I. Sabersky	1	U of Notre Dame/Eng Lib
	1 D. Coles		
		1	New York U/Courant Inst/Lib
1	City College, Wave Hill/Pierson		
		4	Penn State
1	Catholic U of Amer/Civil &		1 B.R. Parkin
	Mech Eng		1 R.E. Henderson
			1 ARL Lib
1	Colorado State U/Eng Res Ctr		1 G.H. Hoffman

Copies		Copies	
1	Princeton U/Mellor	2	Boeing Company/Seattle
			1 Marine System
1	U of Rhode Island/F.M. White		1 P. Rubbert
1	SIT/Lib	1	Bolt, Beranek & Newman/Lib
1	U of Texas/Arl Lib	1	Exxon, NY/Design Div/Tank Dept
1	Utah State U/Jeppson	1	Exxon Math & System, Inc.
2	Southwest Res Inst	1	General Dynamics, EB/Boatwright
	1 Applied Mech Rev		
	1 Abramson	1	Flow Research
3	Stanford U	1	Gibbs & Cox/Tech Info
	1 Eng Lib		
	1 R. Street, Dept Civil Eng	1	Grumman Aerospace Corp/Lib
	1 S.J. Kline, Dept Mech Eng		
		4	Hydronautics
1	Stanford Res Inst/Lib		1 Lib
			1 E. Miller
1	U of Virginia/Aero Eng Dept		1 V. Johnson
			1 C.C. Hsu
1	U of Washington/Arl Tech Lib		
		1	Lockheed, Sunnyvale/Waid
2	VPI		
	1 Dept Mech Eng	1	Lockheed, California/Lib
	1 J. Schetz, Dept Aero &		
	Ocean Eng	1	Lockheed, Georgia/Lib
2	Webb Inst	1	McDonnell Douglas, Long Beach
	1 Lib		1 T. Cebeci
	1 Ward		
		1	Newport News Shipbuilding/Lib
1	Woods Hole/Ocean Eng		
		1	Nielsen Eng & Res
1	Worchester PI/Tech Lib		
		1	Northrop Corp/Aircraft Div
1	SNAME/Tech Lib		
		1	Rand Corp
1	Bell Aerospace		
		1	Rockwell International
1	Bethlehem Steel/Sparrows Point		1 B. Ujihara
1	Bethlehem Steel/New York/Lib	1	SAI (C. von Kerczek)

Copies		
1		Sperry Rand/Tech Lib
1		SRA (S.J. Shamroth)
1		Sun Shipbuilding/Chief Naval Arch
1		Robert Taggert
1		TRW Systems Group/Lib
1		TRACOR
1		United Technology/East Hartford, Conn
1		Westinghouse Electric
	1	Gulino

CENTER DISTRIBUTION

Copies	Code	Name
1	1500	W.B. Morgan
1	1504	V.J. Monacella
1	1507	D.S. Cieslowski
1	1508	R.S. Rothblum
1	152	W.C. Lin
1	1521	P. Pien
1	1521	W. Day
1	1522	G. Dobay
1	1522	M. Wilson
1	154	J. McCarthy
1	154	P. Granville
1	1540.1	B. Yim
1	1540.2	R. Cumming
30	1542	T.T. Huang
3	1542	N.C. Groves
1	1542	G.S. Belt
1	1542	Y.T. Lee
1	1542	M.S. Chang
1	1544	T. Brockett
1	1544	R. Boswell
1	1544	E. Caster

Copies	Code	Name
1	1544	S. Jessup
1	1544	K.F. Lin
1	1560	M. Martin
1	1561	G. Cox
1	1563	W.E. Smith
1	1564	J. Feldman
1	1572	E. Zarnick
1	1606	T.C. Tai
1	1615	R.J. Furey
1	1802.1	H. Lugt
1	1802.2	F. Frenkiel
1	1840	J. Schot
1	1843	H. Haussling
1	1843	K. Rao
1	19	M.M. Sevik
1	1940	J.T. Shen
1	1942	B.E. Bowers
1	1942	T.M. Farabee
1	1942	F.E. Geib
1	1942	T.C. Mathews
10	5211.1	Reports Distribution
1	522.1	Unclassified Lib (C)
1	522.2	Unclassified Lib (A)

FILM

2-8

DTI